LAWRENCE
LIVERMORE
NATIONAL
LABORATORY

LLNL-JRNL-402664

Heavy flavor in heavy-ion collisions at RHIC and RHIC II

A. D. Frawley, T. Ullrich, R. Vogt

April 2, 2008

Physics Reports

Disclaimer

This document was prepared as an account of work sponsored by an agency of the United States government. Neither the United States government nor Lawrence Livermore National Security, LLC, nor any of their employees makes any warranty, expressed or implied, or assumes any legal liability or responsibility for the accuracy, completeness, or usefulness of any information, apparatus, product, or process disclosed, or represents that its use would not infringe privately owned rights. Reference herein to any specific commercial product, process, or service by trade name, trademark, manufacturer, or otherwise does not necessarily constitute or imply its endorsement, recommendation, or favoring by the United States government or Lawrence Livermore National Security, LLC. The views and opinions of authors expressed herein do not necessarily state or reflect those of the United States government or Lawrence Livermore National Security, LLC, and shall not be used for advertising or product endorsement purposes.

Heavy flavor in heavy-ion collisions at RHIC and RHIC II

A. D. Frawley,[a] T. Ullrich,[b] and R. Vogt[c,d,e]

[a] *Physics Department, Florida State University, Tallahassee, FL, USA*

[b] *Physics Department, Brookhaven National Laboratory, Upton, NY, USA*

[c] *Lawrence Livermore National Laboratory, Livermore, CA, USA*

[d] *Physics Department, University of California at Davis, Davis, CA, USA*

[e] *Nuclear Science Division, Lawrence Berkeley National Laboratory, Berkeley, CA, USA*

Abstract

In the initial years of operation, experiments at the Relativistic Heavy Ion Collider (RHIC) have identified a new form of matter formed in nuclei-nuclei collisions at energy densities more than 100 times that of a cold atomic nucleus. Measurements and comparison with relativistic hydrodynamic models indicate that the matter thermalizes in an unexpectedly short time, has an energy density at least 15 times larger than needed for color deconfinement, has a temperature about twice the critical temperature predicted by lattice QCD, and appears to exhibit collective motion with ideal hydrodynamic properties - a "perfect liquid" that appears to flow with a near-zero viscosity to entropy ratio - lower than any previously observed fluid and perhaps close to a universal lower bound. However, a fundamental understanding of the medium seen in heavy-ion collisions at RHIC does not yet exist. The most important scientific challenge for the field in the next decade is the *quantitative* exploration of the new state of nuclear matter. That will require new data that will, in turn, require enhanced capabilities of the RHIC detectors and accelerator. In this report we discuss the scientific opportunities for an upgraded RHIC facility - RHIC II - in conjunction with improved capabilities of the two large RHIC detectors, PHENIX and STAR. We focus solely on heavy flavor probes. Their production rates are calculable using the well-established techniques of perturbative QCD and their sizable interactions with the hot QCD medium provide unique and sensitive measurements of its crucial properties making them one of the key diagnostic tools available to us.

Key words: Heavy Flavor, Quarkonium, Bottomonium, Quark Gluon Plasma, Relativistic Heavy-Ion Collisions, Relativistic Heavy-Ion Collider, RHIC

Contents

1	Introduction	3
1.1	Motivation	4
1.2	Overview of results from the heavy flavor program at RHIC	6
1.3	Overview of the proposed heavy flavor program at RHIC II	9
1.4	Overview of the relationship of RHIC II to the LHC program	11
2	Detector upgrade program at RHIC	12
2.1	PHENIX upgrades	12
2.2	STAR upgrades	15
3	Projected RHIC yields	18
3.1	Projected PHENIX yields	19
3.2	Projected STAR yields	19
3.3	Yields at higher energies	22
4	Open heavy flavor	23
4.1	Open Heavy Flavor Theory	24
4.2	Models of Heavy Quark Energy Loss	28
4.3	RHIC open heavy flavor measurements to date	32
4.4	Proposed open heavy flavor experimental program at RHIC II	40
5	Hidden heavy flavor: quarkonium	44
5.1	Theoretical results	44
5.2	Status of Quarkonium Physics at the CERN SPS	60
5.3	Quarkonium measurements to date at RHIC	64
5.4	Proposed RHIC II quarkonia measurements	76
6	Relationship to the LHC program	83
7	Conclusions	86

Acknowledgements 87

References 87

1 Introduction

During the last 7 years, heavy-ion experiments at the Relativistic Heavy-Ion Collider (RHIC) have recorded a wealth of data in Au+Au, d+Au, Cu+Cu, and *pp* collisions at a variety of energies, ranging from $\sqrt{s_{NN}} = 19.6$ GeV to the highest available Au+Au energy, 200 GeV. It is at these high energies that QCD predictions of new phenomena come into play under conditions where, over nuclear volumes, the relevant degrees of freedom are expected to be those of quarks and gluons rather than of hadrons, the realm of the quark-gluon plasma.

Measurements from the four RHIC experiments, BRAHMS, PHENIX, PHOBOS and STAR, have revealed compelling evidence for the existence of a new form of nuclear matter at extremely high densities and temperatures [1–4]. Detailed analyses of these data also make it clear that this hot, dense medium has surprising properties.

The properties of the medium are those of a strongly coupled plasma, or sQGP, that behaves like a "perfect liquid" flowing with a near-zero viscosity to entropy ratio [5]. The RHIC observations have spurred significant advances in theory. However, a fundamental understanding of the medium seen in heavy-ion collisions at RHIC does not yet exist. It requires new data that, in turn, necessitate enhanced capabilities of the RHIC detectors and accelerator. A detailed plan is being developed by BNL to implement these upgrades in collaboration with the RHIC scientific community.

The main focus of this report is to outline the scientific opportunities in the heavy flavor sector provided by upgrades of the two large RHIC detectors [1], PHENIX and STAR, in conjunction with an upgrade of the accelerator/collider facility, referred to as RHIC II. The detector upgrades will improve the acceptance, particle identification and secondary vertex detection capabilities of PHENIX and STAR. The RHIC II accelerator luminosity upgrade was originally proposed to be done using electron cooling. It is now planned to use a scheme that employs stochastic cooling and other upgrades to achieve for Au+Au a factor of 5 increase in luminosity over present capabilities. This will provide about 70% of the average luminosity expected from electron cooling, but much sooner and at a much lower cost. The accelerator upgrades will

[1] The two smaller experiments BRAHMS and PHOBOS were decommissioned in 2006.

include a new ion injector, EBIS, which will provide high-intensity beams of nuclei as massive as uranium.

This report is the result of the collaboration and research efforts of a RHIC-wide Heavy Flavor Working Group. It provides a comprehensive overview of the physics questions than can be addressed by studies of open charm, open bottom and quarkonia at RHIC II. It also includes a detailed assessment of the accelerator and detector capabilities required to carry out these measurements with sufficient precision to resolve many of the outstanding issues by providing detailed results with which to make thorough comparisons to current and future theoretical calculations.

This report is organized as follows. After a general introduction to heavy flavor physics, section 2 discusses the detector upgrade program at RHIC. The projected yields of various heavy flavor measurements that can be achieved utilizing these upgrades and the higher RHIC II luminosities are discussed in section 3. In sections 4 and 5 we present a more detailed discussion of the motivation for studying open heavy flavor and quarkonia in heavy-ion collisions, respectively. We also include a review of the current theoretical and experimental status as well as the proposed experimental program. In section 6 we review the relationship between heavy flavor physics at RHIC II and the LHC. We conclude in section 7.

1.1 Motivation

Because charm and bottom quarks are massive, they are produced almost exclusively in the initial parton-parton interactions in heavy-ion collisions at RHIC energies. In the absence of any nuclear effects, the heavy flavor cross sections in $A + A$ collisions at RHIC would simply scale with the number of binary collisions. Thus departures from binary scaling for heavy flavor production in $A + A$ collisions provide information about nuclear effects. These can be divided into two categories: effects due to embedding the colliding partons in a nucleus (cold matter effects) and effects due to the large energy density in the final state. The main focus of the heavy flavor program at RHIC is to investigate the properties of the dense matter produced in $A + A$ collisions by studying its effects on open heavy flavor and quarkonium production. This in turn requires a detailed understanding of cold matter effects so that they can be unfolded from the dense matter effects.

The program thus requires detailed measurements and calculations of pp and $p + A$ heavy flavor cross sections to characterize the cold matter effects, if we are to quantify the differences between QGP and non-QGP effects. Up-to-date benchmark calculations of the total open heavy flavor (charm and bottom

hadrons) and quarkonium (J/ψ and Υ families) yields and spectra are imperative. Cold matter effects that need to be included are nuclear shadowing, for both open heavy flavor and quarkonium production, and nuclear absorption of quarkonium. Recent calculations of charm and bottom production to Fixed-Order Next-to-Leading Logarithm (FONLL) in pp collisions have been published [6], along with a discussion of the inherent theoretical uncertainties [7] and reference calculations of heavy quark, heavy flavor meson and their decay lepton spectra [6]. Similar calculations have been made for quarkonium production, including studies of shadowing and absorption effects as a function of rapidity and centrality in d+Au [8] and $A + A$ [9] collisions at RHIC.

A number of dense matter effects on heavy flavor production have been predicted. Some of these do not change the total cross section but, instead, modify the p_T spectra of heavy flavor hadrons and their decay products. Heavy quark energy loss [10–14] by collisional and radiative processes steepens the p_T distribution relative to that in pp collisions. On the other hand, random p_T kicks result in transverse momentum broadening, increasing the average p_T in both cold nuclear matter [15] and in passage through hadron bubbles in the mixed phase of a QGP [16]. If the medium surrounding the heavy quarks after production exhibits collective motion, such as transverse flow [17, 18], the low p_T heavy quarks ($p_T < m$) may be caught in this flow. Strong effects of energy loss [19, 20] on heavy flavor decays to electrons and charm flow [20] have already been seen in Au+Au collisions at RHIC. Studying heavy flavor energy loss using single electrons requires being able to separate electrons from c and b decays since the large bottom and charm quark mass difference suggests that bottom quark energy loss is weaker than that for charm [10]. Some QGP studies require accurate baseline determinations of the total heavy flavor cross sections to interpret other effects. For example, if more than one $c\overline{c}$ pair is produced in an $A + A$ event, uncorrelated c and $\overline{c}$ quarks might coalesce to form a J/ψ in a QGP [22–25]. The total $c\overline{c}$ yield is needed to normalize the J/ψ production rate from this process.

Suppression of J/ψ production was one of the most exciting proposed QGP signatures at the CERN SPS [26]. This J/ψ suppression was predicted to occur due to the shielding of the $c\overline{c}$ binding potential by color screening, leading to the breakup of the quarkonium states, first the χ_c and ψ', and finally the J/ψ itself as the temperature increases [27, 28]. The QGP suppression may not be so simple, as lattice gauge theory studies of the J/ψ spectral function above the critical temperature for deconfinement, T_c, attest. The J/ψ may exist as a bound state for temperatures considerably larger than T_c [29]. However, the J/ψ may instead be dissociated by hot thermal gluons in medium [30] before it could be suppressed by color screening. Secondary quarkonium production from uncorrelated $Q\overline{Q}$ pairs, either in the plasma phase [23, 25, 31–33] or in the hadron phase [34, 35], could counter the effects of suppression, ultimately leading to enhanced quarkonium production. Such secondary J/ψ's

would have different kinematic distributions than those from the initial production. Because the underlying $c\bar{c}$ distribution falls rapidly with p_T, the p_T distribution produced by coalescence will be softer. If the underlying $c\bar{c}$ distribution peaks at midrapidity, the J/ψ rapidity distribution from coalescence will be narrower than that produced in the primordial collisions. The coalescence rapidity distribution should be calculated with shadowing effects on the underlying $c\bar{c}$ distribution taken into account since these can cause the $c\bar{c}$ distribution to flatten in more central $A+A$ collisions [9]. Elliptic flow is also expected to affect quarkonium as well as open heavy flavors [17, 18].

With higher luminosity at RHIC, the Υ yields could also be measured accurately. Since the Υ radius is smaller than that of the J/ψ [28], direct color screening in the QGP would not occur until much higher temperatures. The higher mass bottomonium states, however, would likely be suppressed at RHIC, as would the χ_c and ψ' in the charmonium family. The feed down structure is more complicated for the Υ since there are three S states (Υ, Υ' and Υ'') and two sets of P states (χ_{b1} and χ_{b2}) below the $B\overline{B}$ threshold. The Υ family suppression should be measurable over a large p_T range, with QGP suppression possible on the Υ' and Υ'' up to $p_T \sim 40$ GeV/c at the LHC [36]. Because of the small number of $b\bar{b}$ pairs produced at RHIC, bottomonium formation by coalescence of unrelated pairs should be negligible.

1.2 Overview of results from the heavy flavor program at RHIC

Heavy flavor measurements capable of discriminating between theoretical models need large integrated luminosity. In RHIC runs so far, useful data sets have been acquired at 200 GeV for *pp*, d+Au, Cu+Cu and Au+Au collisions. The Run 6 *pp* data are not fully analyzed yet, but a sizable data set is available from Run 5. Recent runs for two species greatly increase the statistical reach over earlier runs: Au+Au (Run 7) and d+Au (Run 8). The data are still being analyzed, but some preliminary results are available from Run 7.

The *pp* data collected to date provide an essential reference for the heavy-ion program in the form of the underlying heavy flavor production rates as functions of rapidity and p_T. Equally essential, the data from d+Au collisions provide baseline information about cold nuclear matter effects which must also contribute to heavy flavor production in heavy-ion collisions. The analyzed d+Au data from Run 3 have limited statistical precision, but they provide useful tests of models that include the effects of shadowing on heavy flavor production and of J/ψ absorption in cold nuclear matter [8].

The easiest way by far to measure open heavy flavor yields in heavy-ion collisions at RHIC is via the semileptonic decays of D and B mesons. Two

very striking and unexpected results have already been seen by studying decay electrons from open heavy flavor in heavy-ion collisions at RHIC. The first is the observation that the nuclear modification factor, $R_{AA}(y, p_T) = (d\sigma_{AA}/dp_T dy)/(\langle T_{AB}\rangle d\sigma_{pp}/dp_T dy)$, for electrons from open heavy flavor decays shows very strong suppression in central Au+Au collisions [19, 20], similar to that seen for pions. The second striking result is that the elliptic flow parameter, v_2, of electrons from open heavy flavor decays appears to favor charm quark flow at low p_T [20]. Until recently, it had been expected that heavy quark energy loss would be considerably smaller than that for light quarks due to interference effects [10]. Generating the necessary energy loss for charm and bottom quarks with realistic gluon densities in the material is a major challenge for models [10, 37]. The relatively large v_2 values at low p_T imply at least some degree of charm quark equilibration with the medium. This also implies very strong interactions of charm quarks with the medium at lower p_T [17, 18].

A serious shortcoming of open heavy flavor measurements employing semileptonic decays is the difficulty of separating the contributions to the lepton spectra from charm and bottom decays. Perturbative calculations of the relative contributions from charm and bottom as a function of p_T have large theoretical uncertainties: at midrapidity the crossover point at which bottom decays become dominant is between 3 and 9 GeV/c. Recently, however, the ratio of charm to bottom contributions has been extracted by STAR and PHENIX from pp data, although with still large uncertainties. The STAR measurements [38] cover an electron p_T of $3-9$ GeV/c and are based on small azimuthal angle correlations between the decay electrons and hadrons as well as correlation between electrons and identified D^0 mesons. The PHENIX bottom/charm ratio as a function of electron p_T [39] was inferred from the shape of the electron-hadron correlation function. The STAR and PHENIX ratios are in good agreement and indicate that bottom becomes the dominant contribution to the electron spectra at $p_T \sim 3.5$ GeV/c (see Fig. 6). A separate PHENIX measurement of the bottom and charm cross sections was also obtained from fits to the dielectron invariant mass spectrum, after removal of all other contributions [40]. The results are in agreement with the cross sections inferred by PHENIX by combining the correlation measurements with electron p_T distributions.

PHENIX has also measured open heavy flavor yields at forward rapidity, $y = 1.65$, using single muons [41]. The charm cross section is $d\sigma/dy = 0.145 \pm 1.1\%^{+42.7\%}_{-49.8\%}$ μb. This is consistent with the measured values at $y = 0$ but the precision is currently insufficient to meaningfully define the rapidity dependence. It is likely that the displaced vertex measurement from the planned vertex detector upgrades will be needed to determine the rapidity distribution.

The first high statistics charmonium results for heavy-ion collisions at RHIC are now available [42, 43], along with high statistics pp reference data [44]. These include Au+Au and Cu+Cu results for the J/ψ R_{AA} as a function of the number of participant nucleons, $N_{\rm part}$, in the rapidity intervals $|y| < 0.35$ and $1.2 < |y| < 2.2$. A striking feature of the Au+Au J/ψ data is that, for $N_{\rm part} > 150$, the suppression is considerably stronger at forward rapidity than at midrapidity. Comparison with existing models at midrapidity shows that cold nuclear matter baseline calculations [9] which approximately reproduce the RHIC d+Au J/ψ rapidity distributions [8] somewhat underpredict the suppression observed in Cu+Cu and Au+Au collisions. On the other hand, several suppression models [25, 45, 46] which were successful in describing J/ψ suppression at the SPS are found to strongly overpredict the suppression at RHIC. Models which incorporate strong suppression combined with J/ψ coalescence from uncorrelated $c\bar{c}$ pairs seem to agree best with the data although the existing models slightly underpredict the suppression. A major source of uncertainty in all of this is due to the poor precision of the existing d+Au data, leading to poor constraints on the baseline cold nuclear matter effects.

A recent reanalysis of the Run 3 d+Au J/ψ data [47] used the higher yield Run 5 pp data as the reference for calculating R_{AA}. Theory calculations have been fit to the reanalyzed data to explore how well the data constrain cold nuclear matter effects in heavy-ion collisions. They find that the constraints from the Run 3 d+Au data are insufficient for firm conclusions to be drawn about additional hot matter effects in central heavy-ion collisions [43, 47]. The newly obtained Run 8 d+Au data set, approximately 20 times the yield of Run 3, will provide much improved statistical precision.

In the last few years, theorists have begun exploring the consequences of J/ψ coalescence on observables other than the centrality dependence of the nuclear modification factor [22, 48, 49]. This work has led to the prediction that J/ψ's formed by coalescence of uncorrelated $c\bar{c}$ pairs will have narrower rapidity and p_T distributions due to the presumed shape of the underlying charm quark distributions. The coalescence contribution to J/ψ production will cause many observables to change with centrality, including the rapidity and p_T dependence of R_{AA}, the shape of the p_T distribution (quantified by the average p_T^2, $\langle p_T^2 \rangle$), and the J/ψ elliptic flow parameter, v_2. Predictions of $\langle p_T^2 \rangle$ as a function of centrality have been made for Au+Au and Cu+Cu collisions with and without coalescence [22, 48, 49]. These predictions, compared to the Au+Au and preliminary Cu+Cu data, favor calculations including coalescence. The coalescence contributions predicted for central Au+Au (as well as central Cu+Cu) collisions [22] are also qualitatively expected to narrow the J/ψ rapidity distributions if the underlying charm distributions are peaked at midrapidity. The Au+Au data [42] show some narrowing of the rapidity distribution for the most central collisions although the reduction in RMS is only about 2σ. Work is still needed to quantify both the theoretical predictions and the ex-

perimental observables. A first measurement of the J/ψ v_2 may come out of the Run 7 Au+Au data, albeit with large uncertainties.

The existing, but not yet analyzed Au+Au data from Run 7 will quantitatively improve the measurements of many heavy flavor observables. The J/ψ R_{AA} versus centrality and $\langle p_T^2 \rangle$ as well as R_{AA} and v_2 measurements of charm and bottom semileptonic decays to single electrons will all improve significantly, allowing more stringent model tests. Measurements of other observables will be qualitatively improved. Examples are: definitive v_2 measurements from semileptonic decays at intermediate to high p_T where we might hope to see the transition from charm to bottom dominance and flow to non-flow; a possible first J/ψ v_2 measurement; substantially improved measurements of J/ψ $R_{AA}(y)$ to quantify the coalescence contribution; and improved measurements of J/ψ $R_{AA}(p_T)$, invaluable for understanding coalescence and formation time effects.

However it is clear that the RHIC heavy flavor program is now limited by the capabilities of the accelerator and the detectors. The accelerator upgrades planned over the period 2009-2013 to produce a factor of 5 greater luminosity at RHIC II, combined with the detector upgrades in place by that time, will be required for the heavy flavor program at RHIC to move to the next level, as described below.

1.3 Overview of the proposed heavy flavor program at RHIC II

The increase in luminosity, combined with the increased capabilities of the upgraded PHENIX and STAR detectors, will make it possible to add many important new probes to the heavy flavor program at RHIC.

One of the most powerful benefits of the luminosity upgrade will be the ability to measure yields of the excited charmonium states: the ψ' and χ_c. Lattice calculations predict much smaller melting temperatures for the ψ' and χ_c than for the more tightly bound J/ψ. Thus these excited states should not be able to exist in the QGP at RHIC and comparison of the ψ' and χ_c yields to the J/ψ yield as a function of centrality would be a direct test of deconfinement.

Testing models in which the observed J/ψ yield in heavy-ion collisions is due to competition between gluon dissociation and coalescence formation in the QGP requires very high luminosity. Tests of charm coalescence models include measuring J/ψ v_2 as a function of p_T, J/ψ R_{AA} to much higher p_T to follow the trends of suppression as the J/ψ formation time approaches the QGP crossing time, and J/ψ polarization as a function of collision centrality. The rapidity and p_T dependence of R_{AA} as functions of $\sqrt{s_{NN}}$ and centrality, requiring sufficient luminosity for precision measurements at multiple energies, is not

possible on a reasonable time scale at the present RHIC luminosity.

The detailed study of bottomonium states, the Υ family, is only possible at RHIC II luminosities. Like the charmonium states, the dissociation temperatures of the bottomonium states depend on the binding energies. There are, however, two important differences. First, the bottomonium binding energies, particularly that of the $\Upsilon(1S)$, are higher so that they should dissociate at higher temperatures. Only the higher-lying bottomonium states are thus likely to break up at RHIC energies. Second, the $b\bar{b}$ production rate in central Au+Au collisions is only $\sim$ 0.05 pairs per collision, making coalescence production of bottomonium much less likely. Thus bottomonium production at RHIC II will provide a very different window on color screening effects than charmonium production. The bottomonium yields at RHIC II should be sufficient for measurements of R_{AA} as a function of centrality in heavy-ion collisions for the three Υ S states. The Υ yields at RHIC II and at the LHC will not be sufficient for v_2 or polarization measurements.

As mentioned earlier, measurements of semileptonic open heavy flavor decays at RHIC have already produced strikingly different results than expected. The strong suppression in R_{AA} coupled with the large v_2 suggest very large heavy quark energy loss in the medium. The fact that these semileptonic decay spectra contain both charm and bottom contributions remains a significant complication, in spite of recent successes by STAR and PHENIX at measuring the ratio of b to c quark contributions in the semileptonic decay spectrum of pp collisions. The separation of open charm and bottom can be done in several ways. Charm can be observed via hadronic $D^0 \rightarrow K^{\pm}\pi^{\mp}$ and $D^{\pm} \rightarrow K^{\pm}\pi^{\pm}\pi^{\mp}$ decays, as STAR does. Precise R_{AA} and v_2 measurements are difficult in this channel. Since these events cannot be triggered, they must be extracted from a minimum bias data set that samples only a small fraction of the available luminosity. The combinatorial background is also very large, making statistical precision difficult. The addition of a displaced vertex measurement in STAR will dramatically reduce the combinatorial background but there is still no trigger for these decays. At RHIC II luminosity, bottom can be observed very cleanly in both PHENIX and STAR via $B \rightarrow J/\psi X$ decays using displaced vertices, providing good measurements of the $b\bar{b}$ cross section and bottom quark R_{AA}. However those yields will certainly be too small for v_2 measurements at RHIC II or the LHC. Finally, the combination of RHIC II luminosity with a displaced vertex measurement should allow statistical separation of the charm and bottom contributions to the semileptonic decay spectra, taking advantage of the different c and b quark decay lengths. Such semileptonic decay measurements, while less clean than the direct D and B decay measurements, have the advantage of much larger yields so that separate charm and bottom v_2 measurements should be possible.

Independent measurements of open charm and bottom R_{AA} and v_2 to high p_T

will be a very important capability at RHIC II. At low p_T, these measurements reflect the degree of heavy quark thermalization in the medium. At high p_T, they probe the energy loss of heavy quarks in the medium, providing an independent measurement of the initial energy density relative to the light quark energy loss measurements. The thermalization and energy loss mechanisms at low and high p_T respectively may be quite different due to possible resonance scattering at low p_T.

1.4 Overview of the relationship of RHIC II to the LHC program

The heavy flavor production cross sections are significantly higher at the LHC than at RHIC since the per nucleon Pb+Pb energy at the LHC is a factor of 27.5 higher than the maximum per nucleon Au+Au energy at RHIC. The $c\overline{c}$ and $b\overline{b}$ cross sections increase by factors of 15 and 100 respectively [15] while the J/ψ and Υ cross sections increase by factors of 13 and 55 respectively [50]. But, because of the 10 times higher average luminosity and three times longer heavy-ion runs, the Au+Au integrated luminosity at RHIC II will be much higher than for Pb+Pb at LHC. Therefore the heavy flavor yields per year are expected to be similar at the two facilities.

At $\sqrt{s} = 200$ GeV, bottom decays to leptons begin to dominate the single electron spectrum at $p_T \sim 4$ GeV/c. As the collision energy increases, the lepton spectra from B and D decays move closer together rather than further apart [15]. Thus, the large increase in the $b\overline{b}$ cross section relative to $c\overline{c}$ does not make single leptons from B and D decays easier to separate. Preliminary calculations show that the $B \rightarrow e$ decay does become larger than that of $D \rightarrow e$, but at $p_T > 10$ GeV/c. The yields from the two lepton sources differ by less than a factor of two up to $p_T \sim 50$ GeV/c in the range $|y| \leq 1$. Thus interpretation of single lepton results on heavy flavors will be more difficult at the LHC. Other means of separating charm and bottom must be found. ALICE can reconstruct hadronic D^0 decays from $p_T \sim 0$ to $p_T \sim 25$ GeV/c [51] but, like STAR, will have to rely on minimum bias data for these measurements because of the lack of a trigger. While it is not yet clear what CMS and ATLAS will do to reconstruct charm, they should be able to make b-jet measurements, similar to the Tevatron. One way that B mesons can be measured at the LHC is through their decays to J/ψ, as discussed further below. It has also been suggested that the $B\overline{B}$ contribution to the dimuon continuum, the dominant contribution above the Υ mass, can be used to measure energy loss [52]. That channel would be fairly clean at the LHC but more difficult at RHIC.

The RHIC II upgrades and the high LHC energies make detailed studies of Υ production and suppression possible. At the LHC, higher initial temperatures make Υ suppression more likely than at RHIC II. But the higher $b\bar{b}$ production

rate (~ 5 per central Pb+Pb collision) means that, unlike RHIC, significant coalescence contributions to Υ production may be expected at the LHC. Thus measurements at the two energies complement each other. At RHIC II, it is likely that PHENIX will be able to measure and resolve the three Υ S states. STAR and ALICE will have similar Υ yields but the STAR mass resolution will require fitting to extract yields. The CMS detector at the LHC has sufficient mass resolution to separate all three Υ S states. The Υ states can be measured to $p_T \sim 0$ at all LHC detectors. Only ALICE will be able to measure J/ψ production to $p_T \sim 0$ without a special trigger [50] since CMS and ATLAS require high single muon p_T so that typically only J/ψ with $p_T >$ several GeV/c are accepted. (However, CMS is working on a higher-level trigger to measure lower p_T J/ψ [53].) The larger $b\overline{b}$ cross section at the LHC means that J/ψ production from $B \to J/\psi X$ cannot be neglected. These decay J/ψ should be separable from the initial production using displaced vertices [50].

2 Detector upgrade program at RHIC

Both PHENIX and STAR have extensive upgrade programs underway that are extremely important for the heavy flavor program. The upgrades that are most relevant to heavy flavor measurements are described here. The impact on the heavy flavor program of these detector upgrades, in combination with the RHIC II luminosity increase, will be discussed in sections 4 and 5.

2.1 PHENIX upgrades

Several PHENIX detector upgrades that greatly enhance the heavy flavor capability of the experiment are expected to be available in the RHIC II time frame. The most important upgrades for the heavy flavor program will be the barrel [54] and endcap [55] Silicon Vertex Detectors, the Nose Cone Calorimeter [56] and the Muon Trigger Upgrade [57]. The central region of the PHENIX detector, after installation of the silicon trackers and the Nose Cone Calorimeter, is shown in Fig. 1. The pseudorapidity and azimuthal angle coverages of the new detectors are illustrated in Fig. 2.

The Silicon Vertex Detector (SVTX) consists of a central barrel [54] and two endcap detectors [55], as shown in Fig. 1. The SVTX barrel will have a displaced vertex resolution of ~ 50 μm while the endcap resolution is $\sim 90-115$ μm. Together, this inner tracking system provides full azimuthal coverage over $|\eta| < 2.4$. The SVTX will tag heavy flavor decays using displaced vertices by connecting to tracks in both the central and muon arms, improving

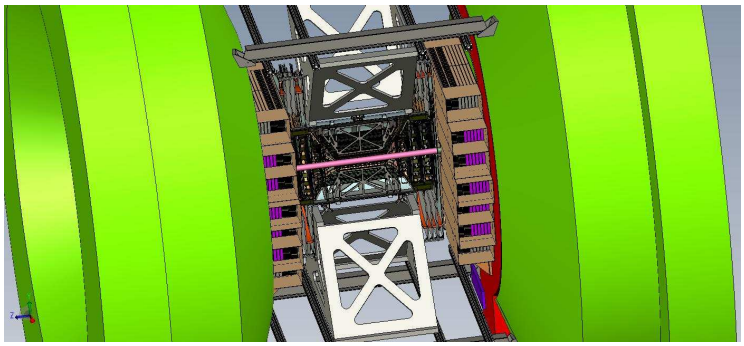

Fig. 1. The central region of the PHENIX detector after the addition of the barrel and endcap silicon vertex detectors and the Nose Cone Calorimeter.

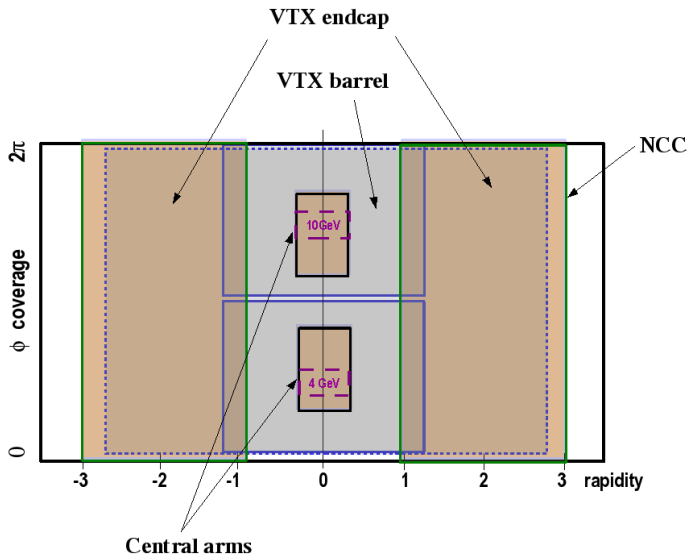

Fig. 2. The pseudorapidity and azimuthal angle coverage of the PHENIX barrel and endcap silicon vertex detectors and the Nose Cone Calorimeter (NCC) [56]. Two areas of the central arms that that provide hadron identification to high $p_T$are also shown.

the quarkonium invariant mass resolution and reducing backgrounds to heavy flavor measurements. In the muon arms, a loose displaced vertex cut will eliminate most muon tracks from light hadron decays and a very tight cut, $\sim 2\sigma$ where σ is the resolution of the displaced vertex measurement, will eliminate most punch-through hadrons. The displaced vertex measurement will greatly enhance $D^0 \rightarrow K^{\pm}\pi^{\mp}$ measurements in the central arms, presently very difficult in PHENIX, by reducing the contribution to the combinatorial background both from prompt tracks (by using a tight vertex cut) and light meson decay tracks (by using a loose cut of ~ 1 cm). A loose displaced vertex cut will also reduce high p_T background tracks in the central arms due to misidentified light hadron decays. In addition to identifying semileptonic heavy flavor decays, displaced vertex measurements can help identify J/ψ's

from B meson decays since all other J/ψ's are prompt.

The SVTX barrel is presently under construction. It will consist of four concentric silicon layers. The two inner layers, at radii of 2.5 and 5.0 cm, consist of pixel detectors with a segmentation of 50 μm by 425 μm. The outer two layers, with radii of 10 and 14 cm, consist of 80 μm by 3 cm strips. The occupancy of the inner layer will be about 4.5% in central Au+Au collisions. The SVTX barrel produces a dramatic improvement in high p_T track resolution in the central arms. The PHENIX Drift Chamber is outside the magnetic field so that, in the present momentum measurement, there is no information about the initial azimuthal angle, ϕ, of the track. The momentum is calculated from the difference between the ϕ angle of the track after passing through the magnetic field and that from the vertex position to the Drift Chamber. This difference is only $\sim$ 40% of the total deflection. By adding a precise measurement of the initial ϕ direction, the SVTX barrel measures the full deflection directly, decreasing the momentum resolution by a factor of ~ 2.5, greatly improving the Υ invariant mass resolution. Installation of the barrel is expected starting in 2009.

The forward silicon detector endcaps will consist of four silicon mini-strip planes. The mini-strips have 75 μm pitch in the radial direction and lengths in the ϕ direction varying from 2.8 mm to 12.1 mm, depending on the polar angle. The maximum occupancy per strip is estimated to be less than 2.8% in central Au+Au collisions. The displaced vertex resolution of $90 - 115$ μm, depending on the number of layers of silicon traversed by the track, should be compared to a mean vertex displacement of 785 μm for the boosted open charm muons. A prototype covering about 1/8 of one muon arm is presently under construction.

The PHENIX Nose Cone Calorimeters (NCCs) [56], tungsten-silicon calorimeters, will replace the two central arm magnet nose cones, and will cover $0.9 < |\eta| < 3.5$. The simulated energy resolution for photons is $\sim 27\%/\sqrt{E}$ GeV. The Nose Cone Calorimeters will contain both electromagnetic and hadronic calorimeter sections. The electromagnetic calorimeter will contain a pre-shower detector and a shower-max detector designed to discriminate between individual electromagnetic showers and overlapping photons from high momentum π^0 decays. The pre-shower and shower-max detectors are expected to resolve showers with separations down to 2 and 4 mm, respectively. The NCCs should thus have good acceptance for $\chi_c \to J/\psi + \gamma$ decays with the J/ψ detected in the muon arms.

The muon trigger upgrade [57] is required for PHENIX to be able to take complete advantage of the RHIC II luminosity upgrade for muon arm measurements. The current muon arm level-1 heavy vector meson triggers have sufficient rejection capability to handle Au+Au collision rates of up to $\sim$ 20

kHz and pp collision rates of up to $\sim$ 0.5 MHz. The muon trigger upgrade adds three layers of Resistive Plate Chamber (RPC) detectors, with two dimensional (θ, ϕ) readout, in each muon arm. These layers follow the design of the CMS muon trigger at the LHC but the cathode pad segmentation is optimized for PHENIX. The front end electronics and trigger processors will be developed within PHENIX. The muon trigger upgrade, with an online momentum measurement, will improve the level-1 trigger rejection for both single muons (with a p_T cut) and muon pairs (with an invariant mass cut). It will also improve the high multiplicity background rejection during the final analysis. The muon trigger upgrade is presently under construction.

2.2 STAR upgrades

To realize the compelling scientific opportunities in heavy flavor physics, upgrades to the STAR detector are required to complete many of the challenging measurements. The collaboration has planned a series of upgrades for the near and intermediate term to overcome the current shortcomings and enhance its heavy flavor capabilities. Implementation of these upgrades will also allow optimum utilization of the increased luminosity expected from RHIC II.

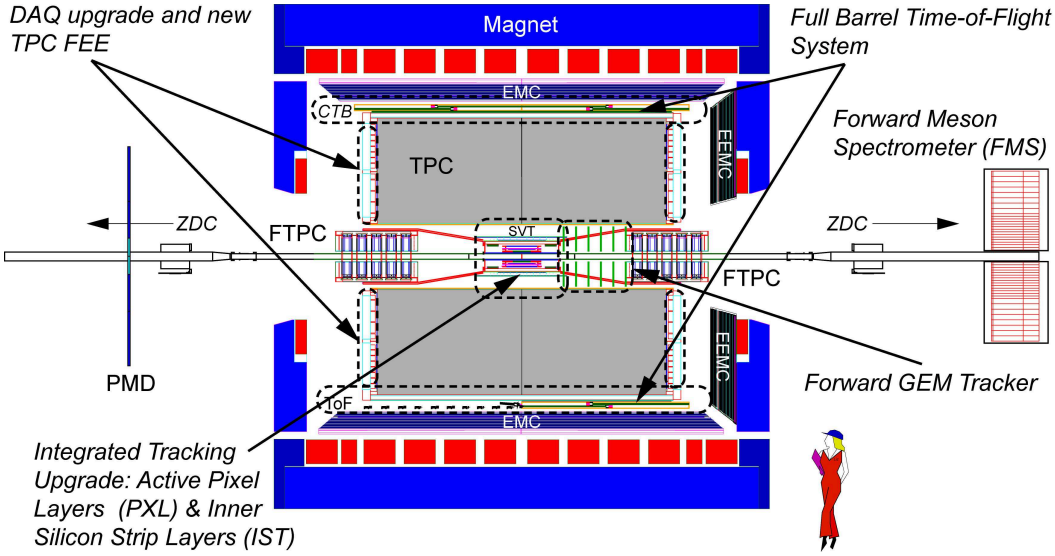

Fig. 3. Layout of the STAR experiment in 2005/2006 (modified from Ref. [58], reprinted with permission from Elsevier). The locations of the planned upgrades are indicated by as dashed lines. See text for details.

The current layout of the STAR detector is depicted in Fig. 3. The medium term upgrades to the detector relevant for heavy flavor physics include: a full barrel Time-of-Flight detector (ToF) replacing the current ToF patch and the Central Trigger Barrel (CTB); new front end electronics for the large Time Projection Chamber (TPC); an upgrade to the data acquisition system (DAQ-

1000), and a tracking upgrade including a barrel section with two inner layers of silicon pixel sensors (PXL) and one layer of silicon strip-pad sensors (IST), replacing the current Silicon Vertex Tracker (SVT).

The new ToF system covering the full outer barrel of the TPC is being constructed and installed in STAR over the next two years. The system uses the multi-gap resistive plate chamber (MRPC) technology developed at CERN and will consist of 3840 MRPC modules with 23,000 channels of readout [59]. The modules will cover the TPC outer barrel ($|\eta| < 1$, $0 < \phi < 2\pi$) and will be mounted in 120 trays which will replace the existing CTB scintillation counter trays and ToF patch.

The ToF triples the current momentum range over which π, K, and p can be identified, considerably improving charm meson and baryon reconstruction. When the ToF measurement is combined with the TPC dE/dx measurement, electrons can be cleanly identified from the lowest momentum measured, $\sim$ 200 MeV/c, up to a few GeV/c. This capability complements the electromagnetic calorimeter which works well for momenta above $\sim$ 2 GeV/c. STAR will then be able to reconstruct soft to medium momentum electrons with high efficiency and purity to make a comprehensive J/ψ measurement. The ToF, in conjunction with the electromagnetic calorimeter (EMC), also allows STAR to implement a high-level trigger scheme to select $J/\psi \rightarrow e^+e^-$decays in pp collisions.

A series of improvements to the STAR data acquisition system over the past several years has brought the recorded event rate capability from the original design of 1 Hz to $50-100$ Hz. To acquire the very large data samples and high data rates needed for heavy flavor measurements, a further upgrade has been initiated to achieve a minimum 1 kHz recorded event rate which could produce data volumes that significantly exceed the capacity for analysis and storage. The rare-trigger data sets will especially benefit from the upgrade since the pipelined architecture being implemented will virtually eliminate the front end dead time, allowing STAR to make full use of rare-event triggers such as that designed for the Υ.

An increase in readout speed will be achieved by replacing the TPC front end electronics (FEE), making use of circuits developed for the ALICE experiment at CERN, in conjunction with an upgrade of the STAR DAQ. In addition to the increased physics capabilities from the DAQ upgrade, the replacement of the TPC FEE, specifically the readout boards (RDO) that collect data from the FEE boards, will make space for a future precision tracking chamber between the TPC end planes and the endcap calorimeter. Replacing the TPC FEE also assures that this system can be maintained for the next decade or more. The readouts of the other existing detectors, which will remain in place for the RHIC II era, are being adapted to the new high speed DAQ with only

minor changes.

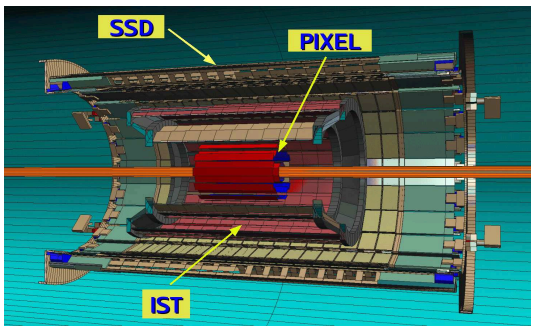

Fig. 4. The proposed geometry for the STAR inner tracking upgrade, the Heavy Flavor Tracker. From the inner to the outer radii, the 2 cm beam pipe, the two PXL layers, the exoskeleton to strengthen the beam pipe, the one IST layers and the existing SSD layer are shown [60].

In order to address heavy quark energy loss and thermalization, it will be necessary to cleanly identify open charm. The recent results from both STAR and PHENIX on the suppression and flow of non-photonic electrons are intriguing. However, without an identified charm sample, the contributions from semileptonic bottom decays and systematic errors on background subtraction make a clear interpretation of these results difficult. Measurement of the yields of various charm species will also allow the study of charm hadrochemistry.

Efficient topological reconstruction of open charm decays requires a tracking "point-back" resolution to the primary collision vertex of $\sim$ 50 μm or less. Further, the beam pipe and innermost detector layers must be very thin to measure the low p_T particles, which comprise the bulk of the cross section, and thus minimize the systematic errors in extrapolating the measured yield to the total yield. A thin beam pipe and inner detector layers are also key elements in efficiently vetoing photon-conversion electrons which, along with electron identification from the TPC, ToF and electromagnetic calorimeter, will measure the soft lepton and dilepton spectra. STAR is thus developing a tracking upgrade for the central rapidity region, the Heavy Flavor Tracker (HFT). The essential elements under consideration for the HFT are a new thin, small-radius beam pipe (0.5 mm thick, 20 mm radius), two layers of thinned (50 μm) CMOS pixel detectors at average radii of 2.5 and 8 cm (PXL) and one layer of low mass silicon strip-pad sensors (IST) at 17 cm, see Fig. 4. The existing layer of double-sided silicon strip sensors at a radius of 23 cm (SSD) will be kept but upgraded to be compliant with the overall higher readout speed (DAQ-1000). The two new IST layers will connect tracks from the TPC and SSD to hits in the pixel layers. These layers will replace the existing three layers of silicon drift detector (SVT). It will be necessary to replace the SVT since, when RHIC II becomes operational, the SVT will be over 10 years old with a readout too slow to be compatible with the upgraded DAQ. Its infrastructure (cables and cooling) also adds undesirable mass in the region

$1 < |\eta| < 2$.

3 Projected RHIC yields

In this section we present some estimates of the quality of the heavy flavor measurements that can be achieved at RHIC with increased luminosities and the upgraded detectors, reflected in the heavy flavor yields.

Species	Energy	Units	Up to 2008 Obtained	2009 Projected	2011 Projected	2013 Projected
Au+Au	200	μb^{-1}	380	610	1450	1820
pp	200	pb^{-1}	7.0	14.6	31.1	40
pp	500	pb^{-1}	–	36.5	78	100

Table 1
The anticipated weekly luminosity delivered by RHIC. When estimating rates, this delivered luminosity has to be reduced by a factor that accounts for detector up time and collision vertex cuts imposed by the detectors. The RHIC projected luminosities are maximum values taken from the RHIC Collider Accelerator Division projections for 2009-2013 as of February 23, 2008. They reflect the progressive implementation of stochastic cooling and other accelerator upgrades and improvements. The numbers in the "obtained" column are the best weekly luminosities observed through Run 8.

Table 1 is a summary of the weekly-integrated, delivered luminosity estimates for RHIC spanning the period when the luminosity upgrade is implemented. The year 2009 should be taken to mean RHIC Run 9. The weekly-luminosity expectations are based on RHIC Collider Accelerator Division guidance as of February 23, 2008. The root-mean square (RMS) of the collision diamond is assumed to be 20 cm beginning in 2009. We assume that 80% of the RHIC beam is in the central bucket (and thus usable by experiments) prior to 2012, when the addition of a 56 MHz RF cavity will bring this up to nearly 100%.

The PHENIX SVTX barrel is expected to be in place starting in 2010. The STAR HFT is expected to be in place starting in 2012. In both cases the usable collision vertex range will be limited to ± 10 cm by the acceptance of the silicon upgrade detectors. Because the RHIC diamond RMS length is ± 20 cm this will result in a reduction in effective luminosity for the experiments. This is taken into account when calculating yields.

The quarkonium cross sections are taken from Ref. [61] with an assumed ψ' to J/ψ ratio of 0.14. The charmonia cross sections are reduced by a factor of 0.43 in Au+Au interactions, approximately accounting for the suppression measured by PHENIX. No Υ suppression is assumed.

3.1 Projected PHENIX yields

Table 2 summarizes the projected PHENIX yields per year for critical heavy flavor signals for the period 2009-2013 for 12 week physics runs, and also includes the yields observed in RHIC runs to date. The estimated yields are based on a number of criteria. The detector acceptances are from PHENIX simulations. The minimum bias trigger efficiency for hard processes is assumed to be 0.75 for *pp* and 0.92 for Au+Au interactions. Where appropriate, an additional, realistic, level-1 trigger efficiency of 0.8 is used.

Realistic lepton pair reconstruction efficiencies of 0.8 in *pp* and 0.4 in Au+Au collisions are used. An additional efficiency factor of 0.4 is assumed for a 1 mm displaced vertex cut to identify $B \to J/\psi X$ decays. The PHENIX vertex detector is assumed to be in place after 2010, requiring a collision vertex cut of ± 10 cm.

3.2 Projected STAR yields

Table 3 shows a summary of the STAR projected yields per year for various critical heavy flavor signals for RHIC and RHIC II. The detector acceptances and efficiencies are from STAR simulations, or, where available, derived from existing measurements. The assumptions of luminosity, interaction vertices, cross sections and suppression effects are identical to those used for the PHENIX projections discussed above.

The upgrade of the inner tracking system is central to the future STAR heavy flavor program. It will provide sufficient tracking resolution to determine the heavy flavor meson decay vertices, providing the means to virtually unambiguously identify these probes. However, the complexity and volume of the data from this subsystem precludes the use of dedicated triggers that are based on the displaced vertex identification. Certain measurements, such as $D^0 \to K^{\pm}\pi^{\mp}$, can only be made by analyzing large quantities of minimum bias data. The substantial increase in readout speed from the DAQ upgrade (DAQ1000) can record events with a rate of up to 1 kHz, *i.e.*, 10 times the current rate. In the projections discussed here, we assume a more conservative rate of 500 Hz. In order to minimize tape costs, STAR plans to filter these events offline in computing farms either before or after transfer to the RHIC Computing Facility (RCF). The D^0 yields reflected in Table 3 are therefore limited not by luminosity but by *bandwidth*.

The same bandwidth limitation holds for the J/ψ trigger in A+A collision. The STAR J/ψ trigger deployed in *pp* events is based on the coincident signal above threshold of two calorimeter towers in conjunction with signals in the referring

Species	Signal	$\|\eta\|$	To Date	2009	2011	2013
pp	$J/\psi \to e^+e^-$	< 0.35	$\sim$ 1,500	30,000	29,000	46,000
	$J/\psi \to \mu^+\mu^-$	$1.2 - 2.4$	$\sim$ 8,000	256,000	249,000	393,000
	$\psi' \to e^+e^-$	< 0.35	–	540	530	830
	$\psi' \to \mu^+\mu^-$	$1.2 - 2.4$	–	4,600	4,500	7,100
	$\chi_c \to e^+e^-\gamma$	< 0.35	–	2,000	1,900	3,000
	$\chi_c \to \mu^+\mu^-\gamma$	$1.2 - 2.4$	–		37,000	116,000
	$\Upsilon \to e^+e^-$	< 0.35	–	115	110	180
	$\Upsilon \to \mu^+\mu^-$	$1.2 - 2.4$	$\sim$ 27	290	280	440
	$B \to J/\psi X \to e^+e^-$	< 0.35	–		155	240
	$B \to J/\psi X \to \mu^+\mu^-$	$1.2 - 2.4$	–		1,500	2,400
Au+Au	$J/\psi \to e^+e^-$	< 0.35	$\sim$ 800	13,500	14,600	22,400
	$J/\psi \to \mu^+\mu^-$	$1.2 - 2.4$	$\sim$ 7,000	119,000	129,000	198,000
	$\psi' \to e^+e^-$	< 0.35	–	240	260	400
	$\psi' \to \mu^+\mu^-$	$1.2 - 2.4$	–	2,150	2,300	3,600
	$\chi_c \to e^+e^-\gamma$	< 0.35	–	890	960	1,500
	$\chi_c \to \mu^+\mu^-\gamma$	$1.2 - 2.4$	–		19,000	59,000
	$\Upsilon \to e^+e^-$	< 0.35	–	120	130	200
	$\Upsilon \to \mu^+\mu^-$	$1.2 - 2.4$	–	310	340	520
	$B \to J/\psi X \to e^+e^-$	< 0.35	–		190	290
	$B \to J/\psi X \to \mu^+\mu^-$	$1.2 - 2.4$	–		1,900	2,900

Table 2
The projected yields of several heavy flavor signals in PHENIX for 12 week physics runs at RHIC. The yields are shown for both pp and Au+Au collisions at $\sqrt{s_{NN}}$= 200 GeV. The approximate yields obtained at RHIC to date are also shown. These reflect the fact that RHIC had not yet achieved the full luminosity development for Au+Au by Run 4, or for pp by Run 5. The Run 6 pp and Run 7 Au+Au data have not yet been fully analyzed. The projected RHIC values for 2011 and 2013 assume that the PHENIX SVTX detector is in place, limiting the usable collision vertex range to $\pm$10 cm. The collision diamond RMS will be $\pm$20 cm. The reduction in usable luminosity is compensated by improvements in signal to background ratio for most measurements. The $\chi_c \to \mu^+\mu^-\gamma$ measurement requires the NCC. It is assumed that one NCC arm is installed for 2011 and both are installed for 2013.

time-of-flight (ToF) segments to veto photon showers. The large multiplicity in $A + A$ events, however, renders this scheme impossible. The J/ψ $A + A$ yields are therefore bandwidth limited while those in pp depend directly on

Species	Signal	$\|\eta\|$	To Date	2009	2011	2013
pp	$J/\psi \to e^+e^-$	< 1.0	~ 400	490,000	1,100,000	750,000
	$\psi' \to e^+e^-$		–	10,400	24,000	16,000
	$\Upsilon \to e^+e^-$		~ 170	4,100	9,300	6,300
	$B \to J/\psi X \to e^+e^-$		–			370
Au+Au	$J/\psi \to e^+e^-$ (min. bias)	< 1.0	~ 350	25,000	25,000	25,000
	$J/\psi_{p_T>5.5\ \mathrm{GeV}/c} \to e^+e^-$		–	1,800	4,400	3,100
	$\psi' \to e^+e^-$ (min.bias)		–	550	550	550
	$\Upsilon \to e^+e^-$		–	5,800	13,800	9,700
	$B \to J/\psi X \to e^+e^-$		–			540
	$D^0 \to K^\pm\pi^\mp$ (min. bias)		400,000	9,000,000	9,000,000	9,000,000
			$(\frac{S}{B} \sim \frac{1}{600})$	$(\frac{S}{B} \sim \frac{1}{600})$	$(\frac{S}{B} \sim \frac{1}{600})$	$(\frac{S}{B} \sim \frac{1}{10})$

Table 3
The projected yields of several heavy flavor signals in STAR for a physics run of 12 weeks at RHIC at $\sqrt{s_{NN}}$= 200 GeV. The approximate yields obtained to date are also shown. The projected values assume that the STAR Heavy Flavor Tracker, the full ToF barrel, and the DAQ upgrades are in place for 2013. From that time on the inner tracking limits the usable collision vertex range to ±10 cm. The collision diamond RMS will be ±20 cm. Projections for signals marked (min. bias) are based on minimum bias events recorded with a rate of 500 Hz and a 33% combined experiment and machine duty cycle. Dedicated triggers cannot be efficiently deployed for these measurements. The corresponding signal-to-background ratios (S/B) are also given for the D^0 measurements.

the delivered luminosity. However, detailed studies from recent runs indicate that a slightly modified J/ψ trigger can be effectively deployed for J/ψ's with $p_T > 5 - 6\,\mathrm{GeV}/c$. Projections for this specific trigger are shown in Table 3.

The bottom measurement, $B \to J/\psi X \to e^+e^-$, is based on a high-$p_T$ J/ψ trigger, thereby avoiding the issues inherent to the low-p_T trigger. The projections shown in Table 3 are based on preliminary results from high-p_T J/ψ measurements in pp, folding in the expected efficiencies of the inner tracking system. The p_T-dependent ratio of J/ψ from B decays to directly produced J/ψ was derived from calculations described later. No bottom quark energy loss was assumed for the Au+Au yields.

The decay electrons from $\Upsilon \to e^+e^-$ are at considerably higher p_T than those of the J/ψ, making the calorimeter-based Υ trigger highly efficient ($\epsilon > 90\%$). The combination of an efficient trigger and large acceptance makes the study of the bottomonium in pp and $A+A$ the main point of the STAR quarkonium program and complements PHENIX's strong charmonium program.

Experiment	Signal	$\|\eta\|$	2009	2011	2013
PHENIX	$J/\psi \to e^+e^-$	< 0.35	166,000	161,000	254,000
	$J/\psi \to \mu^+\mu^-$	$1.2 - 2.4$	1,500,000	1,450,000	2,300,000
	$\psi' \to e^+e^-$	< 0.35	3,000	2,900	4,600
	$\psi' \to \mu^+\mu^-$	$1.2 - 2.4$	27,000	26,000	41,000
	$\chi_c \to e^+e^-\gamma$	< 0.35	28,000	27,000	43,000
	$\chi_c \to \mu^+\mu^-\gamma$	$1.2 - 2.4$		550,000	1,700,000
	$\Upsilon \to e^+e^-$	< 0.35	820	800	1,250
	$\Upsilon \to \mu^+\mu^-$	$1.2 - 2.4$	2,100	2,000	3,200
	$B \to J/\psi X \to e^+e^-$	< 0.35		2,000	3,200
	$B \to J/\psi X \to \mu^+\mu^-$	$1.2 - 2.4$		20,000	32,000
STAR	$J/\psi \to e^+e^-$	< 1.0	1,200,000	2,800,000	1,900,000
	$\psi' \to e^+e^-$		25,000	57,000	39,000
	$\Upsilon \to e^+e^-$		31,000	70,000	47,000
	$B \to J/\psi X \to e^+e^-$				4,100

Table 4
Projected heavy flavor yields in PHENIX and STAR for a 12 week $\sqrt{s} = 500$ GeV *pp* run at RHIC. The projected PHENIX yields for 2011 and 2013 assume that the PHENIX SVTX detector is in place, limiting the usable collision vertex range to ± 10 cm. The STAR HFT is assumed to be in place from 2012, and it also will limit the usable collision vertex range to ± 10 cm. The collision diamond RMS will be ± 20 cm. The $\chi_c \to \mu^+\mu^-\gamma$ measurement requires the NCC. It is assumed that one NCC arm is installed for 2011 and both are installed for 2013.

3.3 Yields at higher energies

Table 4 summarizes the expected PHENIX and STAR heavy flavor yields per year in *pp* collisions at $\sqrt{s} = 500$ GeV. Although not directly comparable with heavy-ion yields from collisions at $\sqrt{s_{NN}} = 200$ GeV, the order of magnitude larger heavy flavor yields at 500 GeV should help in the understanding of the reaction mechanism in *pp* collisions.

Table 5 contains a summary of the projected yields per year from the LHC detector collaborations for various critical heavy flavor signals in 10^6 s of data taking at $\sqrt{s_{NN}} = 5.5$ TeV Pb+Pb run, the standard planning number for a one year run [62–64]. The ALICE muon spectrometer covers only one side of forward rapidity.

Comparison of Tables 2, 3 and 5 reveal that the projected heavy flavor yields

Signal	ALICE	$\|\eta\|$	CMS	$\|\eta\|$	ATLAS	$\|\eta\|$
$J/\psi \to \mu^+\mu^-$	677,000	$2.5-4$	184,000	< 2.4	$8,000-100,000$	< 2.5
$J/\psi \to e^+e^-$	121,100	< 0.9				
$\psi' \to \mu^+\mu^-$	18,900	$2.5-4$			$1,400-1,800$	< 2.5
$\psi' \to e^+e^-$						
$\Upsilon \to \mu^+\mu^-$	9,600	$2.5-4$	37,700	< 2.4	15,000 (21,200)	< 2.0 (< 2.5)
$\Upsilon \to e^+e^-$	1,800	< 0.9				
$D^0 \to K^\pm\pi^\mp$	13,000	< 0.9				

Table 5
The estimated LHC heavy flavor yields for a 10^6 s Pb+Pb run at $\sqrt{s_{NN}} = 5.5$ TeV with 500 μb^{-1} integrated luminosity (one year), reported by the LHC experiments. As for the RHIC tables, the Υ rates include all three states. The ALICE yields [62] assume binary collision scaling and include shadowing. The ALICE dielectron yield estimates are for the 10% most central events while the D^0 yields are for 10^7 central event triggers. The CMS yields [63] assume $dN_{\rm ch}/d\eta = 2500$ and include shadowing with no quarkonia suppression. For ATLAS [64] the range of the J/ψ yield corresponds to different assumed muon p_T trigger thresholds. Good separation of Υ and Υ' states is expected in ATLAS for $|\eta| < 2.0$.

for one year of running are similar at the LHC and at RHIC II. The much larger heavy flavor cross sections at the higher LHC energy are largely compensated at RHIC II by integrated luminosities that result from three times longer runs and a factor of 10 higher luminosity.

4 Open heavy flavor

In this section we present a more detailed discussion of the theoretical motivation for studying open heavy flavor in heavy-ion collisions, of the present experimental and theoretical status, and of the proposed experimental program of open heavy flavor measurements at RHIC II.

As described in the introduction, dense matter effects in nuclear collisions may change the kinematic distributions and the total cross sections of open heavy flavor production. Effects such as energy loss and flow can significantly modify the heavy flavor p_T distributions but do not, in fact, change the total yields. In a finite acceptance detector, however, the measured yields may appear to be enhanced or suppressed, depending on the acceptance. Energy loss steepens the slope of the heavy flavor p_T distribution because the heavy quark p_T is reduced. If the momentum is reduced sufficiently for the quarks to be stopped within the medium, the heavy quarks can take the same velocity as the sur-

rounding medium and 'go with the flow'. The present RHIC results on R_{AA} and v_2 for heavy flavor decays to leptons show that these effects are indeed important for charm quarks and even for bottom quarks. However, higher p_T measurements and reconstructed charm hadrons are needed to solidify and quantify the results. In addition, clean separation of leptons from charm and bottom decays is necessary to provide a sensitive measurement of the electron R_{AA} from bottom decays.

Effects that may modify the total heavy flavor yields are the initial parton distributions in the nuclei and secondary charm production in the medium. The parton distribution functions needed for perturbative QCD calculations of heavy flavor production are modified in the nucleus, as was observed in nuclear deep-inelastic scattering [65]. At very small momentum fractions, x, the gluon fields may be treated as classical color fields. The modifications of the parton distributions in nuclei relative to free protons would affect the total yields. The effect is expected to be small at midrapidity and moderate p_T at RHIC but is likely to be more important at large rapidity where lower x values are probed. Although thermal charm production from the medium is likely to be small at RHIC energies, it could moderately enhance the total yields.

Since the J/ψ yields may be enhanced in nuclear collisions by coalescence of uncorrelated c and $\overline{c}$ quarks in the medium, it is important for charmonium production in heavy-ion collisions to be properly normalized. The ratio of J/ψ to open charm production in pp collisions is not a strong function of energy. Thus the total charm yield sets the scale against which J/ψ suppression relative to enhancement can be quantified, as discussed in more detail in Section 5.

4.1 Open Heavy Flavor Theory

4.1.1 Theoretical Baseline Results

We now discuss the most recent theoretical baseline calculations of the transverse momentum distributions of charm and bottom quarks, the charm and bottom hadron distributions resulting from fragmentation and, finally, the electrons produced in semileptonic decays of the hadrons [6].

The theoretical prediction of the electron spectrum includes three main components: the p_T and rapidity distributions of the heavy quark Q in pp collisions at $\sqrt{s} = 200$ GeV, calculated in perturbative QCD; fragmentation of the heavy quarks into heavy hadrons, H, described by phenomenological input extracted from e^+e^- data; and the decay of H into electrons according to spectra available from other measurements. This cross section is schematically written as

$$\frac{Ed^3\sigma(e)}{dp^3} = \frac{E_Q d^3\sigma(Q)}{dp_Q^3} \otimes D(Q \to H) \otimes f(H \to e) \tag{1}$$

where the symbol $\otimes$ denotes a generic convolution. The electron decay spectrum, $f(H \to e)$, includes the branching ratios.

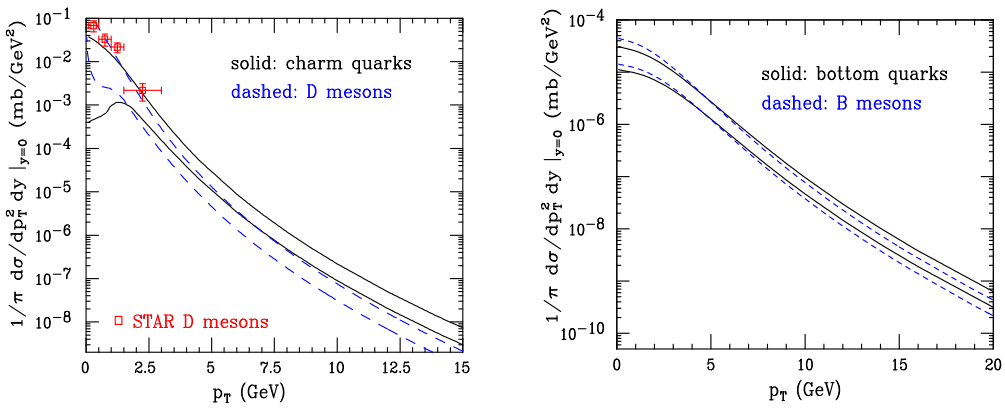

Fig. 5. Left-hand side: The theoretical uncertainty bands for c quark and D meson p_T distributions in pp collisions at $\sqrt{s} = 200$ GeV, using BR$(c \to D) = 1$. The final [66] STAR d+Au data (scaled to pp using $N_{\rm coll} = 7.5$) are also shown. Right-hand side: The same for b quarks and B mesons. Modified from Ref. [67], reprinted with permission from Elsevier.

The distribution $Ed^3\sigma(Q)/dp_Q^3$ is evaluated at Fixed-Order plus Next-to-Leading-Log (FONLL) level [68]. In addition to including the full fixed-order NLO result [69, 70], the FONLL calculation also resums [71] large perturbative terms proportional to $\alpha_s^n \log^k(p_T/m_Q)$ to all orders with next-to-leading logarithmic (NLL) accuracy (*i.e.* $k = n$, $n-1$) where m is the heavy quark mass. The perturbative parameters are the heavy quark mass, m_Q, and the value of the strong coupling, α_s. Since the FONLL calculation treats the heavy quark as an active light flavor at $p_T >> m$, the number of light flavors used to calculate α_s includes the heavy quark, i.e. $n_{\rm lf} + 1$ where, for charm, $n_{\rm lf} = 3$ (u, d and s). The same number of flavors, $n_{\rm lf} + 1$, is also used in the fixed-order scheme where the quark mass is finite. The central heavy quark masses are $m_c = 1.5$ GeV$/c^2$ and $m_b = 4.75$ GeV$/c^2$. The masses are varied in the range $1.3 < m_c < 1.7$ GeV$/c^2$ for charm and $4.5 < m_b < 5$ GeV$/c^2$ for bottom to estimate the mass uncertainties. The five-flavor QCD scale is the CTEQ6M value, $\Lambda^{(5)} = 0.226$ GeV. The perturbative calculation also depends on the factorization (μ_F) and renormalization (μ_R) scales. The scale sensitivity, a measure of the perturbative uncertainty, is calculated using $\mu_{R,F}^2 = \mu_0^2 = p_T^2 + m_Q^2$ as the central value while varying μ_F and μ_R independently within a 'fiducial' region defined by $\mu_{R,F} = \xi_{R,F}\mu_0$ with $0.5 \le \xi_{R,F} \le 2$ and $0.5 \le \xi_R/\xi_F \le 2$ so that $\{(\xi_R, \xi_F)\} = \{$(1,1), (2,2), (0.5,0.5), (1,0.5), (2,1), (0.5,1), (1,2)$\}$. The envelope containing the resulting curves defines the uncertainty. The mass and scale uncertainties are added in quadrature so that

$$\frac{d\sigma_{\max}}{dp_T} = \frac{d\sigma_C}{dp_T} + \sqrt{\left(\frac{d\sigma_{\mu,\max}}{dp_T} - \frac{d\sigma_C}{dp_T}\right)^2 + \left(\frac{d\sigma_{m,\max}}{dp_T} - \frac{d\sigma_C}{dp_T}\right)^2} \tag{2}$$

$$\frac{d\sigma_{\min}}{dp_T} = \frac{d\sigma_C}{dp_T} - \sqrt{\left(\frac{d\sigma_{\mu,\min}}{dp_T} - \frac{d\sigma_C}{dp_T}\right)^2 + \left(\frac{d\sigma_{m,\min}}{dp_T} - \frac{d\sigma_C}{dp_T}\right)^2} \,. \tag{3}$$

where C is the distribution for the central value, μ, max (μ, min) is the maximum (minimum) cross section obtained by choosing the central value with the scale factors in our seven fiducial sets, and m, max (m, min) is the maximum (minimum) cross section obtained with $\xi_R = \xi_F = 1$ and the lower and upper limits on the quark mass respectively.

This range of inputs leads to a FONLL total $c\bar{c}$ cross section (with $n_{\rm lf}+1$ active flavors) in pp collisions of $\sigma_{c\bar{c}}^{\rm FONLL} = 256^{+400}_{-146}$ μb at $\sqrt{s} = 200$ GeV. The theoretical uncertainty is evaluated as described above. The corresponding NLO prediction is 244^{+381}_{-134} μb. The predictions in Ref. [15], using $m_c = 1.2$ GeV/c^2 and $\mu_R = \mu_F = 2\mu_0$ gives $\sigma_{c\bar{c}}^{\rm NLO} = 427$ μb, within the uncertainties. Since the FONLL and NLO calculations tend to coincide at small p_T, which dominates the total cross section, the two results are very similar. Thus the two calculations are equivalent at the total cross section level, within the large perturbative uncertainties. The total cross section for bottom production is $\sigma_{b\bar{b}}^{\rm FONLL} = 1.87^{+0.99}_{-0.67}$ μb.

When the total $c\bar{c}$ cross section is calculated with the next-to-leading order scaling functions of Ref. [69], it does not depend on any kinematic variables, only on the quark mass, m, and the renormalization and factorization scales with central value $\mu_{R,F} = \mu_0 = m$. The heavy quark is always considered massive in the calculation of the total cross section and is thus not an active flavor in the production calculation. Therefore, the number of light quark flavors, $n_{\rm lf}$, does not include the heavy quark. With $n_{\rm lf}$ light flavors and a fixed scale, the charm and bottom NLO total cross sections at $\sqrt{s} = 200$ GeV are $\sigma_{c\bar{c}}^{\rm NLO_{n_{lf}}} = 301^{+1000}_{-210}$ μb and $\sigma_{b\bar{b}}^{\rm NLO_{n_{lf}}} = 2.06^{+1.25}_{-0.81}$ μb, respectively [7]. While the central values are only about 25% and 10% higher respectively than the FONLL results due to a fixed rather than running scale in α_s, the uncertainty is considerably larger, especially for charm. The larger upper limit on the uncertainty is primarily due to the behavior of the CTEQ6M gluon density at factorization scales below the minimum scale of the parton density and the larger value of α_s for $n_{\rm lf}$ light flavors [7]. Other parton densities, with lower initial scales and smaller $\Lambda_{\rm QCD}$ give a reduced upper limit. When both the NLO and FONLL calculations use the same number of light flavors, the results for the total cross section and its uncertainty are in agreement [72].

The fragmentation functions, $D(c \to D)$ and $D(b \to B)$, where D and B indicate a generic admixture of charm and bottom hadrons, are consistently extracted from e^+e^- data in the FONLL context [73].

The measured spectra for primary $B \to e$ and $D \to e$ decays are assumed to be equal for all bottom and charm hadrons, respectively. The contribution of electrons from secondary B decays, $B \to D \to e$, was obtained by convoluting the $D \to e$ spectrum with a parton-model prediction of $b \to c$ decay. The resulting electron spectrum is very soft, giving a negligible contribution to the total. The decay spectra are normalized using the branching ratios for bottom and charm hadron mixtures [74]: $\mathrm{BR}(B \to e) = 10.86 \pm 0.35\%$, $\mathrm{BR}(D \to e) = 10.3 \pm 1.2\%$, and $\mathrm{BR}(B \to D \to e) = 9.6 \pm 0.6\%$.

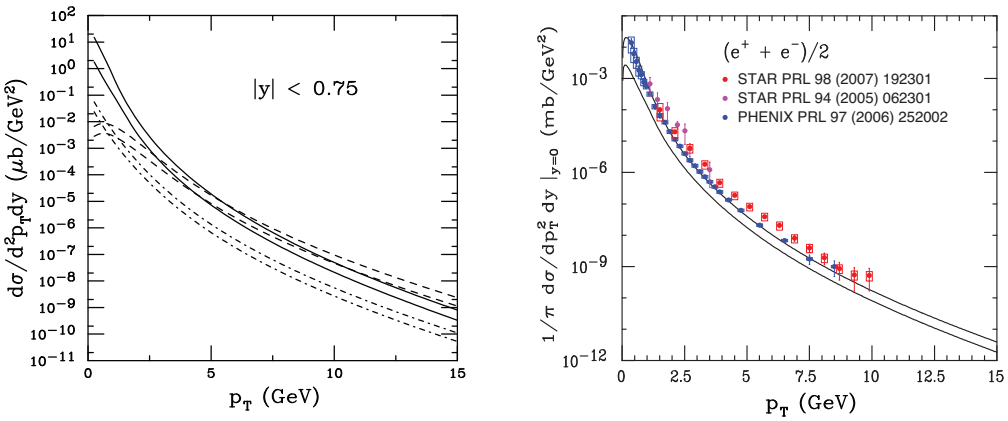

Fig. 6. Left-hand side: The theoretical uncertainty bands for $D \to e$ (solid), $B \to e$ (dashed) and $B \to D \to e$ (dot-dashed) as a function of p_T in $\sqrt{s} = 200$ GeV pp collisions for $|y| < 0.75$. Right-hand side: The final electron uncertainty band in pp collisions is compared to the PHENIX [75] and STAR [19, 66] data. Modified from Ref. [67], reprinted with permission from Elsevier.

The left-hand side of Fig. 5 shows the theoretical uncertainty bands for c quarks and D mesons, obtained by summing the mass and scale uncertainties in quadrature. The band is broader at low p_T due to the large value of α_s and the behavior of the CTEQ6M parton densities at low scales as well as the increased sensitivity of the cross section to the charm quark mass. The rather hard fragmentation function causes the D meson and c quark bands to separate only at $p_T > 9$ GeV/c. The right-hand side of Fig. 5 shows the same results for b quarks and B mesons. The harder $b \to B$ fragmentation function causes the two bands to partially overlap until $p_T \simeq 20$ GeV/c.

Figure 6 shows the individual uncertainty bands for the $D \to e$, $B \to e$ and $B \to D \to e$ decays to electrons on the left-hand side and compares the RHIC data to the total band on the right-hand side. The upper and lower limits of the total band are obtained by summing the upper and lower limits of each component. The secondary $B \to D \to e$ spectrum is extremely soft, only exceeding the primary $B \to e$ decays at $p_T < 1$ GeV/c. It is always negligible with respect to the total yield. While, for the central parameter sets, the $B \to e$ decays begin to dominate the $D \to e$ decays at $p_T \simeq 4$ GeV/c, a comparison of the bands shows that the crossover may occur over a rather broad range of electron p_T, assuming that the two bands are uncorrelated.

While the heavy quarks are in the medium, they can undergo energy loss by two means: elastic collisions with light partons in the system (collisional) and gluon bremsstrahlung (radiative). We will briefly review some of the predicted results for $-dE/dx$ of heavy quarks for both collisional and radiative loss. We then show the predicted effect on the charm and bottom contributions to single electrons at RHIC [10].

The collisional energy loss of heavy quarks through processes such as $Qg \rightarrow Qg$ and $Qq \rightarrow Qq$ depends logarithmically on the extremes of the heavy quark momentum, $-dE/dx \propto \ln(q_{\max}/q_{\min})$. Treatments of the collisional loss vary with the values assumed or calculated for the cutoffs. These cutoffs are sensitive to the energy of the heavy quark and the temperature and strong coupling constant in the medium. Thus the quoted value of the energy loss is usually for a certain energy and temperature. The calculation was first done by Bjorken [76] who found $-dE/dx \approx 0.2$ GeV/fm for a 20 GeV/c quark at $T = 250$ MeV. Further work refined the calculations of the cutoffs [77–79], with similar results. Braaten and Thoma calculated the collisional loss in the limits $E \ll m_Q^2/T$ and $E \gg m_Q^2/T$ in the hard thermal loop approximation, removing the cutoff ambiguities. They obtained $-dE/dx \approx 0.3$ GeV/fm for a 20 GeV/c charm quark and 0.15 GeV/fm for a 20 GeV bottom quark at $T = 250$ MeV [80].

Other models of heavy quark energy loss were presented in the context of J/ψ suppression: Could a produced $c\overline{c}$ pair stay together in the medium long enough to form a J/ψ? Svetitsky [81] calculated the effects of diffusion and drag on the $c\overline{c}$ pair in the Boltzmann approach and found a strong effect. The drag [2] stopped the $c\overline{c}$ pair after traveling about 1 fm but Brownian diffusion drove the quarks apart quickly. The diffusion effect increased at later times. Svetitsky essentially predicted that the heavy quarks would be stopped and then go with the flow. His later calculations of D meson breakup and rehadronization [16] while moving through plasma droplets reached a similar conclusion. Koike and Matsui calculated energy loss of a color dipole moving through a plasma using kinetic theory and found $-dE/dx \sim 0.4 - 1.0$ GeV/fm for a 10 GeV/c $Q\overline{Q}$ [82]. The collisional loss was thus predicted to be small, less than 1 GeV/fm for reasonable assumptions of the temperature. The loss increases with energy and temperature. Using the hard thermal loop approach, Mustafa *et al.* found $-dE/dx \approx 1 - 2$ GeV/fm for a 20 GeV/c quark at $T = 500$ MeV [83].

The first application of radiative loss to heavy quarks was perhaps by Mustafa

[2] The drag coefficient $A(p^2)$ is related to the energy loss per unit length by $A(p^2) = (-dE/dx)/p^2$.

et al. [83]. They included the effects of only a single scattering/gluon emission, $Qq \to Qqg$ or $Qg \to Qgg$. In this case, the loss grows as the square of the momentum logarithm, $\ln^2(q_{\rm max}/q_{\rm min})$, one power more than the collisional loss, but is of the same order in the strong coupling constant [80]. Thus the radiative loss is guaranteed to be larger than the collisional in this approximation. The heavy quark mass enters these expressions only in the definition of $q_{\rm max}$ so that the mass dependence of the energy loss is rather weak. They found, for a 20 GeV/c quark at $T = 500$ MeV, $-dE/dx \approx 12$ GeV/fm for charm and 10 GeV/fm for bottom.

These large values suggested that energy loss could be quite important for heavy quarks. If true, there would be a strong effect on the $Q\overline{Q}$ contribution to the dilepton continuum. Shuryak [84] was the first to consider this possibility for $A + A$ collisions. He assumed that low mass $Q\overline{Q}$ pairs would be stopped in the medium, substantially suppressing the dilepton contribution from these decays. Heavy quarks are piled up at low p_T and midrapidity if stopped completely. However, stopped heavy quarks should at least expand with the medium rather than coming to rest, as discussed by Svetitsky [81]. Lin *et al.* then calculated the effects of energy loss at RHIC, including thermal fluctuations, for constant $-dE/dx = 0.5 - 2$ GeV/fm [14]. These results showed that heavy quark contributions to the dilepton continuum would be reduced but not completely suppressed. In any case, the energy loss does not affect the total cross section.

Dokshitzer and Kharzeev pointed out that soft gluon radiation from heavy quarks is suppressed at angles less than $\theta_0 = m_Q/E$ [13]. Thus bremsstrahlung is suppressed for heavy quarks relative to light quarks by the factor $(1 + \theta_0^2/\theta^2)^{-2}$, the 'dead cone' phenomenon. The radiative energy loss of heavy quarks could then be quite small. However, Armesto *et al.* [12] later showed that medium-induced gluon radiation could 'fill the dead cone', leading to non-negligible energy loss for heavy flavors. They also found that the energy loss would be larger for charm than bottom quarks.

So far the RHIC heavy-ion measurements are not for heavy flavored hadrons but for the electrons from their semileptonic decays. If the effects of energy loss are substantially different for charm and bottom quarks, then the results in Fig. 6 which show that, at high p_T, the single electron spectrum is dominated by b decays, would suggest that, if charm quarks lose more energy than bottom quarks, b-quark dominance of the electron spectra would begin at smaller values of electron p_T in $A+A$ collisions. This would, in turn, limit the electron suppression factor, R_{AA}, at moderate p_T since the large bottom contribution would make R_{AA} larger than expected if the spectrum arose primarily from charm quark decays.

The left-hand side of Fig. 7 is an example calculation comparing the c and

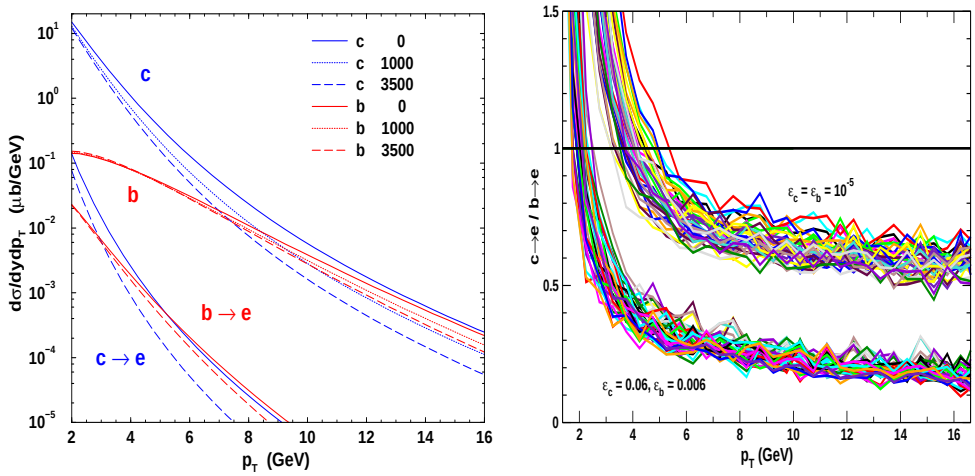

Fig. 7. Left-hand side: The differential cross section (per nucleon pair) of charm and bottom quarks calculated to NLO in QCD [6] compared to single electron distributions calculated with the fragmentation and decay scheme of Ref. [6]. The solid, dotted and long dashed curves show the effects of heavy quark energy loss with initial gluon rapidity densities of $dN_g/dy = 0, 1000,$ and 3500, respectively. Right-hand side: The ratio of charm to bottom decays to electrons obtained by varying the quark masses and scale factors. The effect of changing the Peterson function parameters from $\epsilon_c = 0.06$, $\epsilon_b = 0.006$ (lower band) to $\epsilon_c = \epsilon_b = 10^{-5}$ (upper band) is also illustrated for correlated b and c scales. From Ref. [10], reprinted with permission from Elsevier.

b distributions at midrapidity, as well as their contributions to single electrons. Electrons from bottom decays dominate the single electron spectra at $p_T \sim 5$ GeV/c for all gluon rapidity densities. This conclusion is further supported by the right-hand side of Fig. 7 where the ratio of charm relative to bottom decays to electrons is shown. The crossover region here is rather narrow because μ_F and μ_R for c and b are are assumed to be correlated while they are uncorrelated in Fig. 6. In all cases, the bottom contribution to single electrons is large and cannot be neglected in the computation of single electron suppression, shown in Fig. 8. Since bottom energy loss is greatly reduced relative to charm [10], the possible effect on the electron spectrum is reduced, leading to $R_{AA}(p_T < 6 \text{ GeV}/c;\ e) > 0.5 \pm 0.1$. A calculation by Armesto *et al.* [37], with a somewhat different model of energy loss, showed similar results to those in Fig. 8.

Djordjevic and Heinz found that finite-size effects on radiative energy loss in a dynamical QCD medium induce a nonlinear path length dependence of the energy loss [85]. The light quark and charm quark loss is similar at RHIC while nonlinearities only become large for bottom quarks in LHC conditions. Recent calculations by Wicks *et al.* [86] have revisited the importance of elastic energy loss and have shown that this component may make a larger contribution to the suppression factor than previously expected.

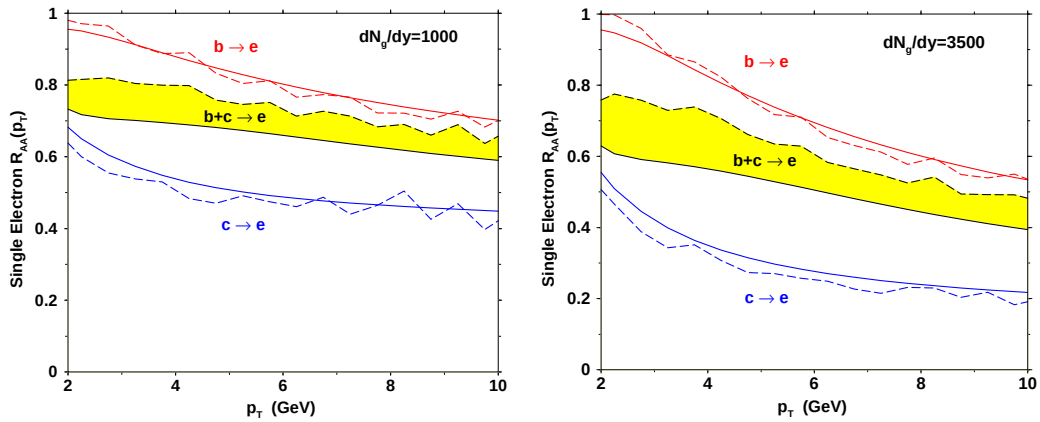

Fig. 8. Single electron attenuation pattern for $dN_g/dy = 1000$, left, and $dN_g/dy = 3500$, right. The solid curves employ the fragmentation scheme and lepton decay parameterizations of Ref. [6] while the dashed curves use the Peterson function with $\epsilon_c = 0.06$ and $\epsilon_b = 0.006$ and the decay to leptons employed by the PYTHIA Monte Carlo. Even for the extreme case on the right, the less quenched b quarks dilute R_{AA} so much that the modification of the combined electron yield from both c and b decays does not fall below $\sim 0.5 - 0.6$ near $p_T \sim 5$ GeV/c. From Ref. [10], reprinted with permission from Elsevier.

A calculation by Adil and Vitev [87] of collisional dissociation of heavy flavor hadrons suggests that the D and B meson attenuation in a quark-gluon plasma are similar. The B dissociation rate is much faster than the D dissociation rate due to its shorter formation time so that it can undergo more fragmentation/dissociation cycles in the plasma than the D, resulting in a similar R_{AA} for D and B mesons and relatively good agreement with the measured nonphotonic electron R_{AA}. The heavy quark flow has not been calculated in this approach.

Moore and Teaney [88] and Rapp *et al.* [89, 90] calculated R_{AA} and the nonphotonic electron elliptic flow, v_2, in a Langevin model of the time evolution of heavy quarks in the medium. Both these groups emphasize that elastic (collisional) energy loss should be important at low p_T relative to radiative loss since the boost for heavy flavor hadrons in the medium should not be large. Both also find a strong correlation between R_{AA} and v_2. Although the approaches differ somewhat, the trends are similar in the two calculations.

Moore and Teaney [88] calculate the diffusion and drag coefficients for charm quarks in perturbative QCD. The diffusion coefficient is proportional to the inverse square of the strong coupling constant, α_s, *e.g.* $D(2\pi T) \propto \alpha_s^{-2}$. They present the effects of a range of values for $D(2\pi T)$ on R_{AA} and v_2, finding the largest effects at high p_T for small $D(2\pi T)$, corresponding to large α_s or strong coupling in the plasma.

Rapp *et al.* [89, 90] calculated the diffusion and drag coefficients assuming that

resonant D and B states in the QGP elastically scatter in the medium. Resonance scattering reduces the thermalization times for heavy flavors relative to those calculated with perturbative QCD matrix elements for fixed $\alpha_s = 0.4$. The effect is larger for charm than for the more massive bottom quarks. Including these states thus reduces the electron R_{AA} at high p_T relative to the results in Ref. [10] while increasing the electron v_2 to $\sim 10\%$ at $p_T \sim 2$ GeV/c, in relative agreement with the data.

Thus, given sufficiently strong coupling and/or resonant states, both R_{AA} and v_2 can be described within transport approaches using elastic scattering. More and better data is necessary to distinguish the two approaches.

4.3 RHIC open heavy flavor measurements to date

Open heavy flavor production cross sections can be measured by reconstructing the invariant mass of the heavy quark hadron from its hadronic decay products or by detecting leptons from semileptonic decays of those hadrons. While both PHENIX and STAR can measure heavy flavor cross sections by either technique, PHENIX has some advantages for semileptonic decay measurements and STAR has advantages for the hadronic decay measurements.

In both cases the signal to background ratio can be greatly improved if a precise measurement of the decay vertex position is available, since hadrons containing c or b quarks typically travel several hundred microns from the collision point before decaying. Both PHENIX and STAR have plans to add secondary vertex detectors capable of the necessary precision. The PHENIX SVTX detectors will be installed starting in 2010, the STAR HFT in 2012. In addition to reducing the background rates for open heavy flavor decays to leptons and hadrons, the secondary vertex detectors make a clean bottom cross section measurement possible using displaced vertex decays to J/ψ, given sufficient luminosity.

Open heavy flavor cross section measurements based on semileptonic decays of charm and bottom mesons are feasible because a small lepton signal can be identified in a very large hadron background. The background lepton sources are both small and well enough understood that they can be subtracted to get the open heavy flavor signal. However, the loss of information about the decaying heavy meson due to the recoil kinematics is a disadvantage of semileptonic decay measurements. Thus charm and bottom decays cannot easily be distinguished. Open charm measurements using hadronic decay products have two advantages: the D meson kinematic properties are reconstructed and separation of charm from bottom is far easier because only a small fraction of D mesons arise from bottom decays [6]. A disadvantage of hadronic decay

measurements is the huge combinatorial background present in heavy-ion collisions.

PHENIX has measured open heavy flavor yields via semileptonic decays to electrons at midrapidity ($|\eta| < 0.35$) using the Ring Imaging Cerenkov detector and electromagnetic calorimeter for electron identification. At forward and backward rapidity ($1.2 < |\eta| < 2.2$) the two muon spectrometers are used. PHENIX results are available for *pp* at midrapidity [75] and forward rapidity [91] as well as for d+Au [92] and Au+Au at midrapidity [20]. No open charm cross sections from hadronic decays have yet been reported by PHENIX since the small central arm acceptance is a disadvantage for such measurements.

STAR has measured open heavy flavor yields at midrapidity ($|\eta| < 1.0$) via semileptonic decays using either a combination of the time projection chamber (TPC) and time of flight (ToF) for electron identification or a combination of the TPC and the electromagnetic calorimeter. The backgrounds that must be subtracted are much larger than they are for PHENIX because of the larger photon conversion rates in STAR and the lack of a hadron blind electron identifier. This is compensated somewhat by the larger acceptance. STAR electron results are available for *pp*, d+Au and Au+Au collisions [19]. STAR has also measured open charm yields in the range $|\eta| < 1.0$ through hadronic D meson decays for d+Au [66], Au+Au [93], and Cu+Cu [21] collisions.

Because the charm cross section is much larger than the bottom cross section at RHIC and dominates the semileptonic decay spectrum for $p_T < 2.5$ GeV/c, the integrated non-photonic lepton cross section is usually assumed to be equal to the charm cross section.

4.3.1 Baseline measurements

Before any conclusions can be drawn about the hot, dense final state from the results for heavy-ion collisions, some baseline information is required. Data from *pp* collisions are needed to establish the underlying cross sections and kinematic distributions for open heavy flavor and $p + A$ data are needed to isolate effects due to gluon saturation and the intrinsic k_T distributions in the colliding nuclei.

Both PHENIX and STAR have measured charm production cross sections at midrapidity. These measurements have been extrapolated to all rapidities to yield total cross sections. These total cross sections are compared to results at other energies and to pQCD calculations in Fig. 9. The results for d+Au and Au+Au collisions are divided by the number of binary collisions, $N_{\rm coll}$, to directly compare with the *pp* results. The STAR data are from combined fits to hadronic and semileptonic decay data. The PHENIX data are from semileptonic decay measurements only.

The STAR values are somewhat higher than those for PHENIX. The total charm cross sections differ by about 1.5 times the combined standard deviations of the two measurements, obtained by adding all statistical and systematic uncertainties in quadrature.

The NLO calculations and their uncertainties are those of the fixed-order calculation with three light flavors for charm, as described in Ref. [7]. While the larger uncertainty of the fixed-order calculation shown here can accommodate the larger STAR cross section, it is not clear which estimate of the uncertainty is best. Obviously the large theoretical uncertainty means that there is little predictive power in the total charm cross section. The FONLL estimate of the uncertainty in the p_T distribution is more reliable for finite p_T [7].

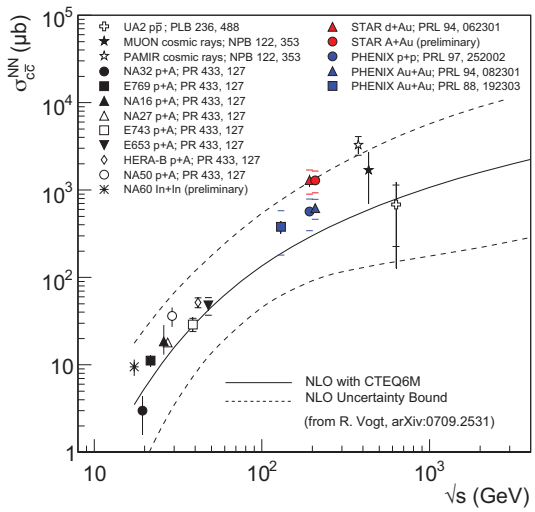

Fig. 9. Comparison of total cross section measurements. The STAR and PHENIX results are given as cross section per binary collisions. Vertical lines reflect the statistical errors, horizontal bars indicate the systematic uncertainties (where available). The NLO calculations and the depicted uncertainty bands are described in the text.

Since charm and bottom quarks are expected to be produced only in the initial nucleon-nucleon interactions, their yield should scale as the number of binary collisions, $N_{\rm coll}$. The left-hand side of Fig. 10 shows the PHENIX measurement of the charm invariant yield in Au+Au collisions, scaled by $N_{\rm coll}$, at midrapidity as a function of $N_{\rm part}$ [20]. The PHENIX data integrated over $p_T > 0.3$ GeV/c are consistent with no $N_{\rm part}$ dependence, as expected. The effect of the final state medium can be seen when the distributions are integrated above 3 GeV/c. These p_T-dependent effects are discussed in the following section. The comparison of charm production measured by STAR in pp, d+Au, Au+Au, and Cu+Cu indicates that the total charm cross section scales with $N_{\rm coll}$, as expected for hard processes, see the right-hand side of Fig. 10. The d+Au and Au+Au cross sections were further constrained by using the low-p_T muons and medium-p_T electrons from semileptonic charm decays. The measured cross

section for each system and centrality was divided by the appropriate value of $N_{\rm coll}$ to reflect the pp equivalent cross section [21]. The NLO lines are the bounds on the total $c\overline{c}$ cross section from Fig. 9.

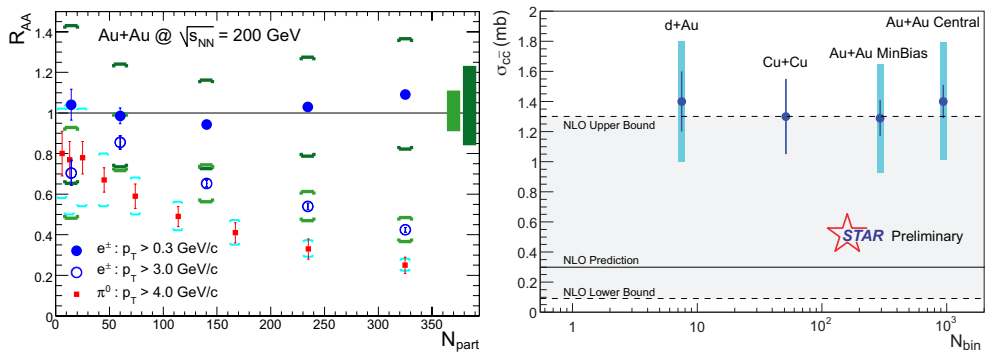

Fig. 10. Left: PHENIX measurements of the midrapidity invariant charm yields scaled by $N_{\rm coll}$ as a function of $N_{\rm part}$ [20]. More than half of the heavy flavor decay electrons included in the integral are above 0.3 GeV/c. Right: STAR measurements of the charm cross section derived from identified D^0 mesons in d+Au, Cu+Cu, and Au+Au collisions as a function of $N_{\rm coll}$.

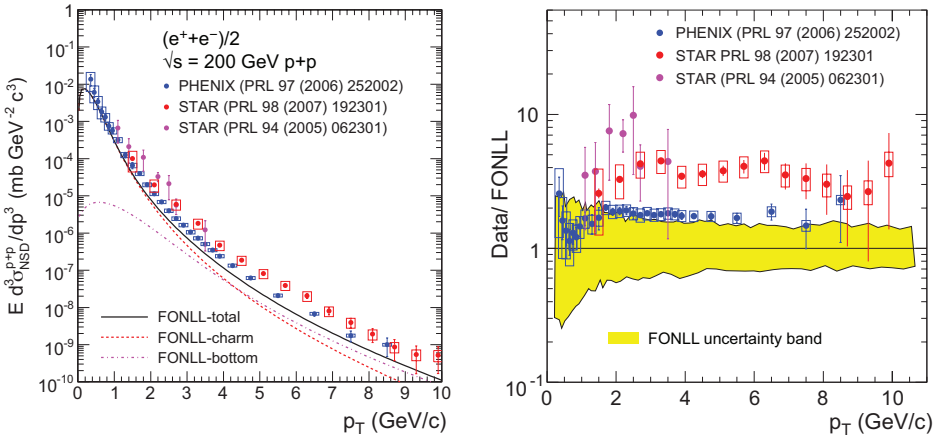

Fig. 11. Left: Compilation of PHENIX [75] and STAR measurements [19, 66] of the p_T dependence of the semileptonic decay open heavy flavor cross section from 200 GeV pp collisions, compared with FONLL calculations [75]. Right: The ratio of the data to the FONLL calculation. The band depicts the theoretical uncertainty of the calculation. Note, that they are smaller than those from the calculation of the total cross-section shown in Fig. 9 and 10 (right) as detailed earlier in this section. From Ref. [94].

The left-hand side of Fig. 11 shows the measured p_T dependence of semileptonic open heavy flavor decays to electrons from 200 GeV pp collisions by PHENIX [75] and STAR [19, 66]. On the right-hand side, the ratio of the measured cross sections to the FONLL calculation [6] is shown. The FONLL calculation reproduces the p_T slope of the data in both cases. The magnitude of

the FONLL cross section is 1.5 times smaller than that of the PHENIX data, just at the limit of the theoretical uncertainty band. However, the FONLL cross section is a factor of $\sim$ 4 smaller than the STAR data, well outside the theoretical uncertainties. The discrepancy of a factor of $\sim$ 2 between the PHENIX and STAR cross sections in Fig. 11 is not yet explained.

A limitation of open heavy flavor measurements using semileptonic decays is the difficulty of separating charm and bottom decay contributions. Recently, the ratio of charm to bottom contributions has been extracted as a function of decay electron p_T from pp data by STAR and PHENIX. STAR measurements were made by fitting measured small angle electron-hadron correlation functions to a combination of the D and B correlation shapes given by their decay kinematics simulated through PYTHIA. Additional p_T integrated measurements were made using like-sign electron-kaon correlations, exploiting the difference in the correlation shape between B and D decays. A new recent measurement is based on the small angle correlation of semileptonic decay electrons with identified D^0 mesons yielding consistent results with the former method [38]. The PHENIX bottom/charm ratio [39] was inferred by fitting the shape of the electron-kaon reconstructed mass spectrum with a combination of the charm and bottom decay line shapes, taken from PYTHIA simulations. The measured STAR and PHENIX $b/(c+b)$ ratios are compared in Fig. 12. They are in good agreement and indicate that bottom decays become dominant at $p_T \sim 3.5$ GeV/c.

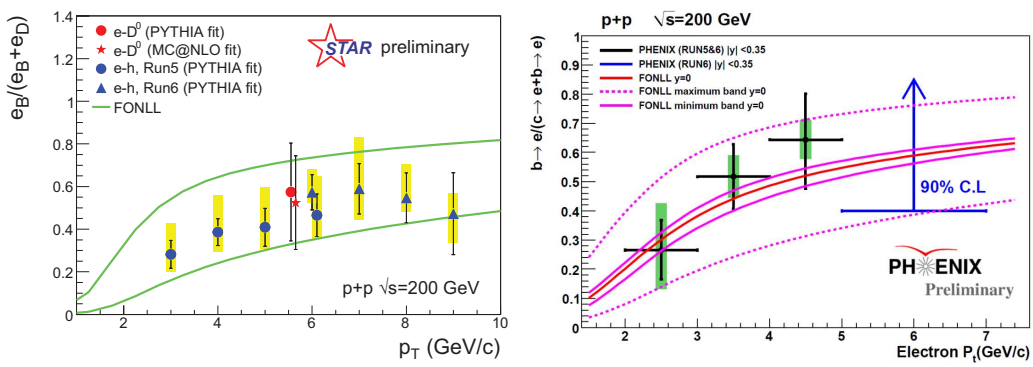

Fig. 12. Measurements of the p_T dependence of $b/(c+b)$ determined from semileptonic heavy flavor decays in 200 GeV pp collisions by STAR [38] (left) and PHENIX [39] (right).

A separate measurement of the bottom and charm cross sections was also obtained by PHENIX from fits to the dielectron invariant mass spectrum, after removal of all non-heavy flavor contributions [40]. The results are in agreement with the cross sections inferred by PHENIX from combining the measured $b/(c+b)$ ratios with semileptonic decay electron p_T distributions. The bottom cross sections determined by PHENIX are summarized in Table 6.

Method	$d\sigma_{b\bar{b}}/dy$ (μb)	$\sigma_{b\bar{b}}$ (μb)
eh mass shape	$1.34 \pm 0.38^{+0.74}_{-0.64}$(sys)	$4.61 \pm 1.31^{+2.57}_{-2.22}$(sys)
e^+e^- mass spectrum	–	$3.9 \pm 2.5^{+3}_{-2}$(sys)

Table 6
Summary of PHENIX [39, 40] measurements of the open bottom cross section in 200 GeV pp collisions.

Unlike the J/ψ measurements discussed in the next section, the current d+Au and pp open heavy flavor results are not precise enough for any conclusions to be drawn about either shadowing or k_T broadening. Obtaining more precise open heavy flavor baseline results is an important priority for the RHIC program over the next few years.

4.3.2 Heavy-ion measurements

Both PHENIX and STAR have released striking results on suppression of single electrons from open heavy flavor decays in central Au+Au collisions. PHENIX also has results for the electron v_2 from open heavy flavor decays.

The nuclear modification factors and elliptic flow parameters for electrons from semileptonic decays of open heavy flavor in Au+Au central collisions from PHENIX [20] are shown in Fig. 13. Figure 14 [19] shows the STAR R_{AA} measured in Au+Au and d+Au collisions. The Au+Au R_{AA} data from the two experiments are in reasonable agreement. Both show very strong suppression in central collisions at high p_T. When comparing the non-photonic electron R_{AA} data to theory, recall that while the electron data contain contributions from both charm and bottom decays, the bottom contribution is expected to dominate for p_T above ~ 4 GeV/c [6]. Since energy loss is predicted to be weaker for bottom, the similarity of the electron R_{AA}, $R_{AA} \sim 0.2 - 0.3$, to light-quark hadrons [4] is surprising.

In Fig. 13, the PHENIX R_{AA} and v_2 data are compared with models that calculate both quantities simultaneously. Curve I is a perturbative QCD calculation with radiative energy loss [37]. It describes the R_{AA} data using a large transport coefficient, $\hat{q} = 14$ GeV^2/fm, that also works well for light hadron suppression. However, in this model v_2 arises only from the path length dependence of energy loss and clearly underpredicts the v_2 data. Band II is a Langevin-based heavy quark transport calculation [90], including elastic scattering mediated by resonance excitation, also compared to the STAR data in Fig. 14. The best simultaneous description of the R_{AA} and v_2 data is achieved with a small heavy quark relaxation time. The curve labeled III is also from a transport calculation [88] where the diffusion and drag coefficients are calculated in perturbative QCD. The diffusion coefficients required by the data are small in both cases, implying a ratio of viscosity to entropy small enough to

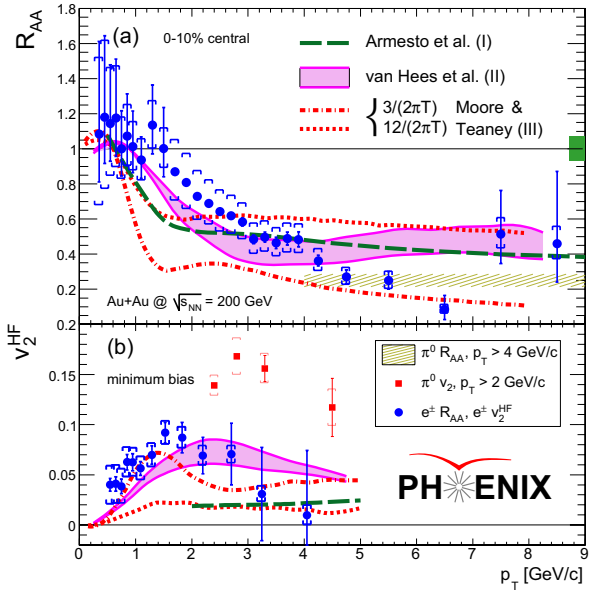

Fig. 13. PHENIX measurement of the non-photonic electron R_{AA} (upper panel) and v_2 (lower panel) in central Au+Au collisions [20]. The theory curves are discussed in the text.

be at or near the conjectured quantum bound [20], consistent with estimates of elliptic flow and fluctuation analyses for light-quark hadrons [95, 96].

The STAR R_{AA} data are compared to model calculations in Fig. 14. The theory curves are from calculations discussed previously. The curves labeled I-IV are calculations of the electron spectra from both D and B decays incorporating final-state c and b quark energy loss. Curve I [10] uses only DLGV radiative energy loss with $dN_g/dy = 1000$, while Curve II [37] employs BDMPS radiative energy loss (Curve I in Fig. 13). Both calculations predict much less suppression than observed. Curves III are from a DLGV-based calculation including both collisional and radiative energy loss [86]. While the addition of collisional energy loss substantially increases the suppression over the calculation with DGLV radiative loss alone, shown in Curve I, it still underpredicts the suppression seen in the data. Curve IV is a Langevin-based calculation [90], the center of Band II in Fig. 13. Resonance effects reduce the R_{AA} for charm-decay electrons to 0.2, but have a smaller effect on bottom quark energy loss, causing R_{AA} to increase at higher p_T. Curve V is the same as Curve II but with only D decays included.

There is considerable interest in the behavior of the non-photonic electron v_2 for $p_T > 2$ GeV/c where, as discussed earlier, the bottom contribution is expected to become important. New preliminary PHENIX semileptonic decay v_2 results were shown at Quark Matter 2008. These show that the v_2 remains high up to 4.5 GeV/c. Together with the observations from PHENIX and

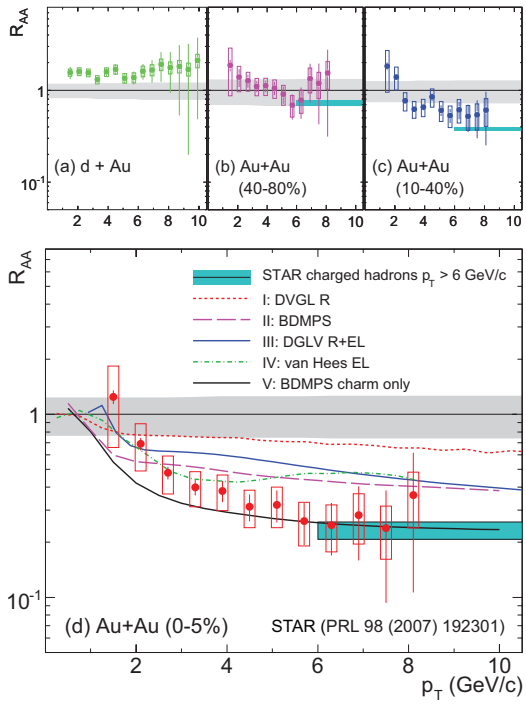

Fig. 14. Measurement of the nuclear modification factor of non-photonic electrons by STAR for d+Au and Au+Au collisions at different centralities [19]. The theory curves are discussed in the text.

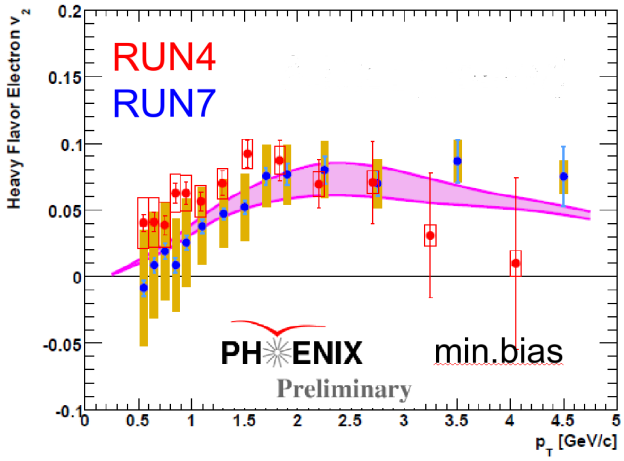

Fig. 15. PHENIX preliminary measurement of the non-photonic electron v_2 in minimum bias Au+Au collisions [39], providing good statistical significance to 5 GeV/c. The band corresponds to Curve III of Fig. 13.

STAR that the bottom cross section starts to dominate the semileptonic decay spectra at about 3.5 GeV/c in pp collisions, the existing R_{AA} data and the new preliminary v_2 data strongly suggest that bottom quarks experience large

energy loss and significant flow at RHIC.

In spite of the recent pp measurements of the ratio of bottom to charm with p_T in the semileptonic decay spectra, the lack of electron separation between charm and bottom decays remains a serious limitation. Sensitive measurements of bottom quark R_{AA} and v_2, in particular, in heavy-ion reactions will require clean separation of bottom and charm contributions. The ways in which this will be addressed in the future RHIC program are discussed in the next section.

4.4 Proposed open heavy flavor experimental program at RHIC II

Here we focus on the new open heavy flavor physics that becomes available with the the RHIC detector upgrades and the RHIC II luminosity upgrade.

The measurement of charm mesons through their *hadronic* decay channels relies on the efficient reconstruction of the secondary decay vertices. With the Heavy Flavor Tracker (HFT) upgrade the STAR experiment will be able to measure D mesons down to low p_T. However, to-date no high-level trigger scheme exist that would allow to trigger on displaced vertices in heavy-ion collisions. Consequently, the direct reconstruction of D mesons does require large minimum bias data sets and the subsequent offline reconstruction of these events. These studies do not depend on large beam luminosity. The situation is different for measurements of open heavy flavor through their *semileptonic* decays where the high-p_T lepton can be used to tag candidate events. Triggers for high-p_T leptons are already deployed in PHENIX and STAR and will be mandatory at RHIC-II luminosities.

The left side of Fig. 16 shows the reconstructed $D^0 \rightarrow K\pi$ channel from STAR simulations. Note that the signal cannot be distinguished from the background (random combinations of K and π tracks) without making topological cuts on the pairs. The plot illustrates the need for high pointing resolution of the two innermost Si-detector layers of the HFT; tight displaced vertex cuts will eliminate most of the prompt hadron tracks from the combinatorial background. The overall reconstruction efficiency, taking into account the acceptance, single track efficiency and D^0 reconstruction efficiency increases from $\sim 10\%$ at low p_T to $\sim 25\%$ at high p_T. The efficiency is small at low p_T because the minimal boost from the parent particle allows the pool of daughter track candidates to be contaminated by primary tracks, diluting the signal and increasing the background.

The right-hand side of Fig. 16 shows the significance of the STAR D^0 signal for 10^8 central Au+Au events as a function of p_T. With the upgraded STAR data acquisition and TPC readout electronics, such a sample is expected in two

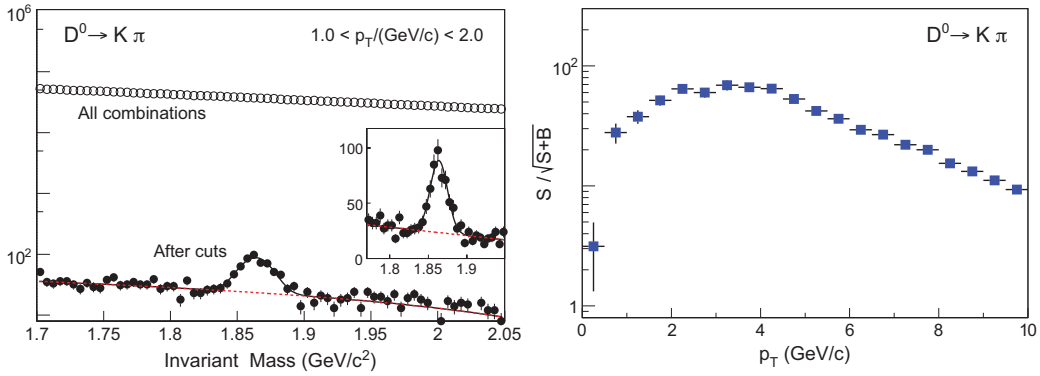

Fig. 16. Left: Illustration of $D^0 \rightarrow K\pi$ reconstruction with the HFT in STAR. The open symbols depict the invariant $K\pi$ mass of all candidate tracks without any topological cuts applied. The closed symbols show the final signal after secondary vertex reconstruction. The dashed line shows the background fit outside the D^0 mass range. The signal peak is shown on a linear scale in the inset. Right: Expected significance of the D^0 measurement in 200 GeV Au+Au collisions with 100 M central events as a function of p_T.

weeks of running. The signal significance is directly related to the precision with which one can determine suppression, R_{AA}, and flow, v_2.

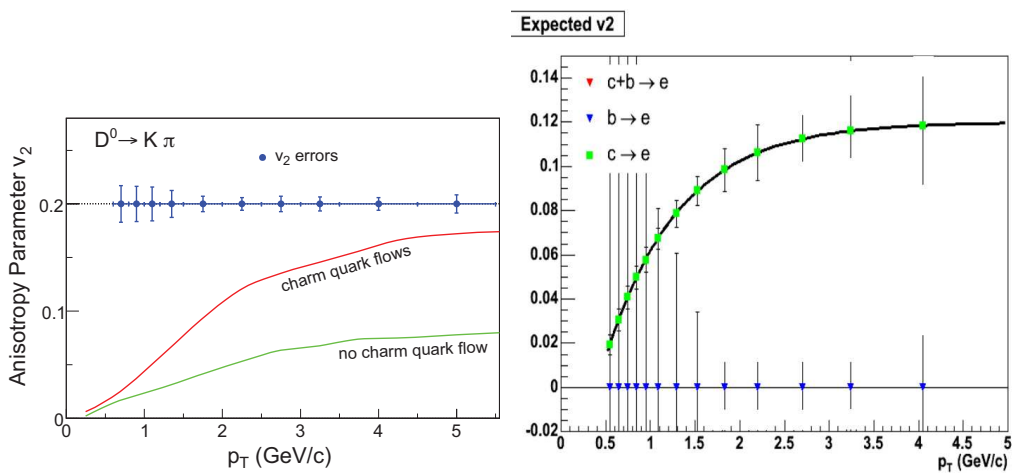

Fig. 17. Left: Estimate by of the D^0 v_2 precision measured by STAR through $D^0 \rightarrow K\pi$ decays. The error bars depict the anticipated errors of the measurement in 10^8 Au+Au minimum bias events. The lower curve illustrates v_2 model predictions if only the light quarks in the D mesons flow. The upper curve illustrates the increase in v_2 if the charm quark also flows [17]. Right: Estimates [97] of PHENIX v_2 precision for open charm and bottom decay electrons using a displaced vertex measurement, calculated for a delivered luminosity of 30 nb^{-1}. The uncertainties on bottom decays at the lowest p_T are dominated by systematic errors.

A precision measurement of charm elliptic flow is one of the main goals for any future RHIC program. In order to simulate minimum-bias Au+Au measurements, it is necessary to make assumptions about the magnitude and the p_T dependence of the anisotropy of the flow distributions. Models of D^0 flow

with and without charm quark flow [17], represent the two possible extremes and thus bracket the expected v_2 range, shown on the left-hand side of Fig. 17. With the known efficiency and the anticipated signal-to-background ratios, the statistical errors on a proposed measurement can be estimated. The small error bars shown (symbols) can be achieved by STAR 10^8 minimum-bias Au+Au events. The most important momentum range for determining the thermodynamic behavior of the D^0 is $p_T < 3$ GeV/c since other dynamical effects such as jet correlations will become important at higher p_T.

Another way to measure open heavy flavor is through semileptonic decays. The azimuthal angle of the D and its decay lepton are closely correlated. With the exception of very low p_T, the v_2 of the lepton is a good proxy for the v_2 of the heavy flavor meson. The disadvantage of this method, however, is the difficulty of separating leptons from charm and bottom decays. With a displaced vertex measurement and the RHIC II luminosity, separation of the charm and bottom contributions to the semileptonic decay spectra can be done statistically using the different decay lengths for charm and bottom mesons (see the right-hand side of Fig. 19). By analyzing data samples with different decay length cuts, the fraction of the signal due to b quarks can be varied. The addition of a displaced vertex measurement greatly reduces the background for all open heavy flavor measurements, improving both statistical and systematic errors. The expected precision for separate v_2 measurements of charm and bottom via electron decays at midrapidity in PHENIX are shown on the right-hand side of Fig. 17.

At forward rapidity in PHENIX, displaced vertex measurements can be used to measure charm and bottom separately using muon decays. In that case, adding a 1 cm displaced vertex cut reduces the muon yields from light hadron decays by about one order of magnitude, reducing a major background source for single muon measurements, and adding a very tight cut around zero vertex displacement also greatly reduces the punch-through hadron background. Figure 18 shows simulations of the expected precision for charm and bottom R_{AA} measurements at forward rapidity in PHENIX in one year of RHIC running. The right-hand side of Fig. 17 shows the estimated v_2 precision [97] from semileptonic charm and bottom decays in the PHENIX central arms for a run with a 30 nb^{-1} delivered luminosity.

Thus, separate R_{AA} and v_2 measurements as a function of p_T and y should be possible for both open charm and bottom over a wide rapidity range at RHIC II.

With a displaced vertex measurement and RHIC II luminosity, the $B \to J/\psi X$ decay channel can provide a very clean measurement of open bottom production by both PHENIX and STAR (see Tables 2 and 3). The displaced vertex distributions for prompt J/ψ and for $B \to J/\psi X$ decays accepted in the

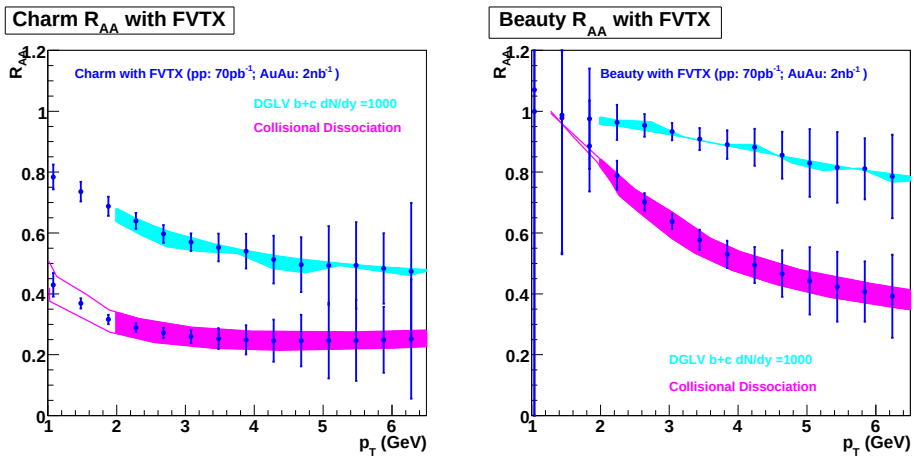

Fig. 18. PHENIX estimates of the precision of the heavy flavor semileptonic decay R_{AA} obtained using a displaced vertex measurement, calculated for a delivered luminosity of 30 nb^{-1} for (left) open charm and (right) open bottom.

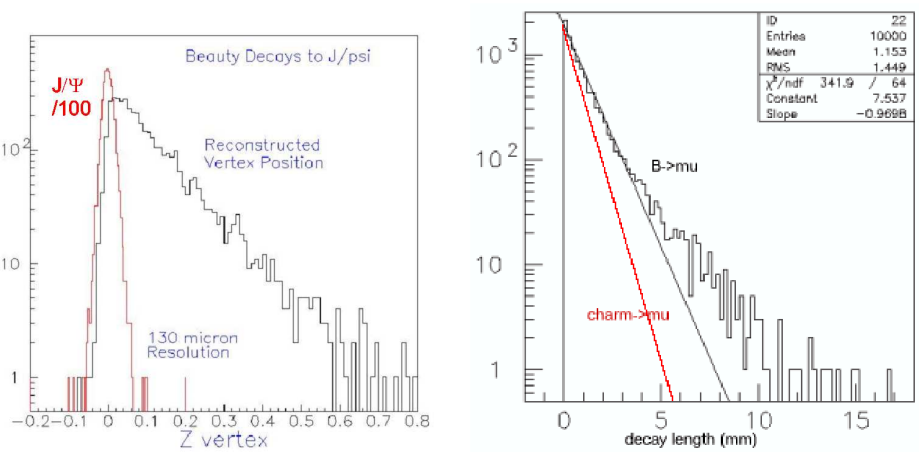

Fig. 19. Left: Comparison of prompt $J/\psi X$ displaced vertex distribution (in cm) with that from $B \rightarrow J/\psi X$ decays [55]. Note that the prompt J/ψ distribution is scaled down by a factor of 100. Right: Decay length distributions (in mm) from open charm and bottom simulations [55].

PHENIX muon arms are compared on the left-hand side of Fig. 19. The yields in Tables 2 and 3 assume a displaced vertex cut of 1 mm. A good measurement of the cross section and R_{AA} as a function of p_T and y for open bottom production will be possible using $B \rightarrow J/\psi X$. Even at RHIC II luminosity, however, the yields are not expected to be large enough to permit a v_2 measurement.

5 Hidden heavy flavor: quarkonium

In this section we present a more detailed discussion of the theoretical motivation for studying heavy quarkonia in heavy-ion collisions. We also summarize the present experimental and theoretical status and describe the proposed RHIC II experimental quarkonia program.

5.1 Theoretical results

5.1.1 Cross sections in pp collisions

We discuss quarkonium production in the color evaporation model (CEM) which can be used to calculate the total quarkonium cross sections. The CEM [98, 99] has enjoyed considerable phenomenological success. In the CEM, the quarkonium production cross section is some fraction F_C of all $Q\overline{Q}$ pairs below the $H\overline{H}$ threshold where H is the lowest mass heavy-flavor hadron. Thus the CEM cross section is simply the $Q\overline{Q}$ production cross section with a cut on the pair mass but without any constraints on the color or spin of the final state. The produced $Q\overline{Q}$ pair then neutralizes its color by interaction with the collision-induced color field—"color evaporation". The Q and the $\overline{Q}$ either combine with light quarks to produce heavy-flavored hadrons or bind with each other to form quarkonium. The additional energy needed to produce heavy-flavored hadrons when the partonic center-of-mass energy, $\sqrt{\hat{s}}$, is less than $2m_H$, the heavy hadron threshold, is obtained nonperturbatively from the color field in the interaction region. Thus the yield of all quarkonium states may be only a small fraction of the total $Q\overline{Q}$ cross section below $2m_H$. At leading order, the production cross section of quarkonium state C in an AB collision is

$$\sigma_C = F_C \sum_{i,j} \int_{4m_Q^2}^{4m_H^2} d\hat{s} \int dx_1 dx_2 \; f_i^A(x_1,\mu^2) \; f_j^B(x_2,\mu^2) \; \hat{\sigma}_{ij}(\hat{s}) \; \delta(\hat{s} - x_1 x_2 s) \quad (4)$$

where $\hat{s}$ is the square of the parton-parton center of mass energy, $ij = q\overline{q}$ or gg and $\hat{\sigma}_{ij}(\hat{s})$ is the $ij \to Q\overline{Q}$ subprocess cross section. The total $Q\overline{Q}$ cross section takes $\hat{s} \to s$ in the upper limit of the integral over $\hat{s}$ in Eq. (4).

The fraction F_C must be universal so that, once it is fixed by data, the quarkonium production ratios should be constant as a function of $\sqrt{s}$, y and p_T. The actual value of F_C depends on the heavy quark mass, m_Q, the scale, μ^2, the parton densities, $f_i^A(x,\mu^2)$ and the order of the calculation. It was shown in Ref. [61] that the quarkonium production ratios were indeed constant, as

expected by the model.

Of course the leading order calculation in Eq. (4) is insufficient to describe high p_T quarkonium production since the $Q\overline{Q}$ pair p_T is zero at LO. Therefore, the CEM was taken to NLO [61, 100] using the exclusive $Q\overline{Q}$ hadroproduction code of Ref. [101]. At NLO in the CEM, the process $gg \to gQ\overline{Q}$ is included, providing a good description of the quarkonium p_T distributions at the Tevatron [100]. In the exclusive NLO calculation [101], both the Q and $\overline{Q}$ variables are integrated to obtain the pair distributions. Thus, although $\mu \propto m_Q$ in analytic LO calculations, at NLO, $\mu^2 \propto m_T^2 = m_Q^2 + p_T^2$ where p_T is that of the $Q\overline{Q}$ pair, $p_T^2 = 0.5(p_{T_Q}^2 + p_{T_{\overline{Q}}}^2)$.

We use parton densities and parameters that approximately agree with the $Q\overline{Q}$ total cross section data, given in Table 7, to determine F_C for J/ψ and Υ production. The fit parameters [102, 103] for the parton densities [104–106], quark masses and scales are given in Table 7 while the $Q\overline{Q}$ cross sections calculated with these parameters are compared to $pp \to Q\overline{Q}$ and $\pi^- p \to Q\overline{Q}$ data in Fig. 20.

$c\overline{c}$					$b\overline{b}$				
Set	PDF	m_c	ξ_T	$F_{J/\psi}$	Set	PDF	m_b	ξ_T	F_Υ
$\psi 1$	MRST HO	1.2	2	0.0144	$\Upsilon 1$	MRST HO	4.75	1	0.0276
$\psi 2$	MRST HO	1.4	1	0.0248	$\Upsilon 2$	MRST HO	4.5	2	0.0201
$\psi 3$	CTEQ 5M	1.2	2	0.0155	$\Upsilon 3$	MRST HO	5.0	0.5	0.0508
$\psi 4$	GRV 98 HO	1.3	1	0.0229	$\Upsilon 4$	GRV 98 HO	4.75	1	0.0225

Table 7
The parton densities (PDFs), quark masses, m_Q, and scale to mass ratios, $\xi_T = \mu/m_T$, used to obtain the 'best' agreement to the $Q\overline{Q}$ cross sections. The quark mass is given in GeV/c^2. The inclusive J/ψ production fraction, $F_{J/\psi}$, and the inclusive Υ production fraction, F_Υ, obtained from the data are also given [50].

We now describe the extraction of F_C in Eq. (4) for the individual quarkonium states. This is done using J/ψ cross sections measured in pp and $p + A$ interactions up to $\sqrt{s} = 63$ GeV. The data are of two types: the forward cross section, $\sigma(x_F > 0)$, and the cross section at zero rapidity, $d\sigma/dy|_{y=0}$. All the cross sections are inclusive with feed down from χ_c and ψ' decays. To obtain $F_{J/\psi}$ for inclusive J/ψ production, the normalization of Eq. (4) is obtained from a fit using the $c\overline{c}$ parameters in Table 7. The comparison of $\sigma_{J/\psi}$ to the $x_F > 0$ data for all four fits is shown on the left-hand side of Fig. 21. The ratios of the direct production cross sections to the inclusive J/ψ cross section can be determined from data on inclusive cross section ratios and branching fractions. These direct ratios, R_C, given in Table 8, are multiplied by the inclusive fitted $F_{J/\psi}$, also shown in Table 7, to obtain the direct production fractions, $F_C^{\rm dir} = F_{J/\psi} R_C$, for the various quarkonium states.

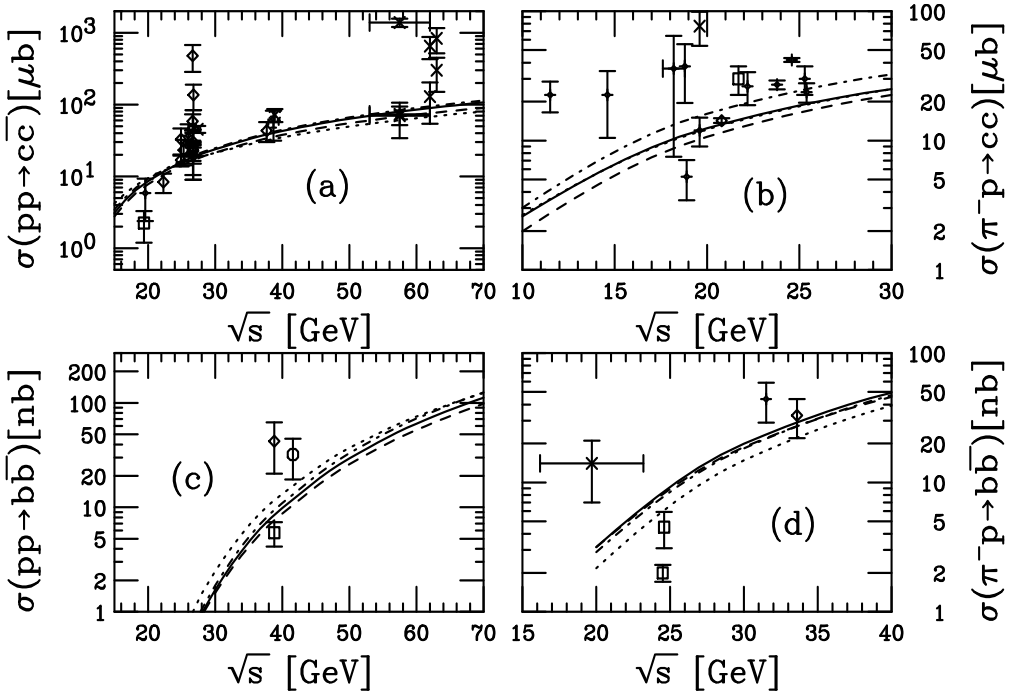

Fig. 20. The $c\overline{c}$, (a) and (b), and $b\overline{b}$, (c) and (d), total cross section data in pp and $\pi^- p$ interactions compared to NLO calculations. In (a) and (b), we show $\psi 1$ (solid), $\psi 2$ (dashed), $\psi 3$ (dot-dashed) and $\psi 4$ (dotted). In (c) and (d), we show $\Upsilon 1$ (solid), $\Upsilon 2$ (dashed), $\Upsilon 3$ (dot-dashed) and $\Upsilon 4$ (dotted) [50].

	J/ψ	ψ'	χ_{c1}	χ_{c2}	Υ	Υ'	Υ''	$\chi_b(1P)$	$\chi_b(2P)$
R_C	0.62	0.14	0.60	0.99	0.52	0.33	0.20	1.08	0.84

Table 8
Direct quarkonium production ratios, $R_C = \sigma_C^{\rm dir}/\sigma_{C'}^{\rm inc}$ where $C' = J/\psi$ and Υ. From Ref. [107].

The same procedure, albeit somewhat more complicated due to the larger number of bottomonium states below the $B\overline{B}$ threshold, is followed for bottomonium. For most data below $\sqrt{s} = 100$ GeV, the three bottomonium S states were either not separated or their sum was reported. No x_F-integrated cross sections were available so that the CEM Υ cross section were fitted to the effective lepton pair cross section at $y = 0$ for the three $\Upsilon(nS)$ states. The extracted fit fraction, $F_{\sum\Upsilon}$, combined with σ_Υ and compared to the data for all parameter sets in Table 7, is shown on the right-hand side of Fig. 21. Using the individual branching ratios of the Υ, Υ' and Υ'' to lepton pairs and the total cross sections reported by CDF [108], it is possible to extract the inclusive Υ fit fraction, F_Υ, given in Table 7. The direct production ratios obtained in Ref. [36] have been updated in Ref. [107] using recent CDF χ_b data. The resulting direct to inclusive Υ ratios, R_C, are also given in Table 8. The sub-threshold $b\overline{b}$ cross section is then multiplied by $F_C^{\rm dir} = F_\Upsilon R_C$ to obtain the direct bottomonium cross sections.

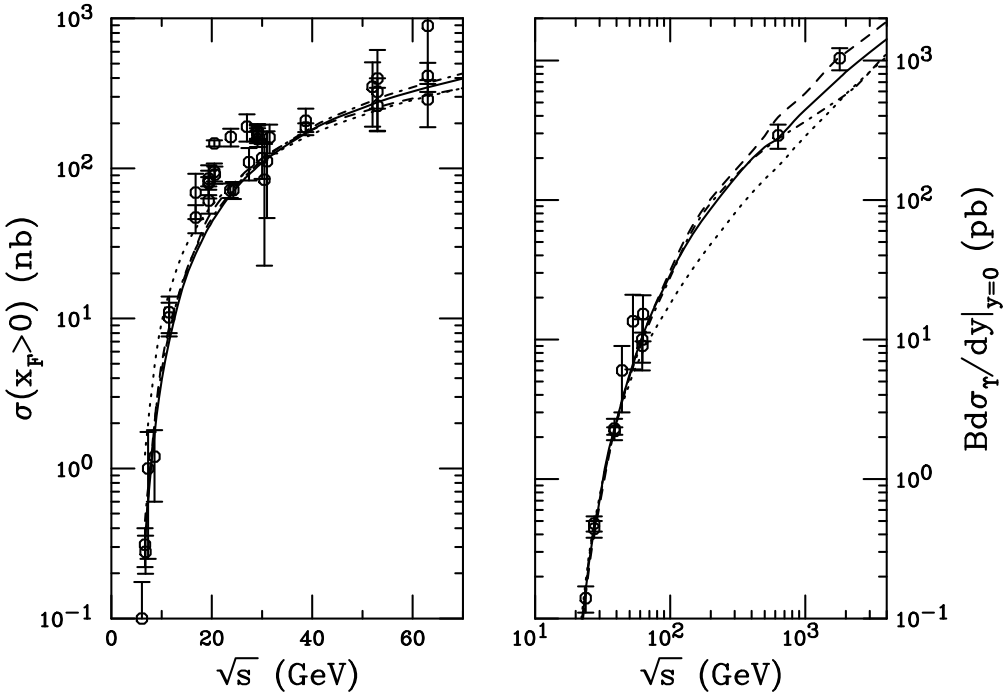

Fig. 21. Forward J/ψ (left) and combined $\Upsilon+\Upsilon'+\Upsilon''$ inclusive (right) cross sections calculated to NLO in the CEM. On the left-hand side, we show $\psi 1$ (solid), $\psi 2$ (dashed), $\psi 3$ (dot-dashed) and $\psi 4$ (dotted). On the right-hand side, we show $\Upsilon 1$ (solid), $\Upsilon 2$ (dashed), $\Upsilon 3$ (dot-dashed) and $\Upsilon 4$ (dotted) [50].

The total cross sections for the charmonium and bottomonium states in pp collisions at $\sqrt{s} = 200$ GeVare shown in Tables 9 and 10 respectively.

	$\sigma^{\rm inc}_{J/\psi}$ (μb)	$\sigma^{\rm dir}_{J/\psi}$ (μb)	$\sigma_{\chi_{c1}}$ (μb)	$\sigma_{\chi_{c2}}$ (μb)	$\sigma_{\psi'}$ (μb)
$\psi 1$	2.35	1.46	1.41	2.33	0.33
$\psi 2$	1.76	1.09	1.06	1.74	0.25
$\psi 3$	2.84	1.76	1.70	2.81	0.40
$\psi 4$	2.10	1.31	1.26	2.08	0.29

Table 9
The charmonium cross sections for 200 GeVpp collisions. The inclusive and direct J/ψ cross sections are both given.

The energy dependence, shown for both states in Fig. 21, is well reproduced by the NLO CEM. All the fits are equivalent for $\sqrt{s} = 100$ GeV but differ by up to a factor of two at 2 TeV. The high energy Υ data seem to agree best with the energy dependence of $\Upsilon 1$ and $\Upsilon 2$ although $\Upsilon 1$ underestimates the Tevatron result by a factor of ≈ 1.4.

	$\sigma_\Upsilon^{\rm inc}$ (nb)	$\sigma_\Upsilon^{\rm dir}$ (nb)	$\sigma_{\Upsilon'}$ (nb)	$\sigma_{\Upsilon''}$ (nb)	$\sigma_{\chi_b(1P)}$ (nb)	$\sigma_{\chi_b(2P)}$ (nb)
$\Upsilon 1$	6.60	3.43	2.18	1.32	7.13	5.54
$\Upsilon 2$	7.54	3.92	2.49	1.51	8.15	6.34
$\Upsilon 3$	5.75	2.99	1.90	1.15	6.21	4.83
$\Upsilon 4$	4.31	2.24	1.42	0.86	4.66	3.62

Table 10
The direct bottomonium cross sections for pp collisions at 200 GeV. The production fractions for the total Υ are multiplied by the appropriate ratios determined from data.

5.1.2 Cold nuclear matter effects on quarkonium production at RHIC

It is essential that the A dependence be understood in cold nuclear matter to set a proper baseline for quarkonium suppression in $A+A$ collisions. The NA50 collaboration has studied the J/ψ A dependence and attributed its behavior to dissociation by nucleons in the final state, referred to as nuclear absorption. However, the parton distributions are modified in the nucleus relative to free protons. This modification, referred to here as shadowing, is increasingly important at higher energies, as emphasized in Ref. [109]. We now discuss the interplay of shadowing and absorption in d+Au and $A+A$ collisions at RHIC.

Shadowing, the modification of the parton densities in the nucleus with respect to the free nucleon, is taken into account by replacing $f_j^p(x,\mu^2)$ in Eq. (4) by $F_j^A(x,\mu^2,\vec{b},z) = \rho_A(\vec{b},z)S^j(A,x,\mu^2,\vec{b},z)f_j^p(x,\mu^2)$ and adding integrals over the spatial coordinates. Here S^j is the shadowing parameterization. The density distribution of the deuteron is also included in these calculations but the small effects of shadowing in deuterium are ignored. The PHENIX J/ψ d+Au data as a function of rapidity show a dependence consistent with nuclear shadowing plus a small absorption cross section, common to all quarkonium states [110], of $1-3$ mb. The J/ψ production cross section is calculated in the CEM using Eq. (4) with the same mass and scale as in $c\overline{c}$ production. The calculations of the d+Au/pp and $A+A/pp$ ratios are done at LO to simplify the calculations since the LO and NLO ratios are equivalent [8].

To implement nuclear absorption in d+Au collisions, the per nucleon production cross section is weighted by the survival probability, $S^{\rm abs}$ [111],

$$S^{\rm abs}(\vec{b},z) = \exp\left\{-\int_z^\infty dz'\rho_A(\vec{b},z')\sigma_{\rm abs}(z'-z)\right\} \ , \tag{5}$$

where z is the longitudinal production point and z' is the point at which the state is absorbed. The nucleon absorption cross section, $\sigma_{\rm abs}$, typically depends on where the state is produced in the medium and how far it travels

through nuclear matter. If absorption alone is active, *i.e.* no shadowing so that $S^j \equiv 1$, then an effective minimum bias A dependence is obtained after integrating $S^{\rm abs}$ over the spatial coordinates. If $S^{\rm abs} = 1$ also, $\sigma_{{\rm d}A} = 2A\sigma_{pN}$. When $S^{\rm abs} \neq 1$, $\sigma_{{\rm d}A} \sim 2A^{\alpha}\sigma_{pN}$ where, if $\sigma_{\rm abs}$ is a constant, independent of the production mechanism for a hard sphere nucleus of constant density inside R_A, *ie.* $\rho_A = \rho_0\theta(R_A - b)$, $\alpha = 1 - 9\sigma_{\rm abs}/(16\pi r_0^2)$ with $r_0 = 1.2$ fm. The contribution to the full A dependence of α from absorption alone is only constant if $\sigma_{\rm abs}$ is constant and independent of the production mechanism [111]. The observed J/ψ yield includes feed down from χ_c and ψ' decays,

$$S^{\rm abs}_{J/\psi}(b,z) = 0.6 S^{\rm abs}_{J/\psi,\,{\rm dir}}(b,z) + 0.3 S^{\rm abs}_{\chi_c}(b,z) + 0.1 S^{\rm abs}_{\psi'}(b,z) \ . \tag{6}$$

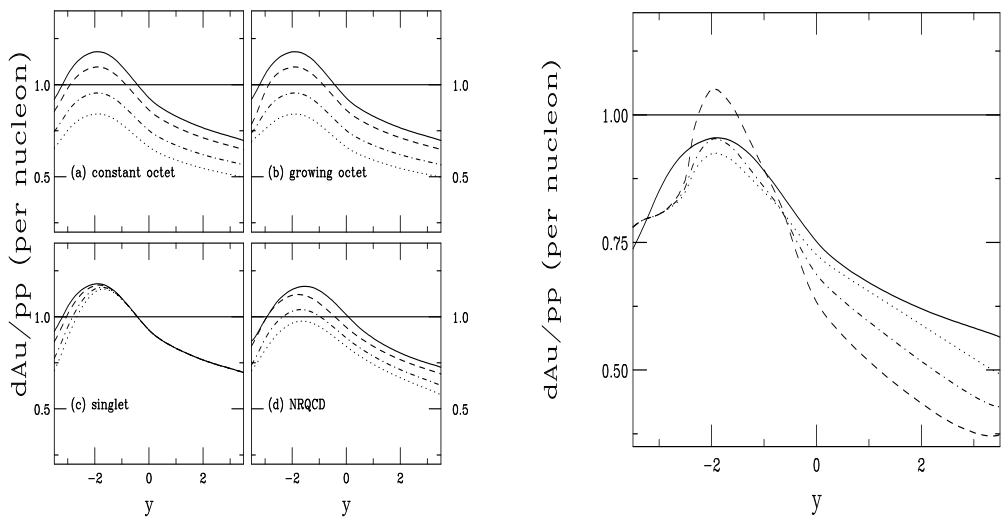

Fig. 22. Left-hand side: The J/ψ d+Au/pp ratio with EKS98 at 200 GeV as a function of rapidity for (a) constant octet, (b) growing octet, (c) singlet, all calculated in the CEM and (d) NRQCD. For (a)-(c), the curves are no absorption (solid), $\sigma_{\rm abs} = 1$ (dashed), 3 (dot-dashed) and 5 mb (dotted). For (d), we show no absorption (solid), 1 mb octet/1 mb singlet (dashed), 3 mb octet/3 mb singlet (dot-dashed), and 5 mb octet/3 mb singlet (dotted). Right-hand side: The J/ψ d+Au/pp ratio at 200 GeV for a growing octet with $\sigma_{\rm abs} = 3$ mb is compared for four shadowing parameterizations. We show the EKS98 (solid), FGSo (dashed), FGSh (dot-dashed) and FGSl (dotted) results as a function of rapidity. From Ref. [8], reprinted with permission from APS.

The J/ψ may be produced as a color singlet, a color octet or in a combination of the two. In color singlet production, the absorption cross section depends on the size of the $c\overline{c}$ pair as it traverses the nucleus, allowing absorption to be effective only while the cross section is growing toward its asymptotic size inside the target. On the other hand, if the $c\overline{c}$ is produced as a color octet, hadronization will occur only after the pair has traversed the target except at very backward rapidity. We have considered a constant octet cross section (hadronization outside the medium at all rapidity), as well as a growing octet

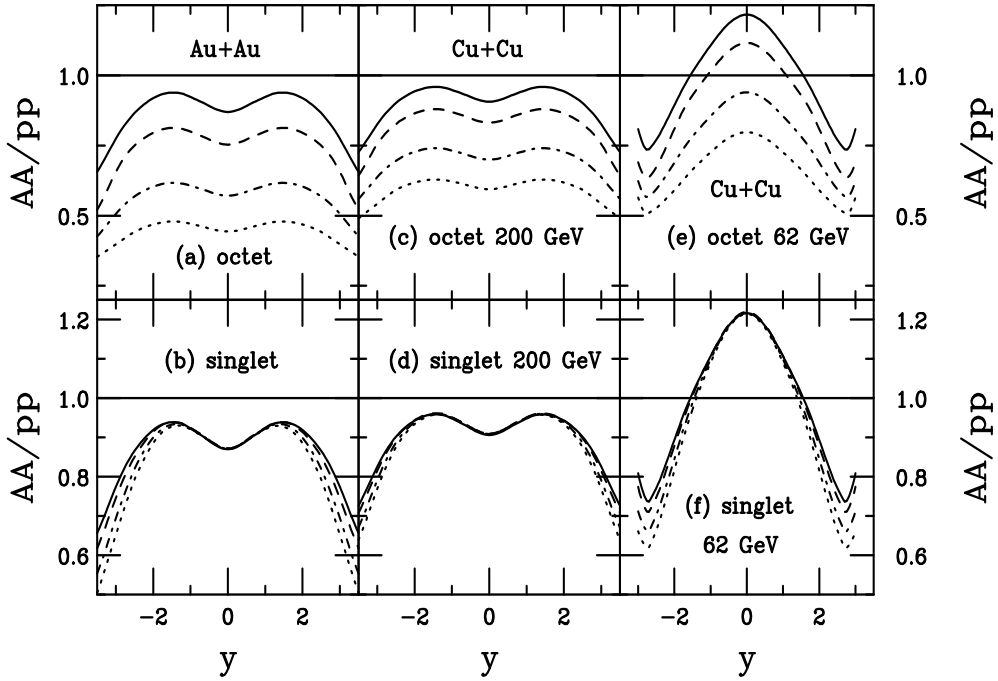

Fig. 23. The AA/pp ratio with the EKS98 parameterization as a function of y for octet (upper) and singlet (lower) absorption. In (a) and (b) we show the Au+Au results at 200 GeV while the Cu+Cu results are shown at 200 GeV (c) and (d) as well as at 62 GeV (e) and (f). The curves are $\sigma_{\rm abs} = 0$ (solid), 1 (dashed), 3 (dot-dashed) and 5 mb (dotted). From Ref. [9], reprinted with permission from Acta Physica Hungarica.

cross section which hadronizes to a color singlet inside the medium at backward rapidities. For singlets, $S^{\rm abs}_{J/\psi,\,{\rm dir}} \neq S^{\rm abs}_{\chi_c} \neq S^{\rm abs}_{\psi'}$ but, with octets, one assumes that $S^{\rm abs}_{J/\psi,\,{\rm dir}} = S^{\rm abs}_{\chi_c} = S^{\rm abs}_{\psi'}$. If this assumption is relaxed and the octet absorption cross sections depend on the final-state size, then $\sigma^{\psi'}_{\rm abs} > \sigma^{\chi_c}_{\rm abs} > \sigma^{J/\psi\,{\rm dir}}_{\rm abs}$ and $S^{\rm abs}_{J/\psi,\,{\rm dir}} > S^{\rm abs}_{\chi_c} > S^{\rm abs}_{\psi'}$. The feed down contributions then effectively lower the value of $\sigma_{\rm abs}$ needed to describe the data. As can be seen in Fig. 22, the difference between the constant and growing octet assumptions is quite small at large $\sqrt{s_{NN}}$ with only a small singlet effect at $y < -2$. Singlet absorption is also important only at similarly negative rapidities. At other rapidities singlet production is dominated by shadowing alone. Finally, we have also considered a combination of octet and singlet absorption in the context of the NRQCD approach, see Ref. [111] for more details. The combination of nonperturbative singlet and octet parameters changes the shape of the shadowing ratio slightly. Including the singlet contribution weakens the effective absorption. The results are shown integrated over impact parameter. The calculations use the EKS98 shadowing parameterization [112] since it gives good agreement with the trend of the PHENIX data. For results with other shadowing parameterizations, see Refs. [8, 9].

Several values of the asymptotic absorption cross section, $\sigma_{\rm abs} = 1$, 3 and 5 mb,

corresponding to $\alpha = 0.98$, 0.95 and 0.92 respectively using Eqs. (5) and (6), are shown in Figs. 22 and 23 for d+Au and $A+A$ collisions respectively. These values of $\sigma_{\rm abs}$ are somewhat smaller than those obtained for the sharp sphere approximation. The diffuse surface of a real nucleus and the longer range of the density distribution result in a smaller value of $\sigma_{\rm abs}$ than a spherical nucleus. As will be seen later, there is good agreement with the trend of the PHENIX data [113] for $\sigma_{\rm abs} = 0 - 3$ mb. Work is in progress to quantify the shadowing parameterization and absorption cross section more precisely over a range of energies [114].

The current RHIC data are not sufficiently precise to distinguish between J/ψ production and absorption in the CEM relative to that in the NRQCD approach. However, a measurement of the χ_c A dependence may be able to clarify the situation [111]. In the CEM, the J/ψ and χ_c distributions differ only in the value of F_C. In the NRQCD approach, the J/ψ is produced primarily in a color octet state while the χ_c is produced as a color singlet state. Thus while the production of both states would exhibit the same shadowing effect, a difference in the J/ψ and χ_c d+Au/pp ratios due to octet relative to singlet absorption may be measurable.

We now turn to the centrality dependence of J/ψ production in d+Au and $A + A$ collisions. In central collisions, inhomogeneous (spatially dependent) shadowing is stronger than the homogeneous (averaged over centrality) result. The stronger the homogeneous shadowing, the larger the inhomogeneity. In peripheral collisions, inhomogeneous effects are weaker than the homogeneous results but some shadowing is still present. Shadowing persists in peripheral collisions in part because the density in a heavy nucleus is large and approximately constant except close to the surface, and because the deuteron wave function has a long tail. Absorption is also expected to be stronger in central collisions.

To study the centrality dependence of shadowing and absorption, the d+Au/pp and $A + A/pp$ ratios are presented as a function of $N_{\rm coll}$,

$$N_{\rm coll}(b) = \sigma_{NN}^{\rm in} \int d^2 s T_A(s) T_B(|\vec{b} - \vec{s}|) \ ,$$

where T_A and T_B are the nuclear thickness functions and the inelastic nucleon-nucleon cross section, $\sigma_{NN}^{\rm in}$, is 42 mb at 200 GeV. In Figs. 24 and 25, the $N_{\rm coll}$ dependence is shown for several representative rapidities, $y = -2$, 0 and 2 for RHIC. The inhomogeneous shadowing parameterization is chosen to be proportional to the path length of the parton through the nucleus [109]. For more results, see Refs. [8, 9].

The dependence of the RHIC ratios on $N_{\rm coll}$ is almost linear, as seen in Figs. 24

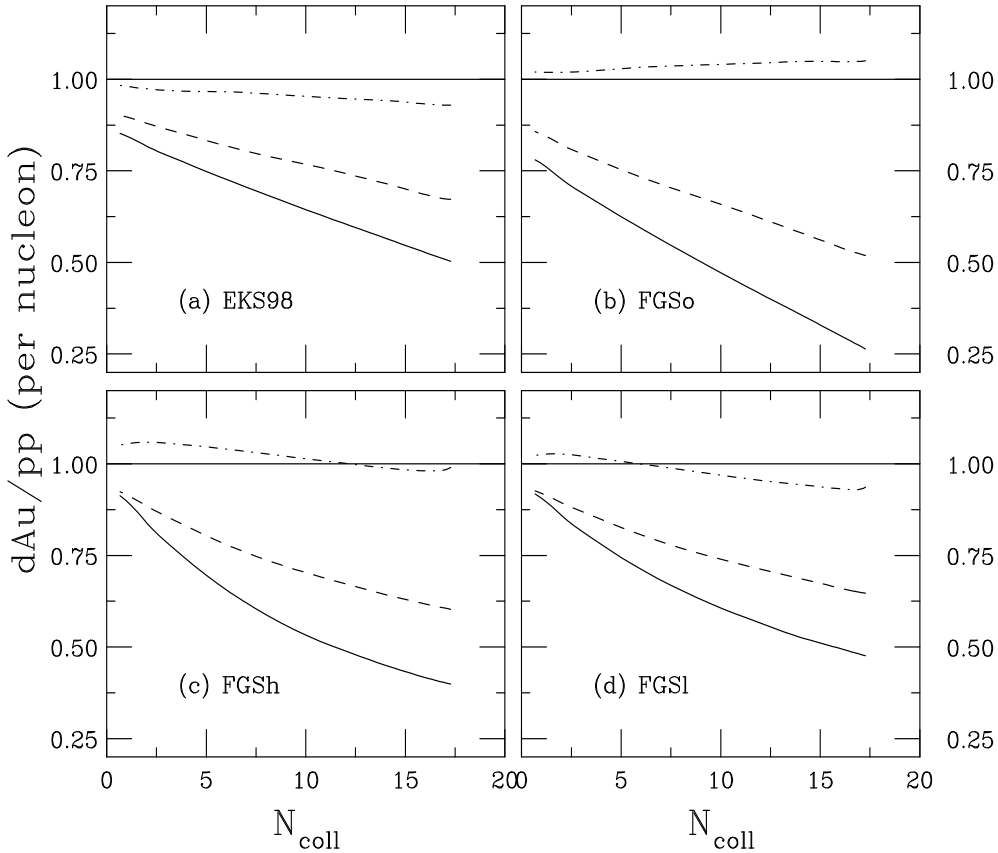

Fig. 24. The ratio d+Au/pp as a function of $N_{\rm coll}$ for the EKS98 (a), FGSo (b), FGSh (c) and FGSl (d) shadowing parameterizations. The calculations with EKS98 and FGSo use the inhomogeneous path length parameterization while that obtained by FGS is used with FGSh and FGSl. Results are given for $y = -2$ (dot-dashed), $y = 0$ (dashed) and $y = 2$ (solid) at 200 GeV for a growing octet with $\sigma_{\rm abs} = 3$ mb. From Ref. [8], reprinted with permission from APS.

and 25. The weakest $N_{\rm coll}$ dependence occurs in the antishadowing region, illustrated by the $y = -2$ result (dot-dashed curve). The overall dependence on $N_{\rm coll}$ is stronger than that obtained from shadowing alone, described in Ref. [109], where inhomogeneous shadowing effects depend strongly on the amount of homogeneous shadowing. Relatively large effects at low x are accompanied by the strongest impact parameter, b, dependence. In the transition region around midrapidity at RHIC, the b dependence of the ratio d+Au/pp due to shadowing is nearly negligible and almost all of the $N_{\rm coll}$ dependence at $y \sim 0$ can be attributed to absorption. The $y = -2$ results for color singlet production and absorption, in the antishadowing region, are fairly independent of $N_{\rm coll}$. The stronger AA/pp effect at $y = 0$ in Fig. 25(a) and (b) can be described by the convolution of antishadowing at $y \sim -2$ in $R_{\rm dAu}$ and shadowing at $y \sim 2$, resulting in the dip in AA/pp at $y = 0$ shown in Fig. 23.

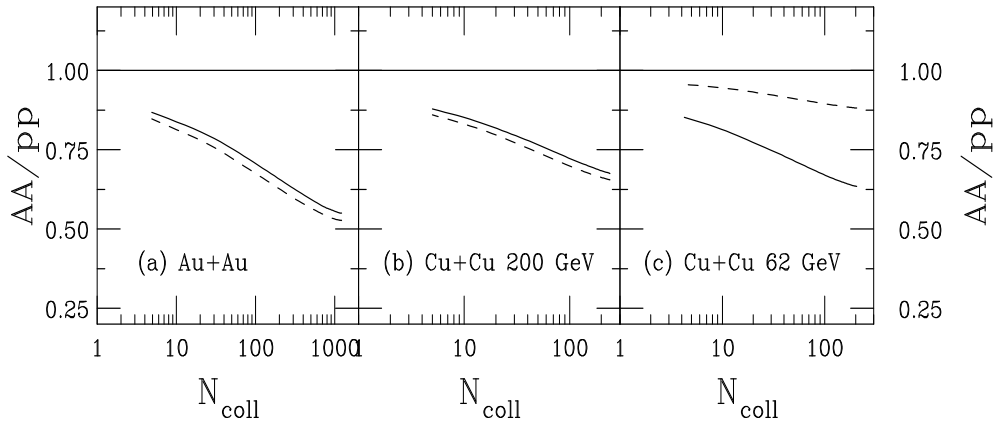

Fig. 25. The ratio AA/pp as a function of $N_{\rm coll}$ for a 3 mb octet absorption cross section and the EKS98 parameterization at $y = 0$ (dashed) and $y = 2$ (solid) for Au+Au at 200 GeV (a) and Cu+Cu at 200 GeV (b) and 62 GeV (c). From Ref. [9], reprinted with permission from Acta Physica Hungarica.

5.1.3 Models of quarkonium production in heavy-ion collisions

In-medium properties of quarkonium from lattice QCD:

Properties of heavy quarks have been used to characterize "thermal properties of the QCD vacuum" ever since the first lattice calculations at non-zero temperature [115]. Modifications of the interactions between heavy, static quarks in a thermal heat bath are clearly reflected by changes of the free energy which, in the zero temperature limit, reduces to the heavy quark potential [116]. To use this information to analyze thermal modifications of quarkonia requires an intermediate, phenomenological step: the construction of a temperature-dependent effective potential which then can be used in a non-relativistic Schrödinger equation [117–119] or a more refined coupled-channel analysis [120, 121]. Quite generically, the potential model analyses suggest a sequential suppression pattern where heavy quark bound states dissociate at temperatures at which their bound state radii become comparable to the Debye screening radius, illustrated in Fig. 26. Table 11 shows quarkonium dissociation temperatures from Ref. [122].

State	$J/\psi(1S)$	$\chi_c(1P)$	$\psi'(2S)$	$\Upsilon(1S)$	$\chi_b(1P)$	$\Upsilon(2S)$	$\chi_b(2P)$	$\Upsilon(3S)$
T_d/T_c	2.10	1.16	1.12	> 4.10	< 1.76	1.60	1.19	1.17

Table 11
Quarkonium dissociation temperatures [122], illustrating the effects of binding energy on the dissociation temperature.

More recently, the calculation of thermal hadron correlation functions and their spectral analysis [124] eliminated some of the ambiguities inherent in

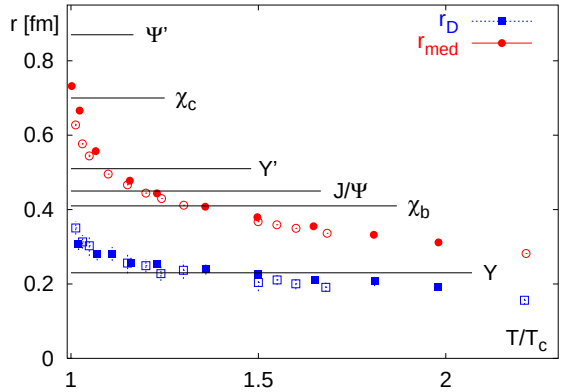

Fig. 26. Mean squared charge radii of some charmonium and bottomonium states compared to the Debye screening radius, $r_D \equiv 1/m_D$, and a related scale, $r_{\rm med}$, an estimate of the distance beyond which the force between a static $Q\overline{Q}$ pair is strongly modified by temperature effects [123]. Open (closed) symbols correspond to SU(3) (2-flavor QCD) calculations. From Ref. [116], reprinted with permission from Springer-Verlag.

the potential model approach. The spectral analysis, at least in principle, provides an ab-initio approach to the calculation of in-medium properties of heavy quark bound states. Its predictive power is reduced only by the application of statistical tools like the Maximum Entropy Method (MEM) which, however, can be steadily improved with further development of the available computing resources and numerical techniques. Predictions based on potential model calculations as well as the spectral analysis have been reviewed in recent studies that have been performed to analyze prospects for quarkonium studies at the LHC [50, 125]. In the following, the analysis of thermal hadron correlation functions and the extracted spectral functions are discussed.

The finite temperature, Euclidean time correlation functions,

$$G_H(\tau, \vec{r}, T) = \langle J_H(\tau, \vec{r}) J_H^\dagger(0, \vec{0}) \rangle \quad , \tag{7}$$

of hadronic currents, $J_H = \bar{q}(\tau, \vec{r}) \Gamma_H q(\tau, \vec{r})$, where Γ_H denotes a suitable product of gamma matrices that projects onto the appropriate quantum numbers of hadron H, are directly related to the spectral functions, $\sigma_H(\omega, T)$. These spectral functions encompass all information about thermal modifications of the hadron spectrum in channel H so that

$$G_H(\tau, \vec{r}, T) = \int_0^\infty d\omega \, \frac{d^3\vec{p}}{(2\pi)^3} \sigma_H(\omega, \vec{p}, T) \, \mathrm{e}^{i\vec{p}\cdot\vec{r}} \frac{\cosh(\omega(\tau - 1/2T))}{\sinh(\omega/2T)} \tag{8}$$

are directly related to experimental observables. In particular, the spectral function in the vector channel, $\sigma_V(\omega, \vec{p}, T)$, is directly related to the differential

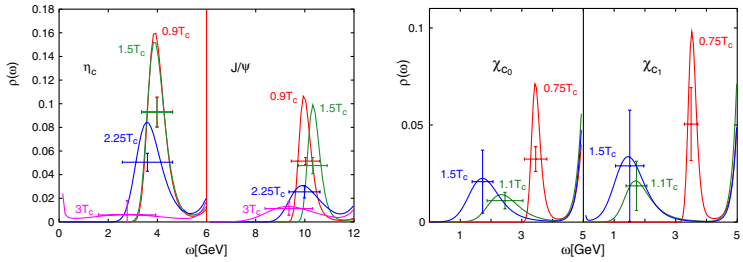

Fig. 27. Spectral functions of η_c, J/ψ (left) and and χ_{c0}, χ_{c1} (right) at various temperatures below and above T_c. The vertical bars give the error on the average value of the spectral function in the bin indicated by the horizontal bars.

cross section for thermal dilepton production,

$$\frac{dW}{d\omega d^3p} = \frac{5\alpha^2}{27\pi^2}\frac{\sigma_V(\omega,\vec{p},T)}{\omega^2(\mathrm{e}^{\omega/T}-1)} \quad . \tag{9}$$

Note that the rates obtained using this method do not include any contributions arising from the feed down of other channels into the vector channel [107, 126].

Some general aspects of the influence of a thermal medium on states with different quantum numbers can be deduced from the temperature dependence of the thermal correlation functions themselves and does not require the additional step of applying the MEM analysis which is based on probabilistic assumptions. Such comparisons show that zero-momentum, thermal hadron correlation functions in the ground state channels, *i.e.* the vector (J/ψ, Υ) and pseudoscalar (η_c, η_b) channels show little modification in a thermal medium up to temperatures $T \gtrsim 1.5\ T_c$. Correlation functions corresponding to radially excited charmonium states (χ_c), however, are already strongly modified close to or at T_c.

These generic features are reflected by the spectral functions. Although results from different groups currently still differ in detail, there are some general trends. The J/ψ and η_c remain unaffected by the thermal medium up to $T = 1.5\ T_c$, shown on the left-hand side of Fig. 27. At higher temperatures it is unclear whether the J/ψ already disappears at $\simeq 1.9\ T_c$ [127] or persists as a strongly modified resonance up to $2.25\ T_c$ [29]. The χ_{c0} and χ_{c1} both disappear at $T \lesssim 1.1\ T_c$, see the right-hand side of Fig. 27. Finite momentum J/ψ states show statistically significant but still small modifications for $T \lesssim 1.5\ T_c$ [128] due to collisional broadening by higher momentum gluons seen by bound states moving relative to the heat bath, see Fig. 28 [129]. Strong J/ψ binding above T_c is also supported by the analysis of spatial correlations [131] and the observed insensitivity of the thermal vector and pseudoscalar correlation functions to spatial boundary conditions [132].

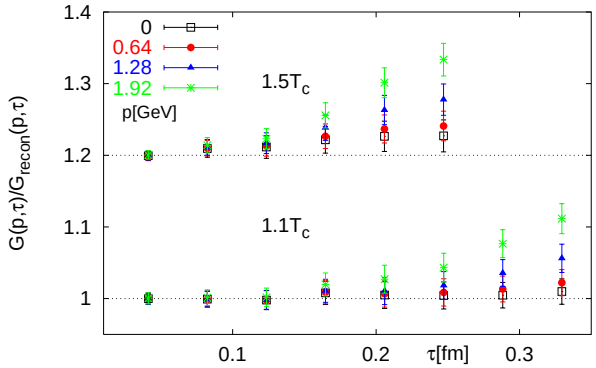

Fig. 28. The ratio of pseudoscalar correlation functions at non-zero momentum above and below T_c [128]. Deviations from the horizontal dotted lines for increasing p indicate stronger temperature-dependent modifications of the spectral functions.

Bottomonium studies are considerably more difficult since a larger lattice cut off is required to properly resolve these states, particularly for temperatures well above 2 T_c where the Υ states are expected to be dissolved. First exploratory finite temperature results on bottomonium have been reported for temperatures up to $\sim 1.5\ T_c$. At this temperature, no thermal modifications of the Υ and η_b have been observed, as expected. The χ_b correlation functions are, however, modified at $T \sim 1.5\ T_c$, similar to the scalar charmonium case at $T \simeq 1.1\ T_c$. To firmly establish the onset of medium modifications in bottomonium states, however, requires further refined studies of the bottomonium system at lower and higher temperatures.

More recent calculations of quarkonia screening by Mocsy and Petreckzy [130] suggest that the quarkonium states break up at lower temperatures. They use $2+1$ flavor lattice results on color screening to fix the parameters of the quarkonium potential used in the calculation of the quarkonium correlators. The most extreme potential compatible with the lattice results is used to derive upper bounds on the quarkonium dissociation temperatures in the quark-gluon plasma. In this case, although resonance structures appear in the spectral functions, the binding energy drops while the thermal width increases. When the width is larger than the binding energy, the state can no longer effectively be observed. These calculations suggest that the χ_c and ψ' break up at or below T_c while the J/ψ and higher Υ family resonances dissolve around $1.2T_c$. Only the $\Upsilon(1S)$ state would persist to $\sim 2T_c$. Further calculations are needed to resolve the issue.

Dynamical Coalescence:

The production of multiple $c\bar{c}$ pairs in a single collision introduces a new charmonium production mechanism [23]. Charmonium states can be formed

in-medium by coalescence of a c and a $\overline{c}$ quark from independently-produced $c\overline{c}$ pairs.

In the plasma phase, there are two basic approaches: statistical and dynamical coalescence. Both these approaches depend on being able to measure the quarkonium rate relative to total $Q\overline{Q}$ production. The first calculations in the statistical approach assumed an equilibrated fireball in a grand canonical ensemble [31, 32]. This approach could be reasonable at the high energies of the LHC, where the number of produced $c\overline{c}$ pairs is large. But, at lower energies, charm conservation is required since a $c\overline{c}$ pair is not produced in every event. More recent calculations assumed a canonical ensemble only for charm production [133–135]. Dynamical coalescence models assume that some of the produced $Q\overline{Q}$ pairs which would not otherwise do so can also form quarkonium. This coalescence can take place in the QGP [23, 46] or at hadronization [33]. The model includes the rapidity differences, $|\Delta y|$, between the Q and $\overline{Q}$ and shows that the enhancement is smaller for large $|\Delta y|$. The impact parameter dependence of statistical and dynamical coalescence is quite different. Statistical coalescence gives the largest enhancement in peripheral collisions where the volume of the plasma is small, with only a minor enhancement in central collisions. Dynamical coalescence produces a larger enhancement in central collisions where the number of $Q\overline{Q}$ pairs per event is greatest but still produces a significant effect in peripheral collisions [136].

Much smaller enhancements are predicted for secondary quarkonium production in the hadron gas, particularly for the J/ψ where the additional production is either small $(20-60\%)$ [34] or about a factor of two [35] at LHC energies and smaller still for RHIC. Larger enhancements may be expected for the ψ' [34]. The predictions depend strongly on the $J/\psi+\pi(\rho)$ cross sections, typically not more than $1-2$ mb [137].

These secondary production models are already testable at RHIC where factors of $2-3$ enhancement are expected from coalescence [23, 135]. Hard scattering of produced particles from different interactions is related to the idea of crosstalk between unrelated interactions [138]. Important crosstalk effects were predicted in e^+e^- collisions at LEP [138] but were not observed. If secondary quarkonium production is found, it would indicate the relevance of such effects. Secondary quarkonium may be separated from primary quarkonium, which is subject to suppression, by kinematic cuts that take advantage of the fact that different mechanisms dominate production in different kinematic regimes.

Predictions of J/ψ production by dynamical coalescence suffer from substantial uncertainties due to the dependence on the charm quark distributions in the medium. In fact, it is possible to turn this uncertainty into an advantage and probe the medium properties using the observed J/ψ momentum distributions. Two extremes can be considered [22]: either the initial c quark

distributions are unchanged by the presence of the medium or the c quarks are thermalized. If the charm quark distributions in the medium are identical to those of the initial production process, the interactions of charm quarks with the medium would be very weak. In this case, both the J/ψ rapidity and p_T distributions will be narrower than if no plasma is formed simply because the center of mass energy of secondary J/ψ production is lower than that of the initial nucleon-nucleon interactions. The lower energy results in a reduced $\langle p_T^2 \rangle$ and a narrower rapidity distribution. Thus, instead of the transverse momentum broadening expected from initial-state multiple scattering going from pp to $p + A$ to $A + A$, the average p_T^2 in $A + A$ would no longer exhibit the monotonic increase seen in pp and $p + A$ interactions for increasing A. On the other hand, if the charm quarks are assumed to be in thermal equilibrium with the surrounding medium, the charm interaction with the medium would be very strong. Any J/ψ's produced from thermalized charm quarks flowing with the medium would have a p_T distribution with a slope characteristic of the temperature of the system at the time they were formed, resulting in even narrower rapidity and p_T distributions. In either case, the effect would be largest in central collisions, reverting to "normal" broadening in peripheral collisions where on the order of one or fewer $c\overline{c}$ pairs will be produced since the number of $c\overline{c}$ pairs scales approximately with the number of collisions.

The $\langle p_T^2 \rangle$ of coalescence and suppression has been calculated by several groups [48, 49, 139]. No realistic calculations of the rapidity distribution from models including J/ψ coalescence are available for heavy-ion collisions so far but, based on the assumption of an underlying open charm distribution peaked at $y = 0$, it is predicted [22] that a strong charm coalescence contribution to J/ψ production will lead to a narrowing of the rapidity distribution, similar to the p_T distribution.

In order to extract the medium properties from secondary J/ψ production, systematic studies of J/ψ production in pp, $p + A$ and $A + A$ interactions are necessary. The pp data determine the intrinsic transverse momentum scale for a particular energy while the $p + A$ results fix the level of broadening due to cold nuclear matter effects which would then apply to $A + A$ interactions at the same energy.

Models of coalescence, of course, also include J/ψ suppression. In addition to the screening effects discussed previously, the J/ψ can scatter with quarks and gluons in the plasma which may break it up more efficiently than screening effects alone, especially if temperatures significantly above T_c are needed for screening to dissociate the directly produced J/ψ, as discussed in Ref. [33]. At low temperatures, relevant for SPS energies, $gJ/\psi \rightarrow c\overline{c}$ is effective for J/ψ breakup by a thermal gluon. However, at higher temperatures where the J/ψ should be more loosely bound, inelastic parton scattering, $g(q, \overline{q})J/\psi \rightarrow g(q, \overline{q})c\overline{c}$, calculated using the leading order matrix elements for gc and gq

scattering, is more effective.

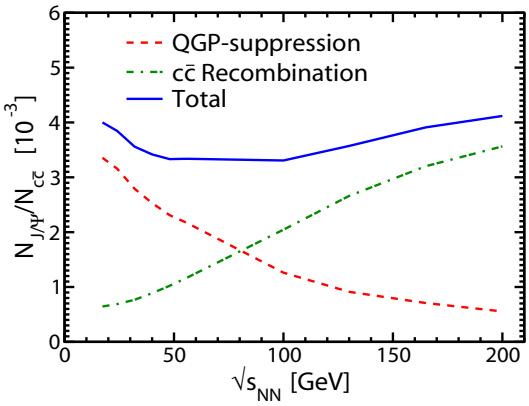

Fig. 29. Excitation function of the ratio of produced J/ψ to the number of $c\overline{c}$ pairs in central heavy-ion collisions for $N_{\rm part} = 360$. From Ref. [140], reprinted with permission from Elsevier.

The relative importance of J/ψ suppression and coalescence will change as a function of energy, as shown in Fig. 29 for central collisions of heavy nuclei with $N_{\rm part} = 360$, from Ref. [140]. The J/ψ yield is dominated by primordial production at SPS energies and by coalescence at the full RHIC energy.

Other Models:

Comovers: The comover model, proposed in Refs. [141–143] and further developed by Capella *et al.*, see most recently Ref. [144], describes J/ψ suppression in nucleus-nucleus collisions by final-state interactions with the dense medium created in the collision, the "comovers". The SPS J/ψ data are reproduced with a small effective dissociation cross section, $\sigma_{\rm co} = 0.65$ mb [145]. At RHIC energies, comover interactions alone would suggest stronger suppression than at the CERN SPS since the density of produced particles is larger at RHIC. Since the produced particle density is largest at midrapidity, comover interactions alone would predict stronger suppression at $y = 0$ than at forward rapidity [146].

However, although the comover model is based on rate equations, the gain term was only previously considered in Ref. [142] and reintroduced by Capella *et al.* in an attempt to account for the stronger observed suppression at forward rapidity at RHIC [144]. The open charm cross section at forward rapidity, where RHIC data are not yet very precise, was obtained from the shape of PYTHIA simulations of the rapidity distribution. As expected, coalescence effects are stronger at midrapidity so that the behavior calculated in Ref. [146] is reversed in Ref. [144] and forward suppression is found to be larger.

Sequential Suppression: As discussed previously, interpretation of the quarkonium dissociation temperatures in Table 11 suggests a sequential suppression pattern in which the quarkonium states dissolve when the system is at or above T_d. Applied to RHIC, the ψ' and χ_c would be completely suppressed above a critical energy density, $\epsilon(T_d)$ while the temperature at RHIC is too high for direct J/ψ suppression by color screening. Since the turn on of suppression at $\epsilon(T_d)$ would result in a step-wise suppression pattern, the suppression is typically smeared over a range of impact parameters.

Several models of sequential suppression have been proposed [147–150]. Most include some level of normal cold nuclear matter effects but neglect gluon dissociation of final-state J/ψ's. The $\langle p_T^2 \rangle$ of J/ψ suppression, is typically flat or decreasing with centrality in these scenarios.

In Ref. [147], the normal absorption cross section is fixed by the RHIC d+Au data in each rapidity region and then applied to the Au+Au data. The threshold energy density model, originally proposed in Ref. [148], suppresses the J/ψ yield above a threshold energy density, neglecting χ_c and ψ' feed down. It was recently applied to RHIC but included no rapidity dependence [149]. The most dynamically complete model of sequential suppression describes suppression in a dynamically-expanding quark-gluon fluid using relativistic hydrodynamics [150].

Conformal Field Theory: Recently, $\mathcal{N} = 4$ super Yang-Mills theory, a conformally-invariant field theory, has been applied to J/ψ suppression [151]. The screening length is described by the dynamics of a color single $Q\overline{Q}$ dipole of velocity v moving through the hot plasma. In its rest frame, the dipole feels the medium as a hot wind moving past it. The screening length in this medium decreases as $\gamma^{-1/2}$ or $(1-v^2)^{-1/4}$ so that the quarkonium dissociation temperature would decrease with increasing v (p_T). Thus high p_T J/ψ's could be suppressed by the plasma while low p_T J/ψ's are unaffected. Such novel suppression patterns are only observable at RHIC for sufficiently high luminosities [151].

5.2 Status of Quarkonium Physics at the CERN SPS

The prospects of a "clean" QGP signature, destruction of the J/ψ by color screening, was discussed in the landmark paper by Matsui and Satz in 1986 [27]. This triggered an extensive experimental program at the CERN SPS. HELIOS-III [152] and NA38 [153] (subsequently NA50 [154] and currently NA60 [155]) made detailed measurements of the dimuon invariant mass spectrum around midrapidity. Despite early enthusiasm and enormous statistics (see Fig. 30), the picture that evolved is still rather ambiguous. The SPS mea-

surements must also be understood in light of the many results on quarkonium production in $p+A$ collisions from fixed target experiments. The status of the SPS program is summarized in this section.

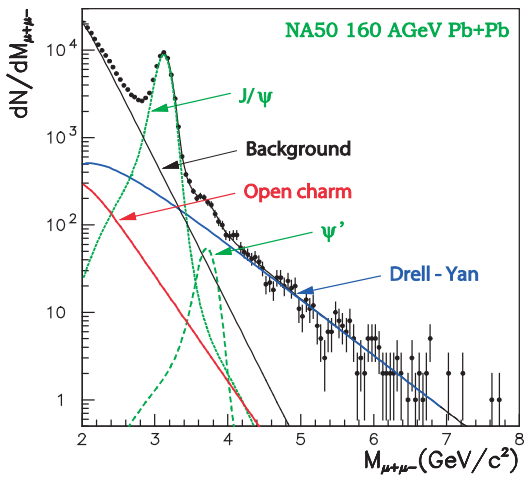

Fig. 30. Dimuon invariant mass spectrum from 158 AGeV Pb+Pb collisions at NA50. Modified from Ref. [26], reprinted with permission from Elsevier.

Feed down contributions (see Fig. 31) from higher charmonium states, $\chi_c \to J/\psi\gamma$ ($\sim 30\%$) and $\psi' \to J/\psi\pi\pi$ ($\sim 10\%$), are important [156, 157]. The χ_c has not yet been measured by the heavy-ion detectors at the SPS although it has been seen in pp and $p+A$ experiments there. These measurements are extremely difficult and the large scatter of available data depicted in Fig. 32 indicates that better measurements are desperately needed. Although the NA60 experiment is planning to conduct this analysis, the feasibility with the present data sets still has to be verified.

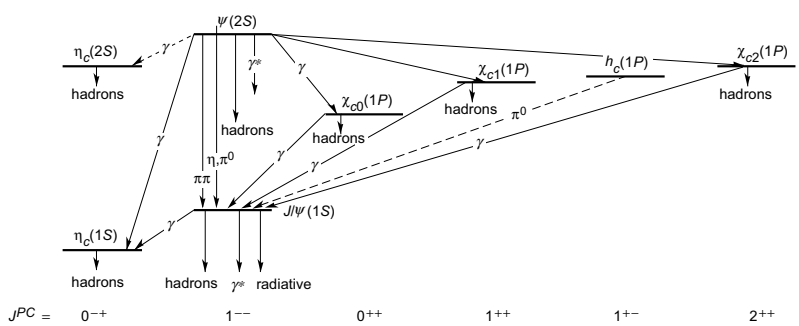

Fig. 31. Charmonium mass levels and spin states. Common feed down channels are indicated.

The J/ψ and ψ' have substantially modified cross sections when produced in normal (cold) nuclear matter. Considerable effort has gone into studying $p+A$ data from six targets covering a wide range of nuclei, from Be to Pb, measured with proton beam energies of 400 and 450 GeV [159]. The $p+A$ J/ψ and ψ' data were fitted assuming a single effective absorption cross section for each charmonium state (*ie.* no explicit treatment of feed down effects), and without

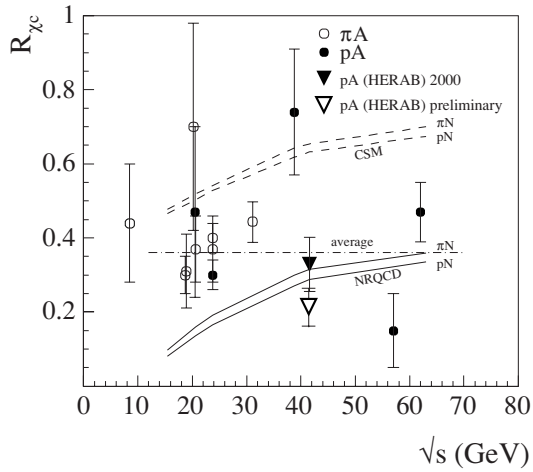

Fig. 32. The fraction, R_{χ_c}, of observed J/ψ's originating from radiative $\chi_{c1,2} \to J/\psi\gamma$ decays as a function of energy for proton and pion beams. From Ref. [156], reprinted with permission from IOP.

shadowing (analyses including shadowing effects are now underway [160]) or comover absorption [45]. It was concluded that absorption cross sections of 4.2 ± 0.5 mb and 7.7 ± 0.9 mb for the J/ψ and ψ' respectively should be used to predict the cold nuclear matter baseline suppression for Pb+Pb collisions at $158A$ GeV beam energy.

Studies of the A dependence in cold matter were also made at Fermilab over a larger x_F range, albeit at higher $\sqrt{s_{NN}}$ [161]. A very strong x_F dependence was observed for $x_F > 0.2$, as depicted in Fig. 33. Effects such as shadowing, absorption and energy loss play roles at different x_F, resulting in the observed dependence [8].

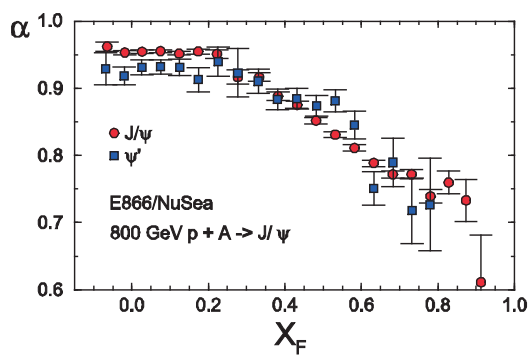

Fig. 33. Measurement of J/ψ and ψ' absorption in 800 GeV $p + A$ collisions as a function of x_F at the Tevatron [161], reprinted with permission from APS.

Figure 34 summarizes the SPS results on J/ψ and ψ' suppression in Pb+Pb S+U and $p + A$ collisions [162, 163]. The figure shows measured J/ψ and ψ' yields (normalized to the Drell-Yan dimuon yield since it is proportional to the number of collisions) as a function of the average path length of the $c\bar{c}$ pair through the nucleus, L, a measure of centrality. The measured yields

are divided by those expected from cold nuclear matter effects, calculated using the effective nuclear absorption cross sections, fit to the $p + A$ data, mentioned earlier. The $p + A$ and S+U data in Fig. 34 have been rescaled to $\sqrt{s_{NN}} = 17.3$ for comparison with the Pb+Pb data. Isospin corrections were applied to the Drell-Yan cross sections. Strikingly, the heavy-ion J/ψ data show no suppression beyond that expected from cold nuclear matter up to $L \sim 7$ fm, after which suppression beyond cold nuclear matter expectations becomes significant.

Alternatives to QGP models of suppression, such as the comover model, are able to describe the observed J/ψ suppression by assuming breakup of the bound state by comoving matter [45]. Although these approaches make some unrealistic assumptions about the hadron density, it is possible that some fraction of the observed suppression is due to comover absorption.

The ψ' suppression in Fig. 34 is similar to that of the J/ψ although suppression beyond cold nuclear matter effects becomes significant at a much shorter path length, $L \sim 4$ fm, *e.g.* in peripheral S+U collisions. Thus the ψ' appears to be more readily suppressed in the final state. This may be because the ψ', lying 50 MeV below the $D\overline{D}$ threshold, can be more easily broken up by interactions in the medium. The strong ψ' suppression measured by NA50 has been interpreted as both total suppression of the ψ' by color screening [164] and a larger interaction cross section for comovers [165].

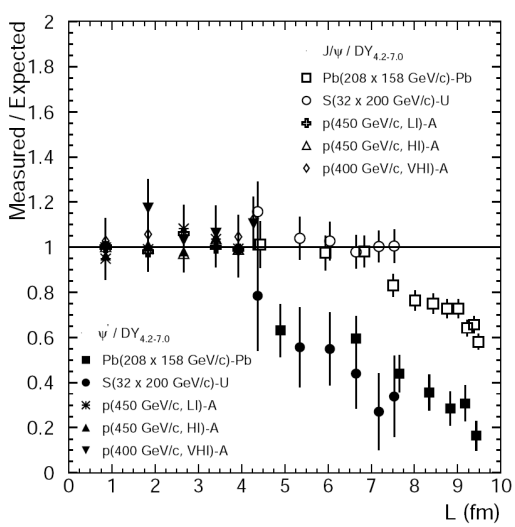

Fig. 34. The ratio of measured J/ψ and ψ' yields to those expected from cold nuclear matter effects in heavy-ion and $p + A$ collisions as a function of the $c\bar{c}$ path length through the colliding nuclei [162]. The measured and expected yields are both normalized to the Drell-Yan yields in the mass range $4.2 < M < 7$ GeV. The lighter systems are scaled to $\sqrt{s_{NN}} = 17.3$ GeV for comparison with the Pb+Pb data and isospin corrections are applied to the Drell-Yan yields.

The NA60 In+In J/ψ measurements exhibit a level of suppression similar to

the NA50 Pb+Pb data [166]. The J/ψ suppression observed in $A+A$ interactions at the SPS can, for the most part, be accounted for by the assumption that the more loosely bound ψ' and χ_c states are both suppressed by plasma production, eliminating their contribution to the inclusive J/ψ measurement. The direct J/ψ contribution is assumed to not be suppressed at the SPS [164, 167]. However this indirect J/ψ suppression picture does not seem to be easily reconciled with the strong observed ψ' suppression for path lengths corresponding to rather peripheral collisions, see Ref. [163], well before any reduction in the J/ψ yield is observed.

Charm production was not measured in heavy-ion experiments at the SPS until very recently. Figure 30 shows that the open charm contribution to the dilepton continuum in the J/ψ mass region is negligible at the SPS. Open charm measurements are, however, key to understanding the intermediate mass dilepton region. The NA60 experiment has used displaced vertices to separate charm decays from prompt dileptons. They have presented preliminary In+In results which show that while the enhancement in the intermediate mass region is confirmed, it is inconsistent with enhanced open charm. Instead, the enhancement is consistent with a prompt dilepton source [168].

The picture emerging from SPS studies is still somewhat ambiguous. In spite of the good precision of the heavy ion data for both J/ψ and ψ', and the effort that went into determining the cold nuclear matter baseline from $p+A$ data, the centrality dependence of the suppression pattern is insufficient to draw unique conclusions. On the other hand, the vast experience gained at the SPS can and should be taken into account at RHIC. The main lesson learned is that a simple J/ψ measurement in $A+A$ collisions as a function of centrality is insufficient to draw unique conclusions, even when a cold nuclear matter baseline is available. Rather, a systematic and detailed study of all related aspects, *i.e.*, a systematic study of open charm, J/ψ, ψ', and χ_c production in pp, $p+A$, and $A+A$ collisions is required. Centrality, rapidity, and A dependence studies are mandatory so that competing models based on different mechanisms can be differentiated.

5.3 Quarkonium measurements to date at RHIC

All of the published J/ψ results from RHIC to date are from PHENIX. Some preliminary J/ψ results from STAR were presented at Quark Matter 2008. PHENIX measures quarkonium yields by reconstructing their invariant mass from dilepton decays. Dielectrons are used in the central arms ($|\eta| < 0.35$) and dimuons are used in the muon arms ($1.2 < |\eta| < 2.2$). STAR uses dielectrons within the TPC acceptance ($|\eta| < 1$).

PHENIX has reported J/ψ results at 200 GeV from pp [44, 113, 169], d+Au [47, 113], Au+Au [42] and Cu+Cu collisions [43]. STAR reported preliminary high p_T J/ψ measurements in pp and Cu+Cu collisions at Quark Matter 2008 [170].

PHENIX reported observation of $\Upsilon \to \mu^+\mu^-$ for $1.2 < |y| < 2.2$ in 200 GeV pp collisions from RHIC Run 5 [171]. This very low statistics measurement (27 counts in both muon arms combined) was used to make a preliminary cross section estimate of $\mathrm{BR}(d\sigma/dy)_{y=1.7} = 45.2 \pm 9.5\,(\mathrm{stat}) \pm 6.3\,(\mathrm{sys})$ nb. STAR observed about 50 $\Upsilon \to e^+e^-$ at $|y| < 1$, leading to a preliminary cross section of $\mathrm{BR}(d\sigma/dy)_{y=0} = 91 \pm 28\,(\mathrm{stat}) \pm 22\,(\mathrm{sys})$ nb [172]. In both cases, the cross section is for the lowest three Υ states combined. It would be difficult to make definitive Υ measurements at present RHIC luminosities, but crude measurements of the Υ nuclear modification factor by both PHENIX and STAR are expected to be possible at RHIC with about 10 times the Run 4 integrated luminosity, which will most likely be available after the next long Au+Au run.

5.3.1 Baseline quarkonium measurements at RHIC

PHENIX has measured J/ψ cross sections in pp [44] and d+Au collisions [47, 113] at 200 GeV. The rapidity dependence is summarized in Fig. 35. The left side shows the invariant J/ψ cross section in pp collisions while the right side shows the nuclear modification factor, R_{dAu}, for minimum bias d+Au collisions.

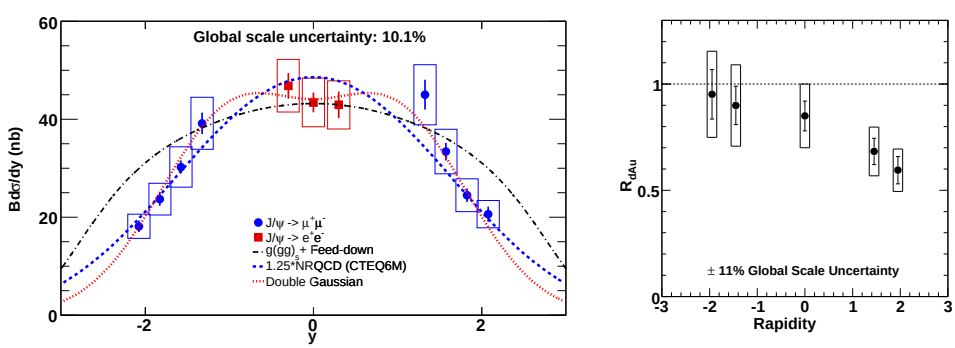

Fig. 35. The rapidity dependence of the pp J/ψ cross section at 200 GeV [44] (left–hand side, reprinted with permission from APS) and the nuclear modification factor for minimum bias d+Au collisions [47] (right-hand side). The curves on the left–hand side are fits used to extract the total cross section and estimate the systematic error. The deuteron is defined to be moving toward positive rapidity.

The data shown on the right-hand side of Fig. 35 are compared [47] with d+Au calculations [8] that include shadowing (EKS98 [112] and nDSg [173])

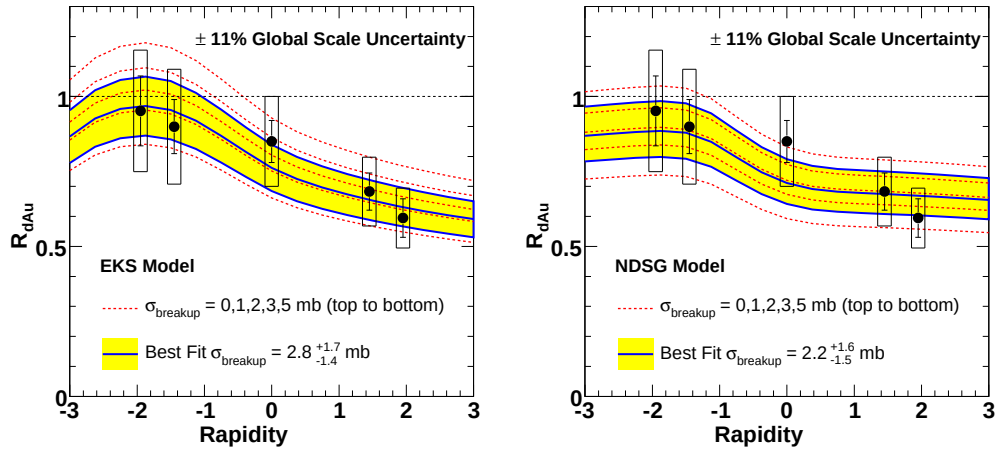

Fig. 36. The rapidity dependence of the d+Au J/ψ invariant yield at 200 GeV [47] compared with calculations [8] including shadowing and a $J/\psi N$ breakup cross section. The left-hand side compares the data with calculations using the EKS98 parameterization [112] while the right-hand side employs the nDSg parameterization [173].

and $J/\psi N$ breakup in Fig. 36. The shaded bands show the one standard deviation limits of fitting the $J/\psi N$ breakup cross section. The extracted values are consistent, within large uncertainties, with the 4.2 ± 0.5 mb cross section determined at the CERN SPS [159, 174].

The J/ψ nuclear modification factor in d+Au collisions is shown as a function of centrality in Fig. 37 [47] for the forward, central and backward rapidity regions covered by the three PHENIX arms. The shaded bands show the same calculation as in Fig. 36 but the breakup cross section is now fit to the data in each rapidity region. The $N_{\rm coll}$ dependence is the same because the impact parameter dependence of the shadowing is assumed to be proportional to the J/ψ path length through the medium in both cases [8]. It is evident that the parameters are not well constrained by the current d+Au data.

5.3.2 Quarkonium measurements in heavy-ion collisions at RHIC

Measurements with the statistical precision needed to provide a strong test of models of J/ψ production in heavy-ion collisions are now available from RHIC. These PHENIX measurements are from the Run 4 Au+Au and the Run 5 Cu+Cu data sets. The main features are summarized here.

Figure 38 shows the J/ψ nuclear modification factor, R_{AA}, measured in 200 GeV Au+Au collisions at both central and forward/backward rapidities [42], along with the ratio of forward to midrapidity R_{AA} values, $R_{AA}^{\rm forward}/R_{AA}^{\rm mid}$. Some

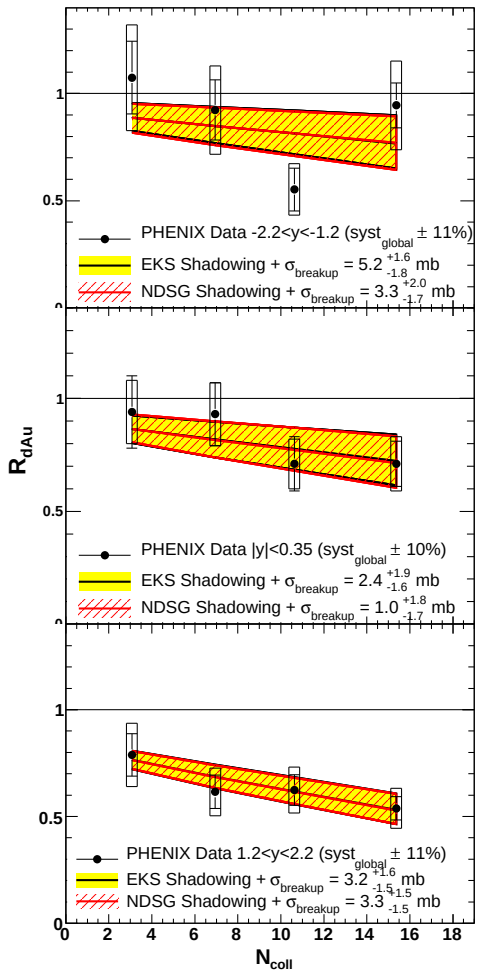

Fig. 37. The nuclear modification factor in d+Au collisions measured at forward (bottom), central (middle) and backward (top) rapidity as a function of centrality. The deuteron is moving toward forward rapidity. The curves, including both shadowing and nuclear breakup, are discussed in the text. From Ref. [47], reprinted with permission from APS.

systematic uncertainties cancel in the ratio. The ratio $R_{AA}^{\rm forward}/R_{AA}^{\rm mid}$, in the lower panel of Fig. 38, shows that when $N_{\rm part} > 150$ the Au+Au nuclear modification factor at forward rapidity is only about 60% of that at midrapidity. Thus the Au+Au data show that the suppression is weaker at the maximum transverse energy density (midrapidity). The weaker suppression could be due to either entrance channel effects (shadowing) or final-state effects such as J/ψ formation by coalescence of uncorrelated charm quarks.

Figure 39 shows the nuclear modification factor for Au+Au and Cu+Cu at central and forward/backward rapidity, along with $R_{AA}^{\rm forward}/R_{AA}^{\rm mid}$. Within un-

certainties, the data for Cu+Cu and Au+Au agree where they overlap in $N_{\rm part}$. It is of considerable interest to see what constraints the d+Au data place on the cold nuclear matter contribution to the heavy-ion R_{AA} by using the fits discussed in the previous section. However, $R_{AA}^{\rm forward}/R_{AA}^{\rm mid}$ is independent of the breakup cross section in those models because the rapidity dependence of the absorption model is small in the range of the data [8]. Thus the model calculation of $R_{AA}^{\rm forward}/R_{AA}^{\rm mid}$ reflects only the effects of the assumed shadowing model. To explore how the d+Au data constrain the forward to midrapidity ratio for heavy ions, an ad hoc model was used to parameterize the d+Au data. In the ad hoc model, the breakup cross section is allowed to vary independently at $y = 0$ and $|y| = 1.7$. The resulting parameterizations of the d+Au data can be used to predict the cold nuclear matter contribution to the heavy-ion R_{AA} independently at each rapidity, with independent uncertainties, and allow the constraints on $R_{AA}^{\rm forward}/R_{AA}^{\rm mid}$ to be quantified. The calculations for EKS98 are compared with the heavy-ion data in Fig. 39. The nDSg results are similar. The cold nuclear matter R_{AA} predicted by the ad hoc fits to the d+Au data are in good agreement with the Cu+Cu R_{AA} measured in more peripheral collisions. This is illustrated in Fig. 40, which shows the survival probability relative to cold nuclear matter effects on the Cu+Cu data, calculated using the ad hoc fits to the d+Au data shown in Fig. 39. Below $N_{\rm part} \sim 50$ the survival probability is consistent with unity within the $\sim 15\%$ uncertainties. Beyond that, the uncertainty in the cold nuclear matter reference rapidly worsens.

The bottom panel of Fig. 39 shows that the existing d+Au data allow the additional suppression from hot nuclear matter at forward rapidity to be anywhere between zero and a factor of two for central Au+Au collisions. Clearly, better d+Au data are required before the effects from cold nuclear matter are quantified for Au+Au collisions. The Run 8 d+Au data set will provide a greatly improved cold nuclear matter reference.

The left-hand side of Fig. 41 [175] compares the PHENIX Au+Au data to the comover model [146], with shadowing and comover interactions, where the suppression is predicted to be larger at $y = 0$ than at $y = 1.7$, in disagreement with the data. The right-hand side of the figures compares the $y = 0$ Au+Au data with calculations containing charmonium dissociation by thermal gluons with no coalescence [48, 176]. All of these calculations overestimate midrapidity J/ψ suppression. Figure 42 [175] compares the midrapidity data to model calculations [22, 48, 176–178] including J/ψ formation by coalescence. These models generally do a better job of describing the magnitude, if not the detailed centrality dependence, of the suppression. However they rely heavily on the rapidity density of charm production as input to the coalescence calculations and the charm distributions are currently not very precisely defined by the RHIC data, especially at forward rapidity.

The extended comover interaction model [144], including J/ψ coalescence as

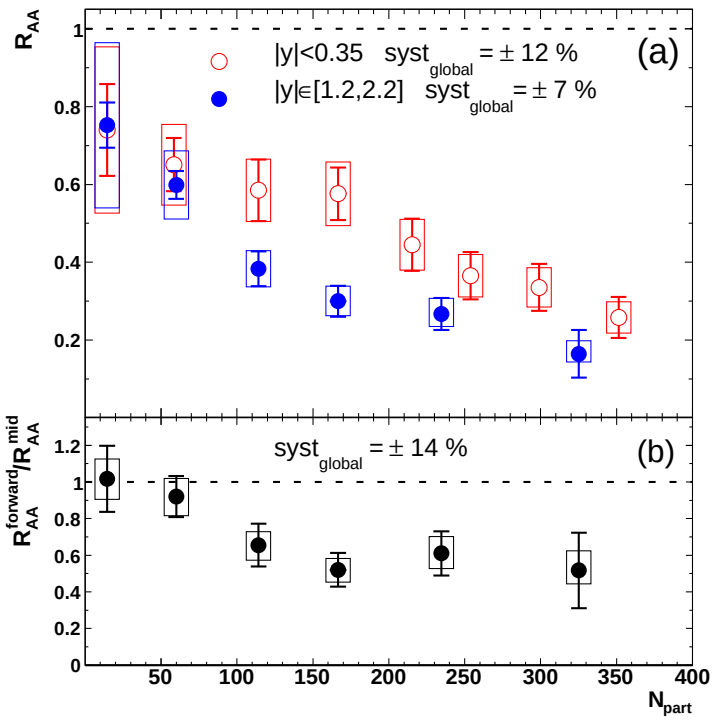

Fig. 38. The nuclear modification factor as a function of centrality for 200 GeV Au+Au collisions measured at central and forward/backward rapidity [42].

well as suppression, shown in Fig. 43, has slightly stronger suppression at forward rapidity than seen in Fig. 41, in better agreement with the data. A midrapidity calculation by Zhao and Rapp [49] extends the suppression and coalescence model [140] to include momentum-dependent dissociation rates. The $J/\psi N$ cross section was reduced to 1.5 mb, closer to the PHENIX d+Au data, and a longer charm quark thermalization time, 7 fm/c was assumed to better match the magnitude of the observed suppression in the most central Au+Au collisions. The calculated centrality dependence of R_{AA} at midrapidity is in good agreement with the data. Reference [49] also presents calculations of $\langle p_T^2 \rangle$ and R_{AA} as a function of p_T, discussed later.

PHENIX also showed a measurement of the nuclear modification factor for 62 GeV Cu+Cu collisions at Quark Matter 2005. While this measurement has relatively low statistics, the 62 GeV data exhibit similar, and perhaps slightly stronger, suppression in the most central collisions than that seen in 200 GeV Cu+Cu collisions, consistent with predictions of color screening and coalescence [140].

There have been recent predictions of $c\bar{c}$ coalescence effects on the rapidity and p_T dependence of the J/ψ yield [48, 49, 139]. Figure 44 shows the average J/ψ p_T^2, $\langle p_T^2 \rangle$, obtained from data below 5 GeV/c, as a function of $N_{\rm part}$ for

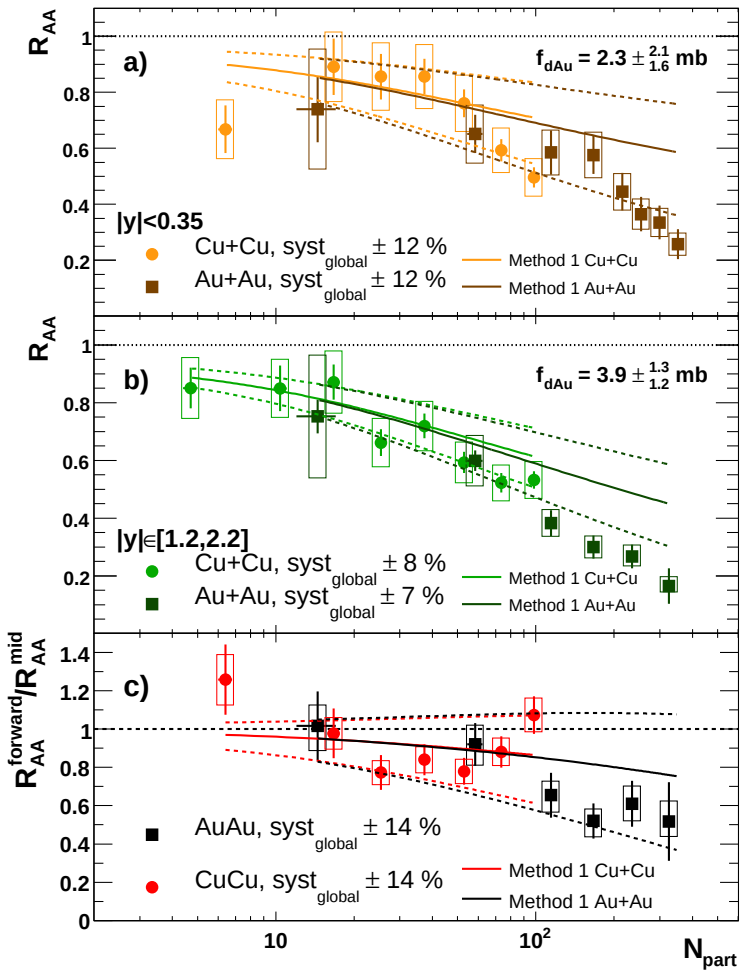

Fig. 39. The nuclear modification factor as a function of centrality for 200 GeV Au+Au and Cu+Cu collisions measured at central and forward/backward rapidity [42, 43].

Au+Au and Cu+Cu collisions in the two rapidity regions covered by PHENIX [42, 43]. The Au+Au and Cu+Cu data are in very good agreement at the same $N_{\rm part}$ and rapidity. Also shown are calculations by Yan, Zhuang and Xu [48] and Zhao and Rapp [49] that incorporate the effect of coalescence on the centrality dependence of $\langle p_T^2 \rangle$. An earlier calculation by Thews [139] predicts a larger and more steeply rising J/ψ $\langle p_T^2 \rangle$ than shown in Fig. 44. However all calculations with J/ψ coalescence agree fairly well with the $\langle p_T^2 \rangle$ data, even though coalescence is a smaller fraction of the J/ψ yield in Refs. [48, 49].

There has been considerable interest in what might be learned about the J/ψ production mechanism from $R_{AA}(p_T)$, since coalescence formation of the J/ψ is generally expected to decrease at high p_T. PHENIX has published data on the p_T dependence of R_{AA} in Au+Au and Cu+Cu collisions [42, 43]. The

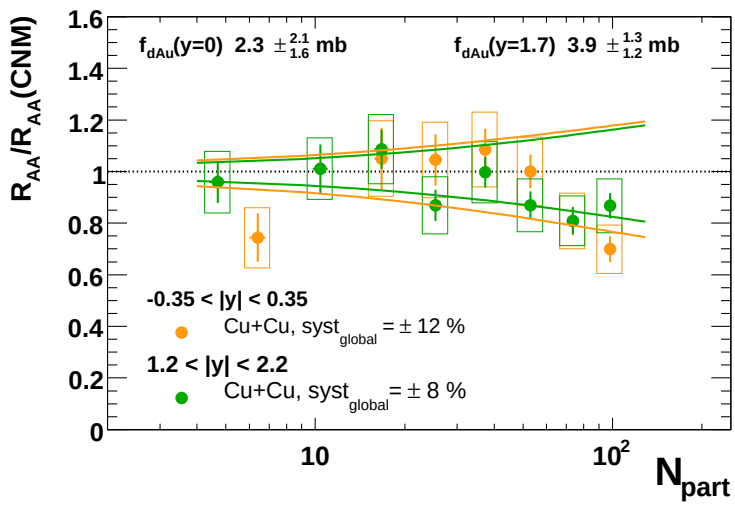

Fig. 40. The ratio of measured R_{AA} to the cold nuclear matter R_{AA} calculated from the ad hoc fits to d+Au data, shown in Fig. 39, for Cu+Cu collisions. The one standard deviation uncertainties in the cold nuclear matter reference are indicated by bands around unity.

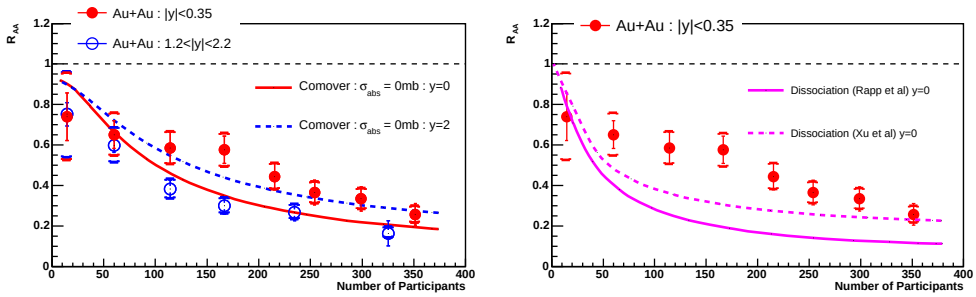

Fig. 41. Left: Nuclear modification factor compared with a comover model calculation at central and forward/backward rapidity. Note that the model predicts maximum suppression at $y = 0$. Right: Comparison with two calculations of gluon dissociation at midrapidity [175].

measured R_{AA} for central collisions is flat within errors over the range of the data, extending only to 5 GeV/c. Zhao and Rapp [49] have calculated the p_T dependence of the J/ψ R_{AA} at midrapidity and compared it with the p_T dependence in Au+Au collisions measured at four different centralities. The calculation agrees well with the data, as seen in Fig. 45. Coalescence is most important for more central collisions at low p_T. It is a negligible effect above 4 GeV/c. An important goal of future measurements is to improve the poor statistical precision of the current data beyond about 3 GeV/c. Any AdS/CFT effects [151] would become important for $p_T > 5$ GeV/c, beyond the current

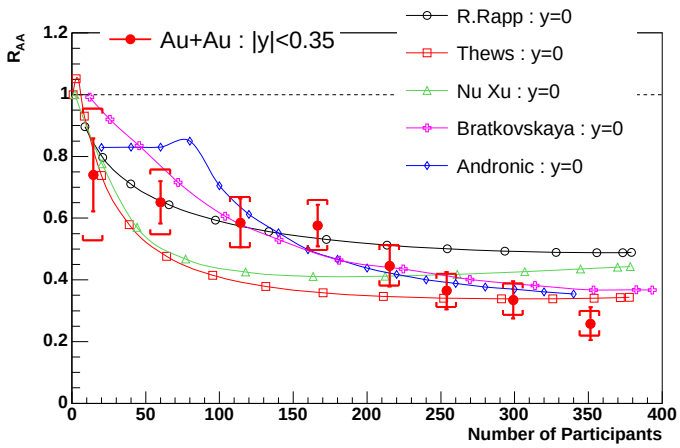

Fig. 42. Nuclear modification factor compared with models that include J/ψ formation by coalescence. The calculations are for $y = 0$ only [175]. See the text for details.

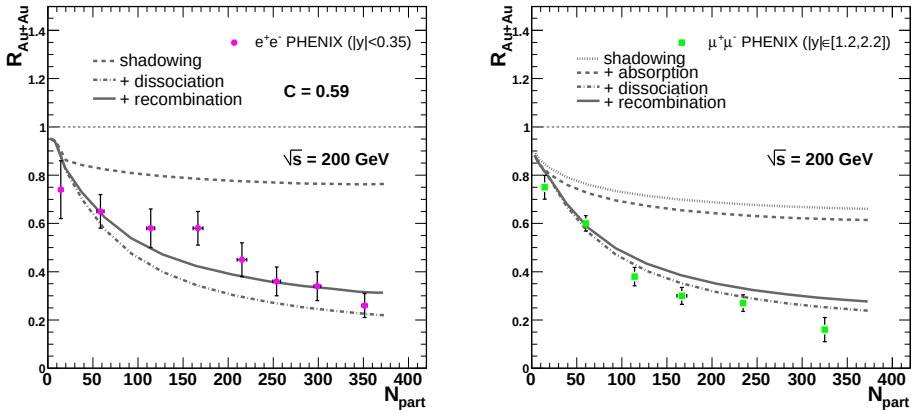

Fig. 43. Calculation of J/ψ R_{AA} at central and forward rapidities in the comover model with coalescence [144].

range of precision. Extending the R_{AA} measurement with good precision to much higher p_T will require RHIC II luminosity, as discussed later.

A strong charm coalescence contribution to J/ψ production will result in a narrower rapidity distribution, similar to the p_T distribution. PHENIX extracted the RMS of the rapidity distribution versus centrality from their Au+Au, Cu+Cu and pp data [42–44]. The extracted Cu+Cu data are independent of centrality within $2-3\%$ uncertainties. The extracted Au+Au values decrease by 10% with increasing centrality, roughly a two standard deviation reduction.

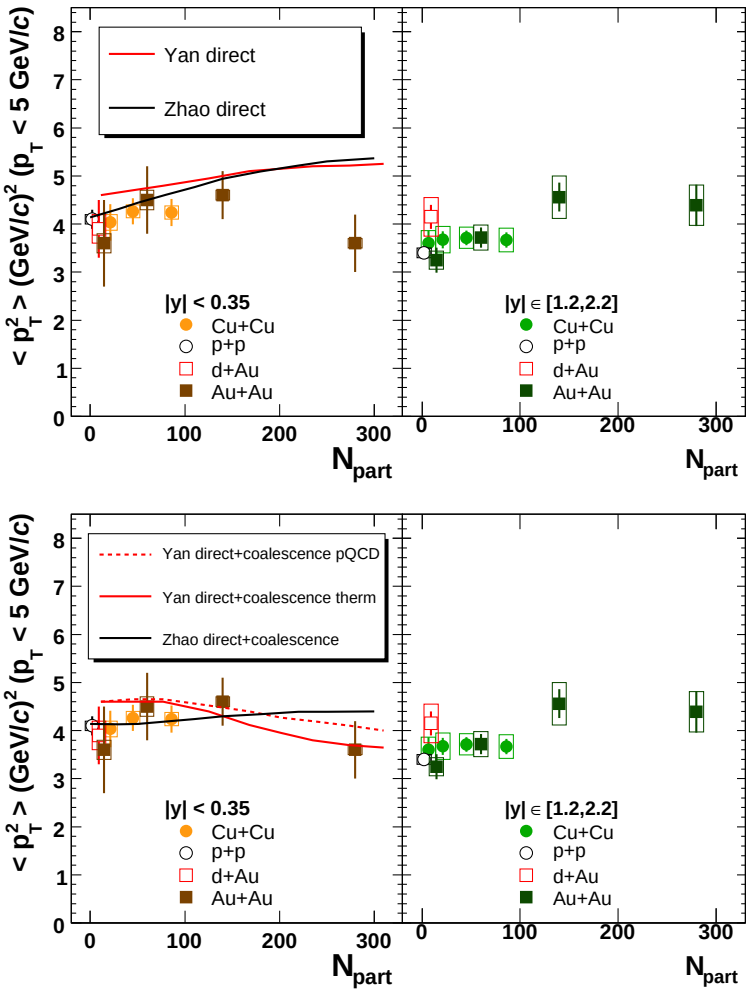

Fig. 44. The $\langle p_T^2 \rangle$ for 200 GeV Au+Au and Cu+Cu collisions measured by PHENIX at midrapidity (left) and forward/backward rapidity (right) [43] compared with calculations without coalescence (top) and including coalescence (bottom) [48, 49]. The p_T integrals are restricted to less than 5 GeV/c to reduce the systematic errors.

In summary, while there is evidence favoring a coalescence contribution to the J/ψ yield in central collisions, it does not seem to be definitive. The suppression as a function of centrality shown in Figs. 42 and 43 is reasonably consistent with models that include coalescence, as is the $\langle p_T^2 \rangle$ in Fig. 44 and $R_{AA}(p_T)$ shown in Fig. 45. The observed narrowing of the rapidity distribution is weak, and its implication will not be clear until the open charm rapidity distribution is better determined experimentally and the effects of shadowing and other initial state phenomena are understood. The initial-state effects should be better constrained by the more precise d+Au data obtained in Run 8. Precise open charm rapidity distributions will require upgrades to the PHENIX and STAR detectors to identify open charm and bottom decays by displaced

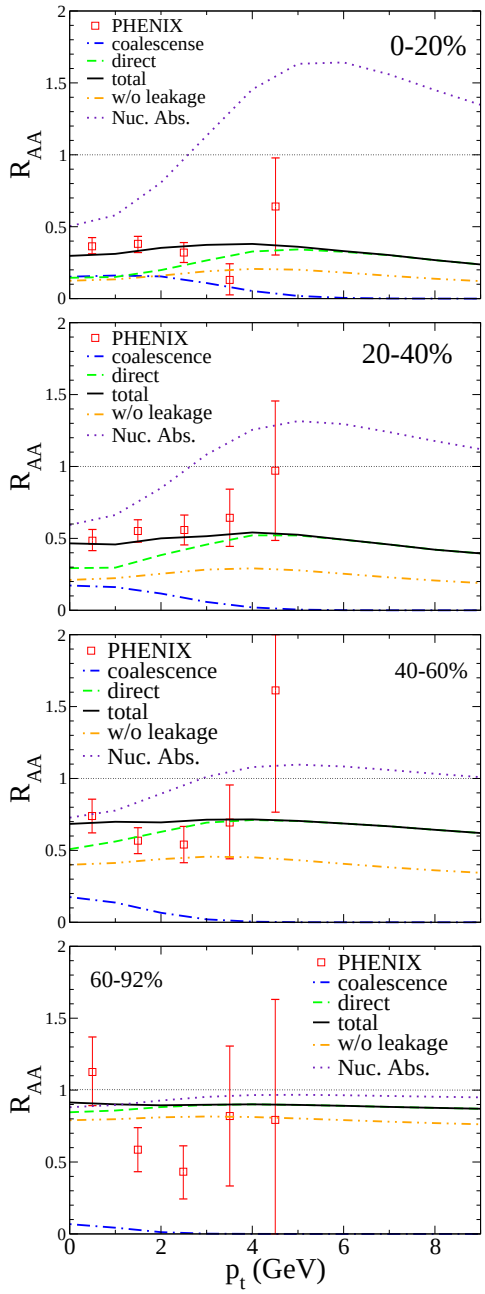

Fig. 45. The J/ψ R_{AA} at midrapidity as a function of p_T in Au+Au collisions in four centrality bins, compared with calculations including formation by coalescence [179].

decay vertices. On the other hand, the predicted narrowing of the p_T distribution relative to broadening of the primordial J/ψ p_T distribution expected in heavy-ion collisions is based on a steeply falling charm p_T distribution, well established by the existing open charm data, and the calculations seem to reproduce the data reasonably well.

PHENIX is attempting to extract the J/ψ v_2 from Run 7 Au+Au data. The current restricted heavy-ion data sets place major limitations on the precision of a v_2 measurement. A statistically meaningful J/ψ polarization measurement is also not feasible with the present data sets. Precise v_2 and polarization measurements will need RHIC II luminosity.

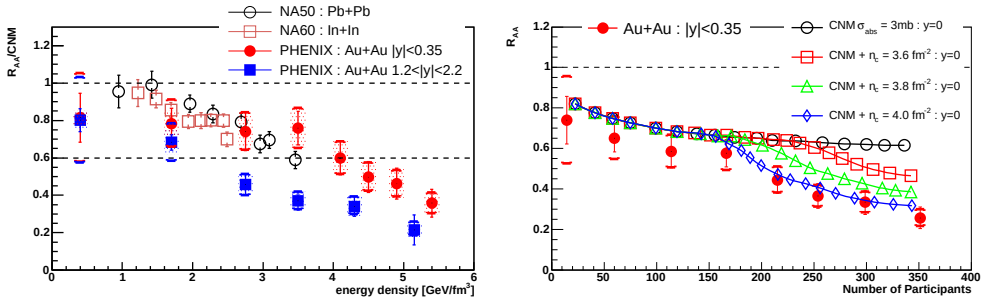

Fig. 46. Left: The RHIC and SPS R_{AA} data compared [175] with sequential charmonium suppression. The two dashed lines indicate no suppression ($R_{AA}/\mathrm{CNM} = 1$) and complete suppression of ψ' and χ_c ($R_{AA}/\mathrm{CNM} = 0.6$). Right: The PHENIX midrapidity data compared with a model including a threshold density for J/ψ suppression [149].

The sequential charmonium suppression model of Ref. [147] has been applied to the preliminary PHENIX data and to the SPS data. Normal nuclear absorption is parameterized by an effective absorption cross section that accounts for all cold nuclear matter effects. The SPS $p + A$ data give a larger effective J/ψ absorption cross section than the RHIC d+Au data, as also implied by Ref. [114]. Three values of σ_{abs} are extracted from the d+Au data, one for each rapidity bin, similar to the ad hoc model applied to the PHENIX data in Figs. 39 and 40. These values are used to obtain the survival probability in $A+A$ collisions. When N_{part} is converted to energy density, ϵ, and the survival probabilities for color screening and cold nuclear matter are included, the SPS and RHIC data were found to lie on a common suppression curve as a function of energy density. However the more precise, final PHENIX data, which show that the forward rapidity J/ψ yield is significantly more suppressed than the midrapidity yield, are inconsistent with such a picture, as can be seen on the left-hand side of Fig. 46 [175]. The measured $\langle p_T^2 \rangle$ is also inconsistent with this scenario.

The threshold energy density model applied to RHIC, Ref. [149], is compared to the midrapidity PHENIX data on the right-hand side of Fig. 46 for several values of the critical density. The model behavior is quite similar to that of the measured midrapidity Au+Au R_{AA} for a critical density of 4 fm^{-2}. However, since it does not have any rapidity dependence, it cannot describe the much stronger suppression for Au+Au at forward/backward rapidity. It also cannot

explain the centrality dependence of the Cu+Cu suppression.

The hydrodynamic model of Ref. [150] fits the critical temperatures to the midrapidity PHENIX Au+Au data but disagrees with R_{AA} as a function of centrality. Since many effects are not included, it is difficult to draw conclusions.

5.4 Proposed RHIC II quarkonia measurements

Unlike other probes, quarkonia measurements are guided by predictions from lattice QCD calculations. Color screening modifies the linear rise of the QCD potential at large distances. The quarkonia spectral functions quantify the temperature dependence of the potential. Since quarkonia suppression is determined by the plasma temperature and the binding energy (equivalently the quarkonium size and the Debye screening length), measuring the sequential disappearance of these states acts as a QCD thermometer.

Thus the importance of a comprehensive study of **all** experimentally accessible quarkonium states cannot be overstated. A systematic study of heavy quarkonium spectroscopy, with a complete determination of the suppression pattern of the quarkonium states, remains the **most direct probe of deconfinement**. It is also the signature that most closely resembles a thermometer of the hot initial state which, with future improved lattice calculations, can be directly compared to QCD.

While J/ψ physics is as compelling as it was in 1986 when first proposed by Matsui and Satz [27], the systematic study of all quarkonia states, and especially bottomonium, feasible at RHIC II, provides a more complete QGP probe than heretofore possible.

Table 12 relates the main physics topics to the relevant probes and subsequent detector requirements. The ability of a program at RHIC II to make these measurements can be judged from the yields given in Tables 2, 3, and 4. The measurements that are possible at RHIC without the luminosity upgrade are the J/ψ rapidity and p_T distributions at full energy. The measurements that are newly possible at RHIC II are those of the excited charmonium states (ψ' and χ_c) and the bottomonium states ($\Upsilon(1S)$, $\Upsilon(2S)$ and $\Upsilon(3S)$). High p_T J/ψ measurements, precise measurements of the J/ψ v_2 and polarization, and excitation functions of heavy flavor measurements will be possible only at RHIC II. The possible statistical precision is illustrated in Fig. 47 which shows the statistical significance of the J/ψ nuclear modification factor R_{AA} in Au+Au at high p_T, and Fig. 48, which presents the expected J/ψ v_2 precision in Au+Au collisions at RHIC II [180]. It is evident that a comprehensive program to use quarkonium as a QCD thermometer to provide direct evidence

of deconfinement is possible only with RHIC II luminosity.

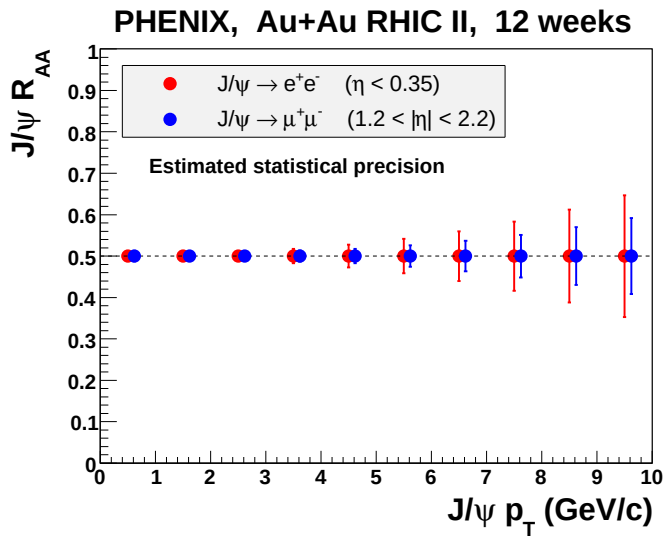

Fig. 47. The statistical significance after background subtraction of the J/ψ $R_{AA}(p_T)$ in PHENIX at central and forward rapidity from a 12 week Au+Au run with RHIC II luminosity (22 nb^{-1} delivered). Values above 5 GeV/c are a p_T extrapolation of current PHENIX data.

The measurements needed to study the excited charmonium states, χ_c and ψ', have quite different problems. The ψ' measurement technique is the same as that for the J/ψ, namely reconstruction of dilepton decays, but requires ~ 100 times greater integrated luminosity for the same yield. In addition, the ψ' measurement is more difficult because the background under the peak in the invariant mass spectrum is significant, increasing the integrated luminosity needed for precision measurements. The presence of the VTX detector in PHENIX will lead to significantly better mass resolution in the central arms by allowing a measurement of the full bend angle of the electrons - only the track angle after the magnetic field is measured at present. The FVTX detector is crucial to the ψ' measurement in the muon arms because it both reduces the combinatorial background and improves the mass resolution, as shown in Fig. 49. A ψ' measurement is certainly feasible at RHIC II. The χ_c measurement can be done with the $\chi_c \rightarrow J/\psi\ \gamma$ channel, where the J/ψ is reconstructed from dilepton decays and the photon is detected in an electromagnetic calorimeter. While the yields are larger than for the ψ', the need to form the χ_c invariant mass by combining each J/ψ candidate with a large number of photons means that combinatorial backgrounds will be quite large in Au+Au collisions. Thus the χ_c measurement will be difficult in central heavy-ion collisions.

PHENIX has very recently carried out detailed simulations of the performance

Physics Motivation	Probes	Measurements	Requirements
Baseline measurements	J/ψ, ψ', χ_c, $\Upsilon(1S)$, $\Upsilon(2S)$, and $\Upsilon(3S)$ decays to dileptons	Rapidity and p_T spectra in $p+A$ and pp as a function of $\sqrt{s_{NN}}$	High luminosity and acceptance for sufficient statistics, especially for the Υ family. Good mass resolution to resolve ψ and Υ states.
Deconfinement and initial temperature	J/ψ, ψ', χ_c, $\Upsilon(1S)$, $\Upsilon(2S)$, and $\Upsilon(3S)$ decays to dileptons	$A+A$ suppression patterns as a function of $\sqrt{s_{NN}}$ and A	High luminosity, acceptance and mass resolution for quarkonium, and triggers that work in Au+Au collisions.
Thermalization and transport	J/ψ	J/ψ v_2 as function of $\sqrt{s_{NN}}$ and A	High luminosity for good statistics in short runs for $\sqrt{s_{NN}}$ and A scans.

Table 12. The main physics goals of the RHIC II quarkonium program with corresponding probes, studies, and requirements.

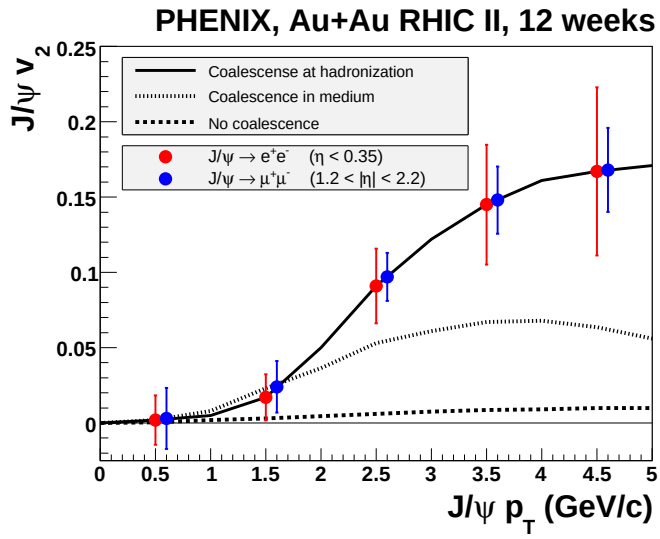

Fig. 48. The vertical bars show the estimated absolute precision of the J/ψ v_2 measurement in PHENIX at central and forward rapidity in a 12 week Au+Au run with RHIC II luminosity (22 nb^{-1} delivered) [180]. The precision is compared with several different models [17, 48].

of the PHENIX muon arms in combination with the Nose Cone Calorimeter for $\chi_c \to J/\psi\,\gamma$ measurements. Figure 50 shows the expected precision for the R_{AA} of the χ_c using the suppression pattern from a simple model in which the χ_c disappears at $1.16T_c$. Note that the maximum $N_{\rm part}$ bin ends at 30% centrality. Extending the measurement beyond 30% to the most central collisions is still being worked on.

As is the case for the J/ψ, the bottomonium states are studied through their dilepton decays. The bottomonium measurements require very large integrated luminosity and good invariant mass resolution. PHENIX expects to be able to resolve the $\Upsilon(1S)$, $\Upsilon(2S)$ and $\Upsilon(3S)$ states, see Fig. 51. Because of its larger acceptance, STAR will have substantially greater Υ yields than PHENIX. To clearly resolve the three S-wave states, STAR needs to reduce the amount of material between the interaction point and the inner field cage of the TPC because energy-loss due to bremsstrahlung deteriorates the mass resolution. Figure 52 shows the Υ mass spectrum without the material from the inner tracking system. Whether the resolution with the new inner tracking system (HFT) installed is sufficient to resolve all 3 states depends on the final design parameters of the new detectors.

Although the yields are small relative to the J/ψ, bottomonium measurements are quite clean. The states are massive ($\sim$ 10 GeV/c^2) so that their decay leptons have relatively large momenta and are thus easily distinguished from background leptons. The combinatorial background is small and multiple

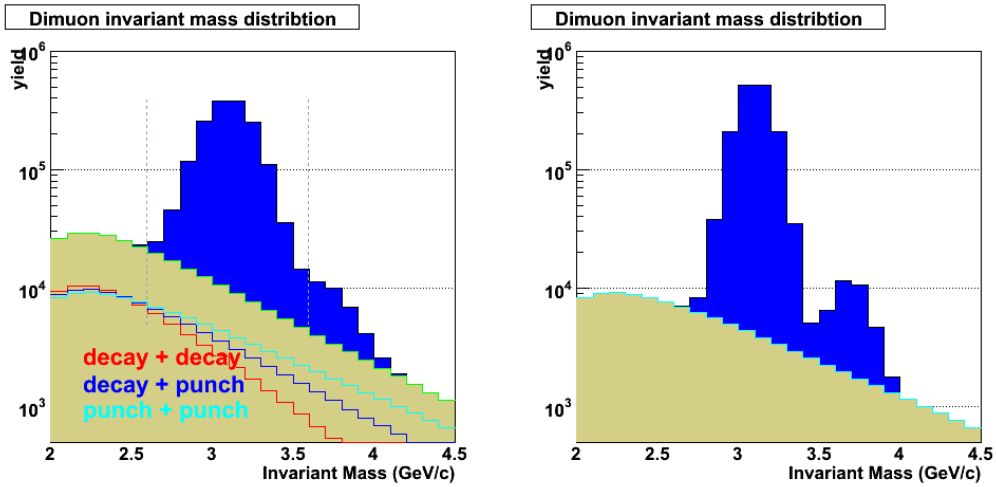

Fig. 49. The J/ψ and ψ' invariant mass spectrum in the PHENIX muon arms without (left) and with (right) the improvement in mass resolution from the FVTX detector.

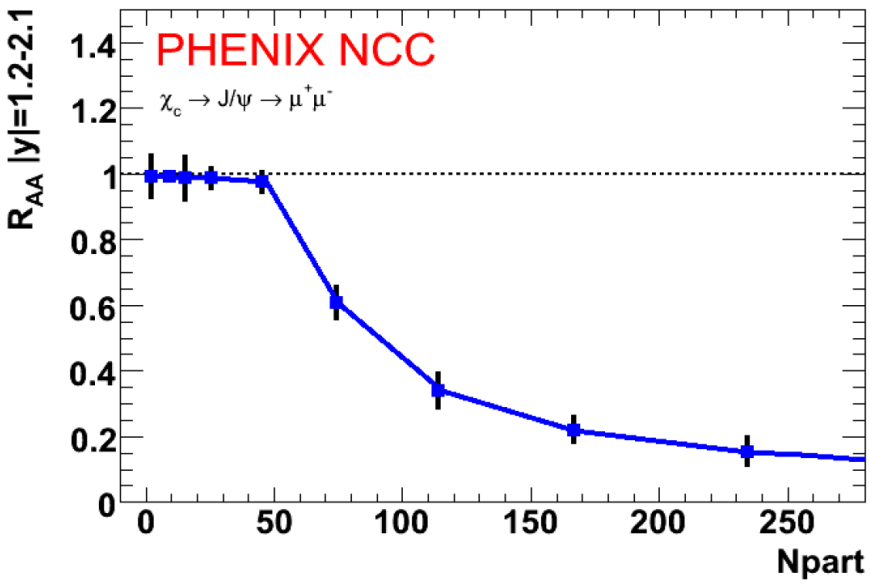

Fig. 50. The expected precision of the R_{AA} for the χ_c from PHENIX using $\chi_c \rightarrow J/\psi\ \gamma$ decays measured in the muon arms and the Nose Cone Calorimeter. The yields shown are for a delivered Au+Au luminosity of 30 nb^{-1}.

scattering is of less concern. While the interpretation of charmonium suppression is made more difficult by the rather large cross section for nucleon and comover absorption, the situation for bottomonium is considerably better. Absorption of directly produced bottomonium by hadronic comovers was shown

to be negligible [181].

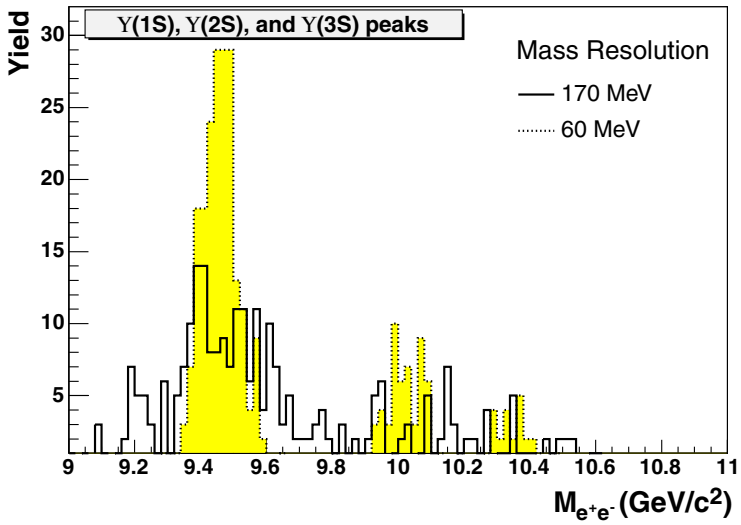

Fig. 51. The dielectron mass spectrum for the Υ family from a PHENIX central arm simulation, showing the expected improvement in Υ mass resolution provided by the initial direction measurement in the SVTX barrel [54]. The number of events shown correspond to a delivered luminosity of 30 nb^{-1} for Au+Au.

The $\sqrt{s_{NN}}$ dependence of produced J/ψ's relative to the number of $c\bar{c}$ pairs, depicted in Fig. 29 [140], is striking. Measurement of the excitation function for this ratio over $30 < \sqrt{s_{NN}} < 200$ GeV could help to disentangle suppression from enhancement. Such measurements, however, are extremely demanding statistically since both heavy quarks and quarkonia will need to be measured with good statistics over a wide energy range.

A measurement of the quarkonium nuclear modification factor at high p_T can provide a unique experimental probe of energy loss and color diffusion [182]. At relatively large transverse momentum, suppression due to color screening and coalescence are predicted to be negligible. Instead, the quarkonium state is a hard probe that interacts with the medium. In particular, any color octet can suffer energy loss. The relative abundance of charmonium resonances can provide an experimental handle on such phenomena as each resonance may have a different octet contribution. We must exercise caution, however, as competing charmonium production models exist. In parallel with nucleus-nucleus studies, it is therefore important to investigate and compare production mechanisms in pp and $p+A$ interactions, at both central and forward rapidities [183–185].

In addition to the baseline quarkonium measurements in pp and $p+A$ collisions listed in Table 12, other measurements are required as model input for description of the $A+A$ measurements. The most prominent of these are listed in Table 13.

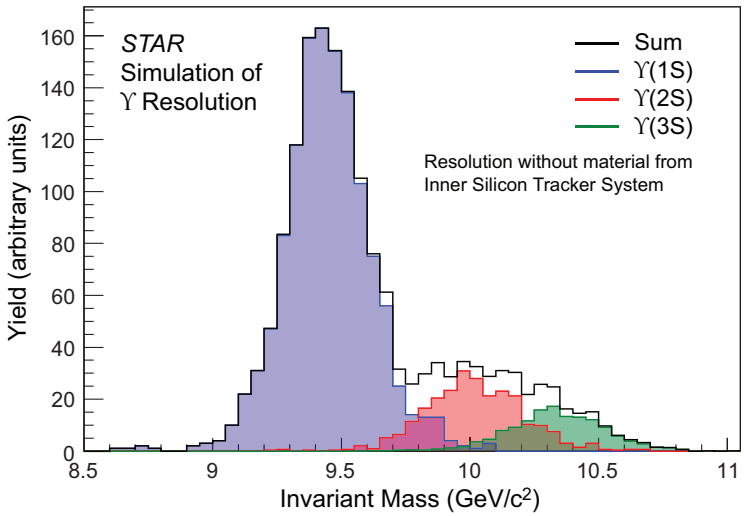

Fig. 52. The Υ family dielectron mass spectrum simulated by STAR. The three states can be clearly separated in the data given sufficient statistics.

The importance of measuring the underlying charm distributions as input to models of J/ψ coalescence is obvious, as is the importance of understanding cold nuclear matter effects on quarkonium production.

It is crucial for the interpretation of the $A+A$ quarkonia yields to understand the feed down contributions from the χ_c states, see Fig. 31. The best feed down measurement will be made in 500 GeV pp collisions because the increased luminosity and increased charmonium production cross sections lead to ~ 10 times larger charmonium yields than in 200 GeV pp collisions. Since the χ_c contribution to the J/ψ yield will not change significantly between 200 and 500 GeV, the increased yield at 500 GeV will provide a definitive baseline measurement of χ_c feed down in pp collisions.

Recently, quarkonium polarization measurements were suggested as signatures of QGP formation [186]. The quarkonium yields at RHIC II will be large enough to permit a J/ψ polarization measurement at low p_T by both PHENIX and STAR.

Topic	Measurements	Requirements
Cold nuclear effects	In pp and $p+A$ collisions: • $x_{1,2}$, x_F and y dependence of quarkonia production • A dependence	Large rapidity acceptance, including forward coverage.
Suppression vs coalescence	In pp, $p+A$ and $A+A$ collisions: • Charm $d\sigma/dp_T dy$ • J/ψ v_2 • $R_{AA}(p_T)$	High resolution vertex detectors (charm).
Feed down	χ_c, at least in pp and $p+A$	Photon detection over wide rapidity range. High rates, good energy and momentum resolution to enhance χ_c signal to background.
Production mechanism	χ_c, polarization at least in pp and $p+A$	Large acceptance for $\cos\theta^*$ measurement.

Table 13
Baseline measurements (beyond Au+Au) required in order to address the main physics questions.

6 Relationship to the LHC program

The major differences between quarkonium studies at RHIC II and at the LHC will be the temperature and lifetime of the medium, the relative production cross sections, luminosities and run times.

The initial temperature in $\sqrt{s_{NN}} = 5.5$ TeV central Pb+Pb collisions at the LHC is expected to be $\sim 4\ T_c$, while it is $\sim 2\ T_c$ in $\sqrt{s_{NN}}$= 200 GeV central Au+Au collisions at RHIC [187]. The QGP lifetime at the LHC is expected to be two to three times longer than at RHIC [187].

Heavy flavor production cross sections are much larger at the LHC. The open charm and bottom production cross sections are ~ 15 and ~ 100 times higher respectively [15]. The charmonium and bottomonium cross sections are ~ 13 and ~ 55 times higher respectively than at RHIC [50]. The higher LHC open

heavy flavor cross sections increase the number of $c\bar{c}$ and $b\bar{b}$ pairs produced in central $A + A$ collisions. There are $\sim$ 10 and $\sim$ 0.05 pairs, respectively, in Au+Au collisions at RHIC, while there should be $\sim$ 115 and $\sim$ 5 pairs in central Pb+Pb collisions at the LHC [15].

The RHIC II Au+Au average luminosity is projected to be 10 times larger than the LHC Pb+Pb luminosity (5×10^{27} cm^{-2} s^{-1} relative to 5×10^{26} cm^{-2} s^{-1}). The yearly heavy-ion runs at RHIC II are also expected to be considerably longer than at the LHC. Taking the polarized pp program at RHIC II into account, the heavy-ion program is expected to get $\sim$ 12 week physics runs on average per year while the LHC heavy ion program will be allocated a one month physics run per year. Thus the annual integrated luminosity at RHIC II is expected to be about 30 times larger for heavy ions than at LHC.

The larger heavy flavor cross sections at the LHC are approximately balanced by the increased luminosity and running times at RHIC II, making the heavy flavor yields per year similar. Thus the types of measurements that can be made at the two facilities will also be similar as well as of similar quality (see Tables 2, 3 and 5). However, there will be important differences in the physics environments prevailing at the two facilities which will make the two programs complementary.

The higher initial energy density at the LHC means that the QGP will be created at a significantly higher temperature with a correspondingly strong potential for new physics effects at the LHC. In addition, the factor of ten increase in $c\bar{c}$ pairs and the factor of 100 increase in $b\bar{b}$ pairs per central collision at the LHC will have a major impact on the interpretation of heavy flavor measurements. We will discuss some of those differences here.

Lattice calculations suggest that the J/ψ may remain bound at the highest RHIC temperatures, while the excited charmonium states are predicted to be unbound. At the LHC, all of the charmonium states should be unbound at the highest temperatures, implying that almost all charmonium production in central Pb+Pb collisions at the LHC will be due to coalescence of $c\bar{c}$ pairs. Thus the prompt charmonium yields at the LHC should reflect only the coalescence mechanism with no contribution from the primordial J/ψ production except in very peripheral collisions. The measurements at RHIC and the LHC will thus provide very different windows on charmonium suppression in the QGP that will help resolve the ambiguities in interpreting data due to the balance between destruction and coalescence formation of charmonium at RHIC.

Because of its higher binding energy, the characteristics of bottomonium production at the LHC should be similar to those of charmonium at RHIC. The bottomonium states are shown in Fig. 53. The $\Upsilon(1S)$ may remain bound at the highest temperatures at the LHC while the other bottomonium states will

be dissociated. Given $\sim 5\ b\bar{b}$ pairs in central Pb+Pb collisions (relative to $\sim 10\ c\bar{c}$ pairs at RHIC), the Υ yield at the LHC is predicted [188] to reflect a balance between dissociation and coalescence reminiscent of the RHIC J/ψ production models. However, at RHIC, the bottomonium dissociation rates will be significantly different. While the $\Upsilon(1S)$ is predicted to be bound, the $\Upsilon(2S)$ may also remain bound. Only the $\Upsilon(3S)$ is likely to dissociate at RHIC. Also, since the $b\bar{b}$ pair yield at RHIC is ~ 0.05 per central Au+Au collision, no significant bottomonium production by coalescence is expected. Thus the bottomonium yields at RHIC II should reflect only QGP suppression. Measurements at RHIC II and the LHC will thus provide very different windows on bottomonium suppression in the QGP that will help to resolve the ambiguities in interpretation due to the balance of bottomonium destruction and coalescence at the LHC.

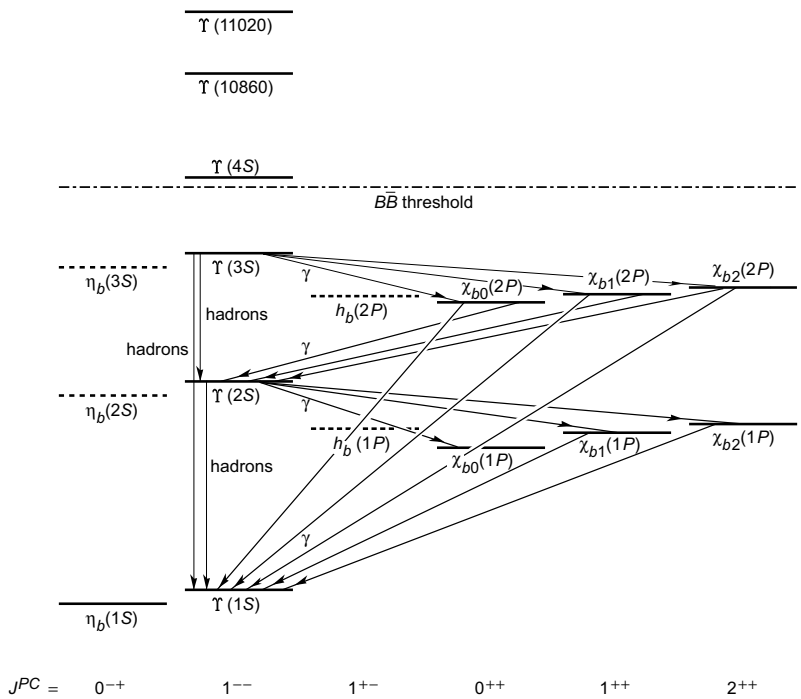

Fig. 53. Bottomonium mass levels and spin states. The common feed down channels are indicated.

The open heavy flavor programs at RHIC II and the LHC will consist of similar measurements with similar goals. They will study energy loss, thermalization and flow of heavy quarks in systems with very different energy densities, interaction cross sections and lifetimes. However, not all challenges in the measurements are similar. At $\sqrt{s_{NN}} = 200$ GeV, bottom decays to leptons begin to dominate the single electron spectrum at $p_T \sim 4$ GeV/c. As the collision energy increases, the lepton spectra from B and D decays move closer together rather than further apart. Thus, the large increase in the $b\bar{b}$ cross section relative to $c\bar{c}$ does not make single leptons from B and D decays easier to separate. Preliminary calculations show that the $B \to e$ decay does

become larger than that of $D \to e$ but only for $p_T > 10$ GeV/c. The two lepton sources differ by less than a factor of two to $p_T \sim 50$ GeV/c in the range $|y| \leq 1$. Separating single leptons from charm and bottom decays will require statistical separation using differences in the displaced vertex distributions at all p_T at the LHC. Thus interpretation of single lepton data from heavy flavor decays will be more difficult at the LHC.

ALICE can reconstruct D^0 decays from $p_T \sim 0$ to $p_T \sim 25$ GeV/c [51]. Like STAR, ALICE will be unable to trigger on D^0's and will have to obtain these events from the minimum bias sample. Thus the longer running times at RHIC are an advantage since more minimum bias data can be taken (see Tables 3 and 5). While it is not yet clear what CMS and ATLAS will do to reconstruct charm, they should be able to do b jets well, similar to the Tevatron measurements. As at RHIC, B mesons can be measured cleanly at the LHC through their decays to J/ψ, although triggering on low p_T J/ψ's is difficult at the LHC.

It has also been suggested that the $B\overline{B}$ contribution to the dimuon continuum, the dominant contribution above the Υ mass, can be used to measure energy loss [52]. That channel would be fairly clean at the LHC but more difficult at RHIC.

7 Conclusions

We have shown that, so far, the RHIC heavy flavor physics program has been very rich and stimulating, with many provocative and challenging results. To fully realize the potential of this compelling program, however, both detector upgrades and a luminosity upgrade are mandatory. Detector upgrades will improve reconstruction of charm hadron decays into hadronic channels and allow detection of $B \to J/\psi X$ decays using secondary vertex measurements. Upgrades will also make χ_c detection possible and, in the case of STAR, lead to significant quarkonium yields. However only increased luminosities will allow high statistics measurements of all of these yields as well as increase the p_T reach of J/ψ and heavy flavor R_{AA} and v_2.

We have also shown that the RHIC II and LHC heavy flavor physics programs are complementary. Both are required for a complete understanding of heavy flavor production as a function of energy and temperature. We have also demonstrated that, despite lower heavy flavor cross sections at RHIC, the longer running times and higher luminosity of RHIC II make the recorded yields similar at the two facilities.

Acknowledgements

We thank F. Karsch for the lattice contribution. The work of R. Vogt was supported in part by the U. S. Department of Energy under Contract Nos. DE-AC52-07NA27344 (LLNL) and DE-AC02-05CH11231 (LBNL) and by the National Science Foundation Grant PHY-0555660. The work of T. Ullrich was supported in part by the U. S. Department of Energy under Contract No. DE-AC02-98CH10886. The work of A. D. Frawley was supported by National Science Foundation grant PHY-04-56463.

References

[1] I. Arsene *et al.* [BRAHMS Collaboration], Nucl. Phys. A **757** (2005) 1 [arXiv:nucl-ex/0410020].

[2] B. B. Back *et al.* [PHOBOS Collaboration], Nucl. Phys. A **757** (2005) 28 [arXiv:nucl-ex/0410022].

[3] J. Adams *et al.* [STAR Collaboration], Nucl. Phys. A **757** (2005) 102 [arXiv:nucl-ex/0501009].

[4] K. Adcox *et al.* [PHENIX Collaboration], Nucl. Phys. A **757** (2005) 184 [arXiv:nucl-ex/0410003].

[5] M. Gyulassy and L. McLerran, Nucl. Phys. A **750** (2005) 30 [arXiv:nucl-th/0405013].

[6] M. Cacciari, P. Nason and R. Vogt, Phys. Rev. Lett. **95** (2005) 122001 [arXiv:hep-ph/0502203].

[7] R. Vogt, arXiv:0709.2531 [hep-ph].

[8] R. Vogt, Phys. Rev. C **71** (2005) 054902 [arXiv:hep-ph/0411378].

[9] R. Vogt, Acta Phys. Hung. New Ser. Heavy Ion Phys. **25** (2006) 97 [arXiv:nucl-th/0507027].

[10] M. Djordjevic *et al.*, Phys. Lett. B **632** (2006) 81 [arXiv:nucl-th/0507019].

[11] M. Djordjevic, M. Gyulassy, and S. Wicks, Phys. Rev. Lett. **94** (2005) 112301 [arXiv:hep-ph/0410372].

[12] N. Armesto, C. A. Salgado, and U. A. Wiedemann, Phys. Rev. D **69** (2004) 114003 [arXiv:hep-ph/0312106].

[13] Yu. L. Dokshitzer and D. E. Kharzeev, Phys. Lett. B **519** (2001) 199 [arXiv:hep-ph/0106202].

[14] Z.-W. Lin, R. Vogt and X.-N. Wang, Phys. Rev. C **57** (1998) 899 [arXiv:nucl-th/9705006]; Z.-W. Lin and R. Vogt, Nucl. Phys. B **544** (1999) 339 [arXiv:hep-ph/9808214].

[15] R. Vogt [Hard Probe Collaboration], Int. J. Mod. Phys. E **12** (2003) 211 [arXiv:hep-ph/0111271].

[16] B. Svetitsky and A. Uziel, Phys. Rev. D **55** (1997) 2616 [arXiv:hep-ph/9606284].

[17] V. Greco, C. M. Ko and R. Rapp, Phys. Lett. B **595** (2004) 202 [arXiv:nucl-th/0312100].

[18] Z.-W. Lin and D. Molnar, Phys. Rev. C **68** (2003) 044901 [arXiv:nucl-th/0304045].

[19] B. I. Abelev *et al.* [STAR Collaboration], Phys. Rev. Lett. **98** (2007) 192301 [arXiv:nucl-ex/0607012].

[20] A. Adare *et al.* [PHENIX Collaboration], Phys. Rev. Lett. **98** (2007) 172301 [arXiv:nucl-ex/0611018].

[21] S. Baumgart [STAR Collaboration], arXiv:0709.4223 [nucl-ex].

[22] R. L. Thews and M. L. Mangano, Phys. Rev. C **73** (2006) 014904 [arXiv:nucl-th/0505055].

[23] R. L. Thews, M. Schroedter, and J. Rafelski, Phys. Rev. C **63** (2001) 054905 [arXiv:hep-ph/0007323].

[24] A. Andronic, P. Braun-Munzinger, K. Redlich and J. Stachel, Phys. Lett. B **571** (2003) 36 [arXiv:nucl-th/0303036].

[25] A. P. Kostyuk, M. I. Gorenstein, H. Stöcker and W. Greiner, Phys. Rev. C **68** (2003) 041902 [arXiv:hep-ph/0305277].

[26] M. C. Abreu *et al.* [NA50 Collaboration], Phys. Lett. B **410** (1997) 327.

[27] T. Matsui and H. Satz, Phys. Lett. B **178** (1986) 416.

[28] F. Karsch, M. T. Mehr, and H. Satz, Z. Phys. C **37** (1988) 617.

[29] S. Datta, F. Karsch, P. Petreczky and I. Wetzorke, J. Phys. G **30** (2004) S1347 [arXiv:hep-lat/0403017].

[30] D. Kharzeev and H Satz, Phys. Lett. B **334** (1994) 155 [arXiv:hep-ph/9405414].

[31] P. Braun-Munzinger and J. Stachel, Phys. Lett. B **490** (2000) 196 [arXiv:nucl-th/0007059].

[32] P. Braun-Munzinger and J. Stachel, Nucl. Phys. A **690** (2001) 119 [arXiv:nucl-th/0012064].

[33] L. Grandchamp and R. Rapp, Phys. Lett. B **523** (2001) 60 [arXiv:hep-ph/0103124].

[34] P. Braun-Munzinger and K. Redlich, Eur. Phys. J. C **16** (2000) 519 [arXiv:hep-ph/0001008].

[35] C. M. Ko, B. Zhang, X.-N. Wang and X. F. Zhang, Phys. Lett. B **444** (1998) 237 [arXiv:nucl-th/9808032].

[36] J. F. Gunion and R. Vogt, Nucl. Phys. B **492** (1997) 301 [arXiv:hep-ph/9610420].

[37] N. Armesto, M. Cacciari, A. Dainese, C. A. Salgado and U. A. Wiedemann, Nucl. Phys. A **774** (2006) 589 [arXiv:hep-ph/0510284]; Phys. Lett. B **637** (2006) 362 [arXiv:hep-ph/0511257].

[38] A. Mischke [STAR Collaboration], in proceedings of Quark Matter 2008.

[39] Y. Morino [PHENIX Collaboration], in proceedings of Quark Matter 2008.

[40] A. Adare *et al.* [PHENIX Collaboration], arXiv:0802.0050 [hep-ex].

[41] D. Hornback [PHENIX Collaboration], in proceedings of Quark Matter 2008.

[42] A. Adare *et al.* [PHENIX Collaboration] Phys. Rev. Lett. **98** (2007) 232301 [arXiv:nucl-ex/0611020].

[43] A. Adare *et al.* [PHENIX Collaboration] arXiv:0801.0220v1 [nucl-ex].

[44] A. Adare *et al.* [PHENIX Collaboration] Phys. Rev. Lett. 98, 232002 (2007) arXiv:hep-ex/0611020v1.

[45] A. Capella and E. G. Ferreiro, Eur. Phys. J. C **42** (2005) 419 [arXiv:hep-ph/0505032].

[46] L. Grandchamp, R. Rapp and G. E. Brown, Phys. Rev. Lett. **92** (2004) 212301 [arXiv:hep-ph/0306077].

[47] A. Adare *et al.* [PHENIX Collaboration], arXiv:0711.3917v1 [nucl-ex].

[48] L. Yan, P. Zhuang, and N. Xu, arXiv:nucl-th/0608010.

[49] X. Zhao and R. Rapp, arXiv:0712.2407 [hep-ph].

[50] M Bedjidian *et al.*, arXiv:hep-ph/0311048.

[51] A. Dainese, R. Vogt, M. Bondila, K. J. Eskola and V. J. Kolhinen, J. Phys. G **30** (2004) 1787 [arXiv:hep-ph/0403098].

[52] I. P. Lokhtin and A. M. Snigirev, Eur. Phys. J. C **21** (2001) 155 [arXiv:hep-ph/0105244].

[53] O. Kodolova, CMS Internal Note 2003-002 (2003).

[54] PHENIX Silicon Vertex Detector proposal, PHENIX Collaboration (2004) BNL Report BNL-72204R-2004.

[55] PHENIX Forward Vertex detector proposal, PHENIX Collaboration (2007) http://www.phenix.bnl.gov/phenix/WWW/docs/upgrades/fvtx/PHENIX_FVTX-proposal_11-1-07.pdf

[56] PHENIX Nose Cone Calorimeter proposal, PHENIX Collaboration (2006) http://www.phenix.bnl.gov/phenix/WWW/docs/upgrades/ncc/PHENIX_NCC_march2006.pdf.

[57] J. Lajoie [PHENIX Collaboration], AIP Conf. Proc. **915** (2007) 490 [arXiv:physics/0612018].

[58] K. H. Ackermann *et al.*, Nucl. Instrum. Meth. A **499** (2003) 624.

[59] W. J. Llope, Nucl. Instrum. Meth. B **241** (2005) 306.

[60] G. Van Nieuwenhuizen [STAR Collaboration] (2007) private communication.

[61] R. V. Gavai, D. Kharzeev, H. Satz, G. A. Schuler, K. Sridhar and R. Vogt, Int. J. Mod. Phys. A **10** (1995) 3043 [arXiv:hep-ph/9502270].

[62] B. Alessandro *et al.* [ALICE Collaboration], J. Phys. G: Nucl. Part. Phys. **32** (2006) 1295.

[63] David G. d'Enterria, (Ed.) *et al.* J. Phys. G **34** (2007) 2307.

[64] L. Rosselet (ATLAS Collaboration) CERN-ATL-PHYS-CONF-2007-011, HEP conference 2007.

[65] M. Arneodo, Phys. Rept. **240** (1994) 301.

[66] J. Adams *et al.* [STAR Collaboration], Phys. Rev. Lett. **94** (2005) 062301 [arXiv:nucl-ex/0407006].

[67] R. Vogt, M. Cacciari and P. Nason, Nucl. Phys. A **774** (2006) 661.

[68] M. Cacciari, M. Greco and P. Nason, JHEP **9805** (1998) 007 [arXiv:hep-ph/9803400]; M. Cacciari, S. Frixione and P. Nason, JHEP **0103** (2001) 006 [arXiv:hep-ph/0102134].

[69] P. Nason, S. Dawson, and R. K. Ellis, Nucl. Phys. B **303** (1988) 607; Nucl. Phys. B **327** (1989) 49 [Erratum: Nucl. Phys. B **335** (1990) 260].

[70] W. Beenakker *et al.*, Nucl. Phys. B **351** 507.

[71] M. Cacciari and M. Greco, Nucl. Phys. B **421** (1994) 530 [arXiv:hep-ph/9311260].

[72] M. Cacciari, private communication.

[73] M. Cacciari and P. Nason, Phys. Rev. Lett. **89** (2002) 122003 [arXiv:hep-ph/0204025].

[74] S. Eidelman *et al.* [Particle Data Group Collaboration], Phys. Lett. B **592** (2004) 1.

[75] A. Adare *et al.* [PHENIX Collaboration] Phys. Rev. Lett. **97** (2006) 252002 [arXiv:hep-ex/0609010].

[76] J. D. Bjorken, FERMILAB-PUB-82-059-THY (1982).

[77] M. H. Thoma and M. Gyulassy, Nucl. Phys. B **351** (1991) 491

[78] M. H. Thoma, Phys. Lett. B **273** (1991) 128.

[79] S. Mrowczynski, Phys. Lett. B **269** (1991) 383.

[80] E. Braaten and M. H. Thoma, Phys. Rev. D **44** (1991) 2625.

[81] B. Svetitsky, Phys. Rev. D **37** (1988) 2484.

[82] Y. Koike and T. Matsui, Phys. Rev. D **45** (1991) 3237.

[83] M. G. Mustafa, D. Pal, D. K. Srivastava and M. Thoma, Phys. Lett. B **428** (1998) 234 [arXiv:nucl-th/9711059].

[84] E. Shuryak, Phys. Rev. C **55** (1997) 961 [arXiv:nucl-th/9605011].

[85] M. Djordjevic and U. Heinz, arXiv:0802.1230 [nucl-th].

[86] S. Wicks, W. Horowitz, M. Djordjevic and M. Gyulassy, Nucl. Phys. A **784** (2007) 426 [arXiv:nucl-th/0512076].

[87] A. Adil and I. Vitev, Phys. Lett. B **649** (2007) 139 [arXiv:hep-ph/0611109].

[88] G. D. Moore and D. Teaney, Phys. Rev. C **71** (2005) 064904 [arXiv:hep-ph/0412346].

[89] H. van Hees and R. Rapp, Phys. Rev. C **71** (2005) 034907 [arXiv:nucl-th/0412015].

[90] H. van Hees, V. Greco and R. Rapp, Phys. Rev. C **73** (2006) 034913 [arXiv:nucl-th/0508055].

[91] S. S. Adler *et al.* [PHENIX Collaboration], Phys. Rev. D **76** (2007) 092002 [arXiv:hep-ex/0609032].

[92] S. Kelly [PHENIX Collaboration], J. Phys. G **30** (2004) S1189.

[93] C. Zhong [STAR Collaboration], J. Phys. G **34** (2007) S741 [arXiv:nucl-ex/0702014].

[94] A. A. P. Suaide, J. Phys. G **34** (2007) S369 [arXiv:nucl-ex/0702035].

[95] R. A. Lacey *et al.*, Phys. Rev. Lett. **98** (2007) 092301 [arXiv:nucl-ex/0609025].

[96] S. Gavin and M. Abdel-Aziz, Phys. Rev. Lett. **97** (2006) 162302 [arXiv:nucl-th/0606061].

[97] B. V. Jacak and M. P. McCumber, J. Phys. G **34** (2007) S543 [arXiv:nucl-ex/0703032].

[98] V. D. Barger, W. Y. Keung, and R. J. Phillips, Phys. Lett. B **91** (1980) 253.

[99] V. D. Barger, W. Y. Keung, and R. J. Phillips, Z. Phys. C **6** (1980) 169.

[100] G. A. Schuler and R. Vogt, Phys. Lett. B **387** (1996) 181 [arXiv:hep-ph/9606410].

[101] M. L. Mangano, P. Nason and G. Ridolfi, Nucl. Phys. B **405** (1993) 507.

[102] R. Vogt, arXiv:hep-ph/0203151.

[103] R. Vogt, Acta Phys. Hung. New Ser. Heavy Ion Phys. **18** (2003) 11 [arXiv:hep-ph/0205330].

[104] A. D. Martin *et al.*, Eur. Phys. J. C **4** (1998) 463 [arXiv:hep-ph/9803445].

[105] H. L. Lai *et al.* [CTEQ Collaboration], Eur. Phys. J. C **12** (2000) 375 [arXiv:hep-ph/9903282].

[106] M. Gluck, E. Reya and A. Vogt, Eur. Phys. J. C **5** (1998) 461 [arXiv:hep-ph/9806404].

[107] S. Digal, P. Petreczky and H. Satz, Phys. Rev. D **64** (2001) 094015 [arXiv:hep-ph/0106017].

[108] T. Affolder *et al.* [CDF Collaboration], Phys. Rev. Lett. **84** (2000) 2094 [arXiv:hep-ex/9910025].

[109] S. R. Klein and R. Vogt, Phys. Rev. Lett. **91** (2003) 142301 [arXiv:nucl-th/0305046].

[110] D. Kharzeev and H. Satz, Phys. Lett. **366** (1996) 316 [arXiv:hep-ph/96xxxx].

[111] R. Vogt, Nucl. Phys. A **700** (2002) 539 [arXiv:hep-ph/0107045].

[112] K. .J. Eskola, V. J. Kolhinen and P. V. Ruuskanen, Nucl. Phys. B **535** (1998) 351 [arXiv:hep-ph/9802350]; K. .J. Eskola, V. J. Kolhinen and C. A. Salgado, Eur. Phys. J. C **9** (1999) 61 [arXiv:hep-ph/9807297].

[113] S. S. Adler *et al.* [PHENIX Collaboration], Phys. Rev. Lett. **96** (2006) 012304 [arXiv:nucl-ex/0507032].

[114] M. Leitch, C. Lourenco and R. Vogt, J. Phys. G **34** (2007) S759.

[115] L. McLerran and B. Svetitsky, Phys. Lett. B **98** (1981) 195; J. Kuti, J. Polonyi and K. Szlachanyi, Phys. Lett. B **98** (1981) 199.

[116] O. Kaczmarek and F. Zantow, Eur. Phys. J. C **43** (2005) 63 [arXiv:hep-lat/0502011].

[117] S. Digal, P. Petreczky and H. Satz, Phys. Lett. B **514** (2001) 57 [arXiv:hep-ph/0105234].

[118] C. Y. Wong, Phys. Rev. C **72** (2005) 034906 [arXiv:hep-ph/0408020].

[119] W. M. Alberico, A. Beraudo, A. De Pace and A. Molinari, Phys. Rev. D **72** (2005) 114011 [arXiv:hep-ph/0507084].

[120] E. V. Shuryak and I. Zahed, Phys. Rev. D **70** (2004) 054507 [arXiv:hep-ph/0403127].

[121] D. Blaschke, O. Kaczmarek, E. Laermann and V. Yudichev, Eur. Phys. J. C **43** (2005) 81 [arXiv:hep-ph/0505053].

[122] H. Satz, J. Phys. G **32** (2005) R25 [arXiv:hep-ph/0512217].

[123] F. Karsch, Eur. Phys. J. C **43** (2005) 35 [arXiv:hep-lat/0502014].

[124] Y. Nakahara, M. Asakawa, and T. Hatsuda, Phys. Rev. D **60** (1999) 091503 [arXiv:hep-lat/9905034].

[125] N. Brambilla *et al.* [Quarkonium Working Group], arXiv:hep-ph/0412158.

[126] F. Karsch and R. Petronzio, Z. Phys. C **37** (1988) 627.

[127] M. Asakawa and T. Hatsuda, Phys. Rev. Lett. **92** (2004) 012001 [arXiv:hep-lat/0308034].

[128] S. Datta, F. Karsch, S. Wissel, P. Petreczky and I. Wetzorke, arXiv:hep-lat/0409147.

[129] K. L. Haglin and C. Gale, Phys. Rev. C **63** (2001) 065201 [arXiv:nucl-th/0010017].

[130] A. Mocsy and P. Petreczky, Phys. Rev. Lett. **99** (2007) 211602 [arXiv:0706.2183 [hep-ph]].

[131] T. Umeda, R. Katayama, O. Miyamura and H. Matsufuru, Int. J. Mod. Phys. A **16** (2001) 2215 [arXiv:hep-lat/0011085].

[132] H. Iida, T. Doi, N. Ishii and H. Suganuma, PoS **LAT2005** (2006) 184 [arXiv:hep-lat/0509129].

[133] M. I. Gorenstein, A. P. Kostyuk, H. Stoecker and W. Greiner, Phys. Lett. B **509** (2001) 277 [arXiv:hep-ph/0010148].

[134] M. I. Gorenstein, A. P. Kostyuk, H. Stoecker and W. Greiner, J. Phys. G **27**(2001) L47 [arXiv:hep-ph/0012015].

[135] M. I. Gorenstein, A. P. Kostyuk, L. McLerran, H. Stoecker and W. Greiner, arXiv:hep-ph/0012292.

[136] R. L. Thews, Nucl. Phys. A **702** (2002) 341 [arXiv:hep-ph/0111015].

[137] K. Martins, D. Blaschke, and E. Quack, Phys. Rev. C **51** (1995) 2723 [arXiv:hep-ph/9806027]; S. G. Matinyan and B. Müller, Phys. Rev. C **58** (1998) 2994 [arXiv:nucl-th/9806027]; K. Haglin, Phys. Rev. C **61** (2000) 031902R [arXiv:nucl-th/9907034]; Z.-W. Lin and C. M. Ko, Phys. Rev. C **62** (2000) 034903 [arXiv:nucl-th/9912046].

[138] K. Geiger and J. R. Ellis, Phys. Rev. D **52** (1995) 1500 [arXiv:hep-ph/9503349]; Phys. Rev. D **54** (1996) 1967 [arXiv:hep-ph/9511321].

[139] R. L. Thews, Eur. Phys. J. A **29** (2006) 15 [arXiv:hep-ph/0511292].

[140] L. Grandchamp and R. Rapp, Nucl. Phys. A **715** (2003) 545 [arXiv:hep-ph/0209141].

[141] S. Gavin, M. Gyulassy and A. Jackson, Phys. Lett. B **207** (1988) 257.

[142] R. Vogt, M. Prakash, P. Koch and T.H. Hansson, Phys. Lett. B **207** (1988) 263.

[143] J. Ftacnik, P. Lichard and J. Pisut, Phys. Lett. B **207** (1988) 194; J. Ftacnik, P. Lichard, N. Pisutova and J. Pisut, Z. Phys. C **42** (1989) 132.

[144] A. Capella *et al.*, arXiv:0712.4331v1 [hep-ph].

[145] N. Armesto, A. Capella and E. G. Ferreiro, Phys. Rev. C **59** (1999) 395 [arXiv:hep-ph/9807258].

[146] A. Capella and E. Ferriero, arXiv:hep-ph/0610313.

[147] F. Karsch, D. Kharzeev and H. Satz, Phys. Lett. B **637** (2006) 75 [arXiv:hep-ph/0512239].

[148] J.-P. Blaizot and J.-Y. Ollitrault, Phys. Rev. Lett. **77** (1996) 1703 [arXiv:hep-ph/9606289].

[149] A. K. Chaudhuri, Phys. Rev. C **75** (2007) 044902 [arXiv:nucl-th/0610031].

[150] T. Gunji, H. Hamagaki, T. Hatsuda and T. Hirano, Phys. Rev. C **76** (2007) 051901 [arXiv:hep-ph/0703061].

[151] H. Liu, K. Rajagopal, and U. A. Wiedemann, Phys. Rev. Lett. **98** (2007) 182301 [arXiv:hep-ph/0607062].

[152] A. L. S. Angelis *et al.* [HELIOS-3 Collaboration], Eur. Phys. J. C **5** (1998) 63.

[153] M. C. Abreu *et al.* [NA50 Collaboration], Phys. Lett. B **466** (1999) 408.

[154] M. C. Abreu *et al.* [NA50 Collaboration], Phys. Lett. B **477** (2000) 28.

[155] A. Baldit *et al.* [NA60 Collaboration], CERN-SPSC-2000-010 (2000).

[156] H. Kolanoski [HERA-B Collaboration], J. Phys. G **31** (2005) S799.

[157] I. Abt *et al.* [HERA-B Collaboration], Phys. Lett. B **561** (2003) 61 [arXiv:hep-ex/0211033].

[158] G. Borges [NA50 Collaboration], J. Phys. G **30** (2004) S1351.

[159] B. Alessandro *et al.* [NA50 Collaboration], arXiv:nucl-ex/0612012.

[160] C. Lourenco, R. Vogt and H. Woehri, in preparation.

[161] M. Leitch *et al.* [FNAL E866/NuSea collaboration], Phys. Rev. Lett. **84** (2000) 3256 [arXiv:nucl-ex/9909007].

[162] B. Alessandro *et al.* [NA50 Collaboration], Eur. Phys. J. C **49** (2007) 559 [arXiv:nucl-ex/0612013].

[163] B. Alessandro *et al.* [NA50 Collaboration], Eur. Phys. J. C **39** (2005) 335 [arXiv:hep-ex/0412036].

[164] M. Nardi and H. Satz, Phys. Lett. B **442** (1998) 14 [arXiv:hep-ph/9805247].

[165] D. Kharzeev, C. Lourenco, M. Nardi and H. Satz, Z. Phys. C **74** (1997) 307 [arXiv:hep-ph/9612217].

[166] R. Arnaldi *et al.* [NA60 Collaboration], arXiv:0706.4361 [nucl-ex].

[167] J.-P. Blaizot, M. Dinh and J.-Y. Ollitrault, Phys. Rev. Lett. **85** (2000) 4012 [arXiv:nucl-th/0007020].

[168] R. Shahoyan [NA60 Collaboration], Eur. Phys. J. C **43** (2005) 209.

[169] S. S. Adler *et al.* [PHENIX Collaboration], Phys. Rev. Lett. **92** (2004) 051802 [arXiv:hep-ex/0307019].

[170] Z. Tang [STAR Collaboration], in proceedings of Quark Matter 2008.

[171] H. Buesching [PHENIX Collaboration], Nucl. Phys. A **774** (2006) 103; M. Leitch, J. Phys. G **34** (2007) S453 [arXiv:nucl-ex/0701021].

[172] P. Djawotho *et al.* [STAR Collaboration], J. Phys. G **34** (2007) S947 [arXiv:nucl-ex/0701075].

[173] D. deFlorian and R. Sassot, Phys. Rev. D **69** 074028 (2004)

[174] B. Alessandro *et al.*, Euro. Phys. J. C **48** 329 (2006).

[175] T. Gunji [PHENIX Collaboration], J. Phys. G **34** (2007) S749 [arXiv:nucl-ex/0703004].

[176] R. Rapp, Eur. Phys. J. C **43** (2005) 91 [arXiv:hep-ph/0502208].

[177] A. Andronic, P. Braun-Munzinger, K. Redlich and J. Stachel, Nucl. Phys. A **789** (2007) 334 [arXiv:nucl-th/0611023].

[178] W. Cassing, E. L. Bratkovskaya, and S. Juchem, Nucl. Phys. A **674** (2000) 249 [arXiv:nucl-th/0001024].

[179] X. Zhao and R. Rapp, arXiv:0712.2407v2 [hep-ph].

[180] M. Wysocki (2007), private communication.

[181] Z.-W. Lin and C. M. Ko, Phys. Lett. B **503** (2001) 104 [arXiv:nucl-th/0007027].

[182] R. Baier, D. Schiff and B. G. Zakharov, Ann. Rev. Nucl. Part. Sci. **50** (2000) 37 [arXiv:hep-ph/0002198].

[183] R. Vogt, Phys. Rev. C **61** (2000) 035203 [arXiv:hep-ph/9907317].

[184] S. Gavin and J. Milana, Phys. Rev. Lett. **68** (1992) 1834.

[185] M. B. Johnson *et al.*, Phys. Rev. C **65** (2002) 025203 [arXiv:hep-ph/0105195].

[186] B. L. Ioffe and D. E. Kharzeev, Phys. Rev. C **68** (2003) 061902 [arXiv:hep-ph/0306176].

[187] I. Vitev, J. Phys. G **30** (2004) S791 [arXiv:hep-ph/0403089].

[188] L. Grandchamp, S. Lumpkins, D. Sun, H. van Hees and R. Rapp, Phys. Rev. C **73** (2006) 064906 [arXiv:hep-ph/0507314].